NORTHWESTERN UNIVERSITY

Second Harmonic Generation Spectroscopy Studies of Polymers and Nanomaterials at Model Biological Surfaces

A DISSERTATION

SUBMITTED TO THE GRADUATE SCHOOL

IN PARTIAL FULFILLMENT OF THE REQUIREMENTS

for the degree

DOCTOR OF PHILOSOPHY

Field of Chemistry

By

Alicia Christine McGeachy

EVANSTON, ILLINOIS

June 2018

Abstract

Second Harmonic Generation Spectroscopy Studies of
Polymers and Nanomaterials at Model Biological Interfaces

Alicia C. McGeachy

The projected increase in the use of nanomaterials raises concerns about adverse impacts new technologies utilizing these materials may have on the environment. These concerns can be addressed from a chemical perspective by studying how emerging nanomaterials interact with biological systems. Fundamentally, the key interactions for nanomaterial uptake into a cell occurs at the nano/bio interface. This interface is difficult to access experimentally, mainly because traditional methods used to probe these interactions do not provide molecular information, are not interface-specific, or are not sensitive enough to detect small surface coverages, even at saturation. As a result, the amount of molecular information regarding how nanoparticles interact with aqueous/solid interfaces, including biological membranes, is limited. There exists therefore an urgent need to bridge this knowledge gap by probing the nano/bio interface with new tools. The motivation of this thesis is to address this need by using advanced spectroscopic techniques that will improve our ability to understand, control, and predict how emerging nanomaterials will impact the environment and biological systems. Herein we take a bottom-up approach to better understand, from a fundamental perspective, what factors contribute to nano/bio interactions.

The interactions that take place at the nano/bio interface are directly influenced by the chemistry of the biological surface, the properties of the nanomaterial (size, shape, functionalization, surface charge, charge density, etc.), and environmental conditions (ionic strength, pH, temperature, etc.). Given the complexity of both nanomaterials and biological surfaces, we simplify our systems to include biomimetic membranes, model nanomaterials, and

polyelectrolytes which are often used to functionalize nanomaterials. We use a combinatorial approach that employs second harmonic generation (SHG) spectroscopy, sum frequency generation spectroscopy (SFG), and quartz crystal microbalance with dissipation monitoring (QCM-D) measurements to explore the influence of surface charge, charge density, chemical functionality, ionic strength, and electrostatics, on nano/bio interactions. Specifically, SHG spectroscopy is used here to estimate equilibrium constants, changes in interfacial potential, and surface charge densities of model biological membranes interacting with nanomaterials and polyelectrolytes. With insights from complementary tools, we discuss the impacts that nanomaterials have on the structure of biomimetic surfaces and provide estimates for the adsorbed mass, number densities, and percent ionizations. In addition to building a better understanding of nano/bio interactions, we aim to use this information to develop better design rules for nano-scale materials, to minimize or attenuate some outcomes, and to exploit more favorable outcomes. The results generated from these studies are reported in collaboration with the Center for Sustainable Nanotechnology.

Professor Franz M. Geiger
Research Advisor

Acknowledgments

At times our own light goes out and is rekindled by a spark from another person. Each of us has cause to think with deep gratitude of those who have lighted the flame within us.
-Albert Schweitzer

First I would like to thank my advisor, Franz Geiger. I am often asked what made me decide that Northwestern was the place for me. My answer is always the same: Franz. Your enthusiasm, encouragement, support, and mentorship has been invaluable. You have supported me in everything that I have wanted to pursue and you have been one of my biggest advocates. I am forever grateful that I had the fortune to join your group. For the many people that I have been able to work with while in the Center for Sustainable Nanotechnology, thank you all. Miriam and Mike, you have gone above and beyond to make sure that me, and other students in the Center, had everything that we needed to be successful, and for that I am grateful.

Thank you to Penny Warren who did more for graduate students than was ever written in her job description. It was a great pleasure to work with Nsombi Ricketts, Brittani, Aireale, and Mychelle and I am thankful that we crossed paths. Working with you has given me a sense of purpose and has opened many doors for me. I cannot thank you enough.

To the Geiger group: Sarah, Mona, Juli, and Laura thank you for your friendship and for being a sharing your knowledge, encouragement, and inspiration. Hilary, I am so thankful for your friendship and for our many coffee walks/venting sessions. Merve, your smile and calm attitude often put things into perspective for me and I am thankful that I got to learn so much about you over the last few years. Paul and Mavis, I am willing to bet (not a lot of money) that one or both of you will win a Nobel Prize. You two are brilliant and I am thankful that I could learn from you both. Ariana, thank you for introducing me to yoga and for your bright smile and light mood that made working with you so enjoyable. Johnny, thanks for all of the laughs (and memes). Dawning,

Naomi, Tian, and HanByul I am thankful that I got to know you over the last few years. Naomi, I am especially happy that I got the chance to mentor you the first year and I am glad that you decided to join our group.

Working alongside Abdallah, Kedy, Lam-Kiu, Andrea, Dana, Ariana, Oliver, Zack, and Jiaqi on NUBonD was the most enriching experience of my graduate school career. Jonathan, you have helped me through a lot of challenges here at Northwestern. Thank you for always knowing the answers to all of the many questions that I have had over the years. Laura and Madison, I am glad that we got to work alongside you on many of our NUBonD initiatives.

To Spelman, thank you for existing and helping to show me my place in the world. My time at Spelman was the most transformative experience of my entire life. I need to especially acknowledge Dr. Virgil Payne who supported me in every step of my academic career and encouraged me to persist. To my very amazing Spelman boss, Yvonne Prabhu, thank you for being there to help me navigate life at a time that I thought it could all fall apart.

To my parents, Sharon and Clive, and my siblings, Lauren and David thank you for your constant push to do my best and your unwavering confidence in me. To my grandparents, Laura, Robert, and Donald, you all have given me the strength to push forward and challenged me to think more critically about the world. My cousins and friends have rooted me on since the beginning of my journey. Tiesha, thank you for always being there for me when I needed you the most. To my sisters from other misters: Breoshshala, Cheyanne, and Tynisha, thank you for being there for me being and for your encouragement, inspiration, and laughter. Where would I be without you all?

Kenneth, you have been there for me to encourage me, to celebrate me, and to restore me when I really believed I had nothing more to give. There is no way that I could ever thank you enough for all that you have been for me along this journey. *Looks like we made it at last.*

TABLE OF CONTENTS

Abstract..... 3

Acknowledgments..... 5

Table of Contents..... 7

List of Figures..... 10

List of Tables..... 12

Chapter 1. Shedding Light on Nano/Bio Interactions: Fundamental Spectroscopic Studies of the Nano/Bio Interface..... 13
1.1. Introduction and Motivation..... 14
1.2. Supported Lipid Bilayers as a Model for Cellular Surfaces..... 15
1.3. Factors Governing Interactions Occurring at Biological Interfaces..... 17
1.3.1. Surface Charge Density..... 19
1.4. Tools for Probing Nanomaterials, Biological Surfaces, and Nano/Bio Interactions..... 19
1.4.1. Fluorescence Techniques..... 20
1.4.2. Optical and Acoustic Mass Sensors..... 20
1.4.3. Other Spectroscopies/Microscopies..... 21
1.5. Nonlinear Optical Spectroscopic Studies of Biological Interfaces..... 21
1.6. Scope and Organization of Thesis..... 22

Chapter 2. Theoretical Foundation of Second Harmonic Generation Spectroscopy Experiments..... 25
2.1. Second Harmonic Generation Spectroscopy (SHG) Theory..... 26
2.1.1. SHG: An Optical Voltmeter..... 26
2.2. Resonantly Enhanced SHG Spectroscopy..... 28
2.3. Modeling Interfacial Adsorption Processes..... 29
2.3.1. Surface Complexation Models..... 29
2.3.2. Adsorption Models..... 35
2.3.3. Estimating Thermodynamics from SHG Spectroscopy..... 36
2.4. SHG Laser System and Procedures..... 36
2.4.1. Laser System..... 36
2.4.2. Sample Cell, Flow System, and Substrate Preparation..... 37

Chapter 3. Resonantly Enhanced Nonlinear Optical Probes of Oxidized Multiwalled Carbon Nanotubes at Supported Lipid Bilayers..... 40
3.1. Introduction..... 41
3.2. Experimental Details..... 43
3.2.1. Laser System..... 43
3.2.2. Flow Cell, Substrate, Solution, and Bilayer Preparation..... 43
3.2.3. Preparation and Characterization of O-MWCNT Suspensions..... 45
3.2.4. SHG Experiments..... 45

3.2.5. SFG Experiments…… 46
3.2.6. QCM-D Experiments…….. 48
3.3. Results and Discussion…….. 48
3.3.1. Assessing the Stability of O-MWCNT Suspensions…….. 48
3.3.2. Attachment of O-MWCNTs to Supported Lipid Bilayers Prepared from DMPC…… 49
3.3.3. SHG Control Studies…….. 51
3.3.4. SHG Adsorption Isotherm Measurements……. 58
3.3.5. O-MWCNT Adsorption to SLBs Prepared from DOPC and DOPC/DOTAP……... 60
3.4. Possible Interaction Mechanism and Conclusions……. 60
Chapter 4. Interfacial Electrostatics of Poly(vinylamine hydrochloride), Poly(diallyldimethylammonium chloride), Poly-L-lysine, and Poly-L-arginine Interacting with Lipid Bilayers..... 64
4.1. Introduction…… 65
4.2. Experimental Methods……... 70
4.2.1. Vesicle and SLB Preparation…….. 70
4.2.2. Polymer Solution Preparation……. 72
4.2.3. Fluorescence Recovery after Photobleaching Measurements……. 72
4.2.4. SHG Adsorption Experiments…… 75
4.3. Results and Discussion…….. 77
4.3.1. Polycation Adsorption to SLBs…….. 77
4.3.2. Reversibility and Timescales…….. 79
4.3.3. Comparable Binding Free Energies Across All Polymers Despite Differences in Molecular Structure and Mass…… 80
4.3.4. Charge Densities of Polycations Attached to SLBs…… 84
4.4. Conclusions…… 89
Chapter 5. Counting Charges on Membrane-bound Peptides……... 92
5.1. Introduction…… 93
5.2. Experimental Methods……... 95
5.2.1. Oligopeptide and Lipid Vesicle Preparation……... 95
5.2.2. Determination of Lys_8 and Arg_8 Surface Mass Densities……... 95
5.3. Results and Discussion…….. 97
5.3.1. Peptide Mass Adsorbed to Bilayers Formed from 9:1 DMPC/DMPG…… 97
5.3.2. Interfacial Free Binding Energy and Cooperativity…… 97
5.3.3. Interfacial Charge Densities and Number of Charges per Attached Peptide……. 103
5.3.4. Bound Confirmation of Peptides and Interfacial Electrostatics from Atomistic Simulations…… 105
5.3.5. Comparing SHG Results for PLL/PLR to Lys_8/Arg_8..... 110
5.4. Conclusions…… 110
Chapter 6. Improving Biomimetic Models for Probing Nano/Bio Interactions…..... 115
6.1. Introduction and Motivation……..... 116
6.2. Experimental Details……..... 117

6.2.1. Lipid Vesicle Preparation……..... 117
6.2.2. DMPC/DMPS……..... 117
6.2.3. DOPC/CL and DOPC/LPI…….. 118
6.2.4. Charge Screening of Bare Silica Substrate Exposed to HEPES Buffer……..... 118
6.2.5. Cytochrome *c* (Cyt*c*) Adsorption to SLBs…….. 121
6.2.6. Characterization of Vesicles with/without Cytc……. 121
6.3. Integrating PS Lipids into the SLB Matrix…… 121
6.4. Cytochrome *c* as a Model Peripheral Membrane Protein…….. 122
6.4.1. Adsorption of Cyt*c* to Lipid Vesicles……. 124
6.4.2. Nonlinear Optical Studies of SLBs Containing PS,CL, and PI….. 127
6.4.3. Future Studies Employing Cyt*c*-containing SLBs…….. 127
6.5. Future Directions for Modifying Biomimetic Systems……..... 130
6.5.1. Addition of Cholesterol to SLBs……. 130
6.5.2. Biologically Relevant Proteins for Fundamental Studies……... 131
6.5.3. Naturally-Derived Membranes for Spectroscopic Studies……..... 132

References
Chapter 1……. 133
Chapter 2……. 146
Chapter 3……. 152
Chapter 4……. 159
Chapter 5……. 164
Chapter 6……. 170

Curriculum Vitae…… 174

LIST OF FIGURES

Scheme 1.1. Summary of chemical structures of lipids……... 18

Figure 2.1. Illustration of Gouy-Chapman model…… 30

Figure 2.2. Illustration of triple layer model…… 34

Figure 2.3. Cross sectional illustration of flow cell used in SHG studies…… 39

Figure 3.1. TEM images of O-MWCNTs and absorbance spectra and hydrodynamic diameters of O-MWCNT solution……. 47

Figure 3.2. *ssp*-Polarized SFG spectra of DMPC SLBs before, during, and after exposure to O-MWCNTs……... 50

Figure 3.3. QCM-D Frequency shifts as a function of O-MWCNT oxygen content for O-MWCNTs adsorbing to DMPC SLBs……... 52

Figure 3.4. SHG data for the adsorption of O-MWCNTs to bare SiO_2 as a function of ionic strength……. 54

Figure 3.5. SHG data for O-MWCNTs adsorbing to SLBs formed from DMPC as a function of ionic strength and incident wavelength……... 55

Figure 3.6. SHG control studies (power, bandwidth, and polarization studies) for O-MWCNTs adsorbed to DMPC SLBs……. 57

Figure 3.7. SHG data for O-MWCNT adsorbed to DMPC SLB with associated Langmuir fit……... 59

Figure 3.8. SHG data for O-MWCNT adsorption to SLBs with varying surface chemistry…… 61

Figure 4.1. Structures of polycations used in SHG studies…….. 69

Figure 4.2. Illustration of FRAP experimental setup……... 74

Figure 4.3. Representative simFRAP plots for SLBs formed via various preparation methods…….. 76

Figure 4.4. SHG adsorption and reversibility studies for polycations adsorbing to SLBs formed from DMPC and 9:1 DMPC/DMPG……... 78

Figure 4.5. SHG data for polycations adsorbed to SLBs formed from 9:1 DMPC/DMPG as a function of polymer and charge concentration…….. 83

Figure 4.6. Individual SHG adsorption isotherms for polycations adsorbed to SLBs formed from 9:1 DMPC/DMPG with associated Gouy-Chapman/Hill fits.. 87

Figure 4.7. Polymer number density and percent ionization on SLBs formed from 9:1 DMPC/DMPG as a function of water content……... 90

Figure 5.1. Optical and acoustic mass estimates for octamers of lysine and arginine to SLBs formed from 9:1 DMPC/DMPG…….. 98

Figure 5.2. SHG data for adsorption of arginine and lysine octamers to SLBs formed from 9:1 DMPC/DMPG…… 100

Figure 5.3. Charge densities estimated from SHG as a function of extrapolated data for arginine and lysine octamers adsorbed to SLBs formed from 9:1 DMPC/DMPG……... 104

Figure 5.4. Snapshots from molecular dynamics simulations for arginine and lysine octamers interacting with SLBs formed from 9:1 DMPC/DMPG…… 107

Figure 5.5. Charge densities and electrostatic potentials of SLBs formed from 9:1 DMPC/DMPG as determined in molecular dynamics simulations……... 109

Figure 6.1. SHG charge screening of bare fused silica substrate in the presence of HEPES buffer adjusted to pH 7.4…….. 120

Figure 6.2. SHG charge screening of SLB formed from 9:1 DMPC/DMPS in the presence of Tris buffer……... 123

Figure 6.3. DLS and absorbance spectra for the interaction of Cyt*c* with CL-containing vesicles……. 126

Figure 6.4. SHG data for the adsorption of Cyt*c* to SLBs containing CL and LPI 128

Figure 6.5. SHG adsorption isotherms for Cyt*c* adsorbing to SLBs containing varying CL contents…… 129

LIST OF TABLES

Table 4.1. Summary of experimental data for polycations adsorbing to SLBs formed from 9:1 DMPC/DMPG at 0.1 M NaCl…….. 81

Table 4.2. Summary of estimates for charge densities and equilibrium constants determined via different adsorption models…… 85

Table 5.1. Summary of experimental data for arginine and lysine octamers adsorbed to 9:1 DMPC/DMPG……... 102

Table 5.2. Comparison of fitting parameters and free energies of adsorption of polymers or oligomers of arginine and lysine……. 111

Table 6.1. Hydrodynamic diameters and zeta potentials of CL and LPI containing vesicles…… 125

CHAPTER 1

Shedding Light on Nano/Bio Interactions: Fundamental Spectroscopic Studies of the Nano/Bio Interface

1.1. Introduction and Motivation. The desire for new materials that can address a number of technological and societal needs drives the study, development, and use of a relatively new class of materials: engineered nanomaterials.[1-4] Characteristically, nanomaterials have at least one dimension between 1-100 nm (or 1-100 billionth of a meter)[5-7] and can be engineered or naturally occurring.[8] Nanoscale materials are sought after because of characteristics that can differ significantly from those of their macroscopic scale counterparts.[2,5,9] These unique chemical, optical, and electronic properties are largely a result of the orders of magnitude increase in surface area-to-volume ratio.[10-12] Many of these features and properties can be tuned simply by manipulating the size, shape, and morphology of the nanomaterial, thus establishing an ideal platform on which many technologies can be built and designed.[6,9,13] Research in this area is still relatively new, as our understanding of nanoscale phenomena, development of synthesis strategies, and technologies for characterizing and visualizing nanoscale materials and their properties, develops.[14]

Engineered nanomaterials have applications ranging from environmental remediation[15-17] and energy storage[15,18] to medicine[2,19-21] and clothing.[22,23] Nanomaterials can be found in batteries for cars and electronics, cosmetic products such as lotions, makeup, and sunscreen, and have a plethora of other potential applications.[5,9,24] For instance, carbon nanotubes, which are discussed more in Chapter 3, have proposed applications in environmental remediation as sorbent materials, in energy storage solutions, and as an additive for composites.[1,15,25] One of the most widely studied nanomaterials, titanium dioxide (TiO_2), is not only found in research laboratories, but also in the hands of consumers in the form of cosmetics and sunscreens.[5,9] In fact, the global value of nanomaterials and nano-technologies and products is expected to reach over $4 trillion by this year.[26] Yet, considering the number of nano-enabled technologies that are proposed, developing,

and in use, and the existing evidence of environmental release,[27] there is rising concern about the impacts that these materials may have on biological and environmental systems.[8,28,29] As a response to these concerns, and also motivated by scientific interest, many researchers are focusing on understanding the interactions between nanomaterials and biological systems ranging from model systems,[30-41] to bacteria,[40,42-45] to whole organisms.[46-48]

Given the ubiquity of interfaces in environmental and biological systems and the ever rising concentrations of engineered nanomaterials in the environment, the interface between nanomaterials and biological systems (the "nano/bio interface"),[49] has gained significant attention.[10,26,31,34,36,49-56] Indeed, knowledge of the processes that occur at the nano/bio interface is critical for understanding the fate, transport, and toxicity of nanoparticles.[49] Developing a clear understanding of the fundamental interactions occurring at the nano/bio interface is nontrivial and requires knowledge of 1) the nature of the biological interface (surface charge, composition, structure, etc.), 2) the surface chemistry and physical properties of the nanomaterial, and 3) the transformations that can occur under experimental, environmental, and biological conditions.[26,53] The aim of the work outlined in this thesis is motivated by these questions and focuses on developing a molecular-level view of the nano/bio interface in order to understand the fundamental interactions that occur between nanomaterials and biological systems.

1.2. Supported Lipid Bilayers as a Model for Cellular Surfaces. Upon interaction of a nanomaterial with living systems, one of the first surfaces that will be encountered is the cellular membrane which serves as a barrier to intra- and extra- cellular environments, provides structural support for, and mediates many functions, of the cell.[57] As such, many studies have focused on exploring the interactions occurring at the interface between cellular membranes, both natural and synthetic, and engineered nanomaterials.[32-35,37,40,41]

Mammalian cellular membranes are composed of lipids (phospholipids, sphingolipids, and sterols), proteins, and carbohydrates (glycoproteins and glycolipids).[58] Several hundred different types of lipids exist in a single cellular membrane, and, depending on the type of cell,[57] the composition or distribution of the principal components varies.[59] To circumvent the complex nature of cellular membranes, biomimetic systems like supported lipid bilayers (SLBs) are often used in the study of processes occurring on the cellular level,[60-66] including cell-cell interactions,[67] immune recognition processes,[60] and nano-bio interactions.[10,26,32-35,37,38,40,49,68,69] SLBs are advantageous model systems because they allow for the assessment of the fundamental role that various cellular components play in mediating nano-bio interactions.[37] Moreover, SLBs can be easily formed on SiO_2 via the vesicle fusion method, allowing for more controlled interaction studies, and are amenable to a number of surface techniques.[61,70,71] Other biomimetic systems that are used include small ($d < 100$ nm),[35,65] large ($d > 100$ nm),[39,72] and giant ($1 < d < 100$ μm)[65,73-75] unilamellar vesicles, suspended lipid membranes,[38,76,77] lipid monolayers,[41,75,78-80] and supported vesicle layers.[37,58] Due to the advantages described above, the present work, outlined in Chapters 2–6, focuses exclusively on SLBs as models for cellular membranes.

Typically, SLBs are formed on glass,[81,82] SiO_2,[31,32,34,69,83-88] and mica,[87,89] but TiO_2,[87,90,91] Al_2O_3,[87,92] noble metals,[93-95] and polymer cushions[96-102] can also serve as suitable substrates.[58,83] Although SLBs do not capture all of the properties of cellular membranes, SLBs have been shown to mimic the lateral mobility,[60] gel-to-liquid phase transition[63] and cellular functionality, under some conditions,[62] of natural cellular membranes.

Zwitterionic phosphatidylcholine (PC) lipids, with varying degrees of saturation and acyl chain lengths, can account for as much as 50% of the lipids comprising most eukaryotic cellular membranes,[103] motivating our use of PC lipids. Overall, the surface charge of the cellular

membrane is dictated by the presence of anionic phospholipids, such as phosphatidylserine (PS), phosphatidylglycerol (PG), and phosphatidylinositol (PI), which are typically localized in the cytosolic leaflet (on the interior of the cell).[104] While PG lipids are more abundant in bacterial membranes, PG lipids are also present in mammalian cells[105] where they play a critical, yet not well understood, role in neonatal development[106] and mitochondrial electron transport chain.[107] Given that many of the systems explored in this thesis employ PC lipids, the findings from these studies can potentially provide information about interactions occurring in PC-rich cellular membranes and thereby may be applied to a broad range of cellular membranes. (See Scheme 1.1 for a summary of the chemical structures relevant to this thesis).

1.3. Factors Governing Interactions Occurring at Biological Interfaces. In addition to the complexity introduced by the diverse and dynamic surface of cellular membranes, the physical properties of the nanomaterial also play a critical and complicated role in the interactions at the nano/bio interface and their subsequent biological and environmental fate.

Some of these physical properties include size, shape, surface charge, morphology, and surface functionalization (through ligands, coatings, and covalent linkages), all of which can be strategically tuned to achieve a desired function.[49,108,109] In biologically- and environmentally-relevant matrices, nanomaterials can undergo physical and chemical transformations (ex. dissolution, aggregation, redox chemistry, corona formation, etc.) that are dictated by solution conditions such as pH, ionic strength, temperature, and the presence of ions, proteins, and other biomacromolecules.[42,49,110,111]

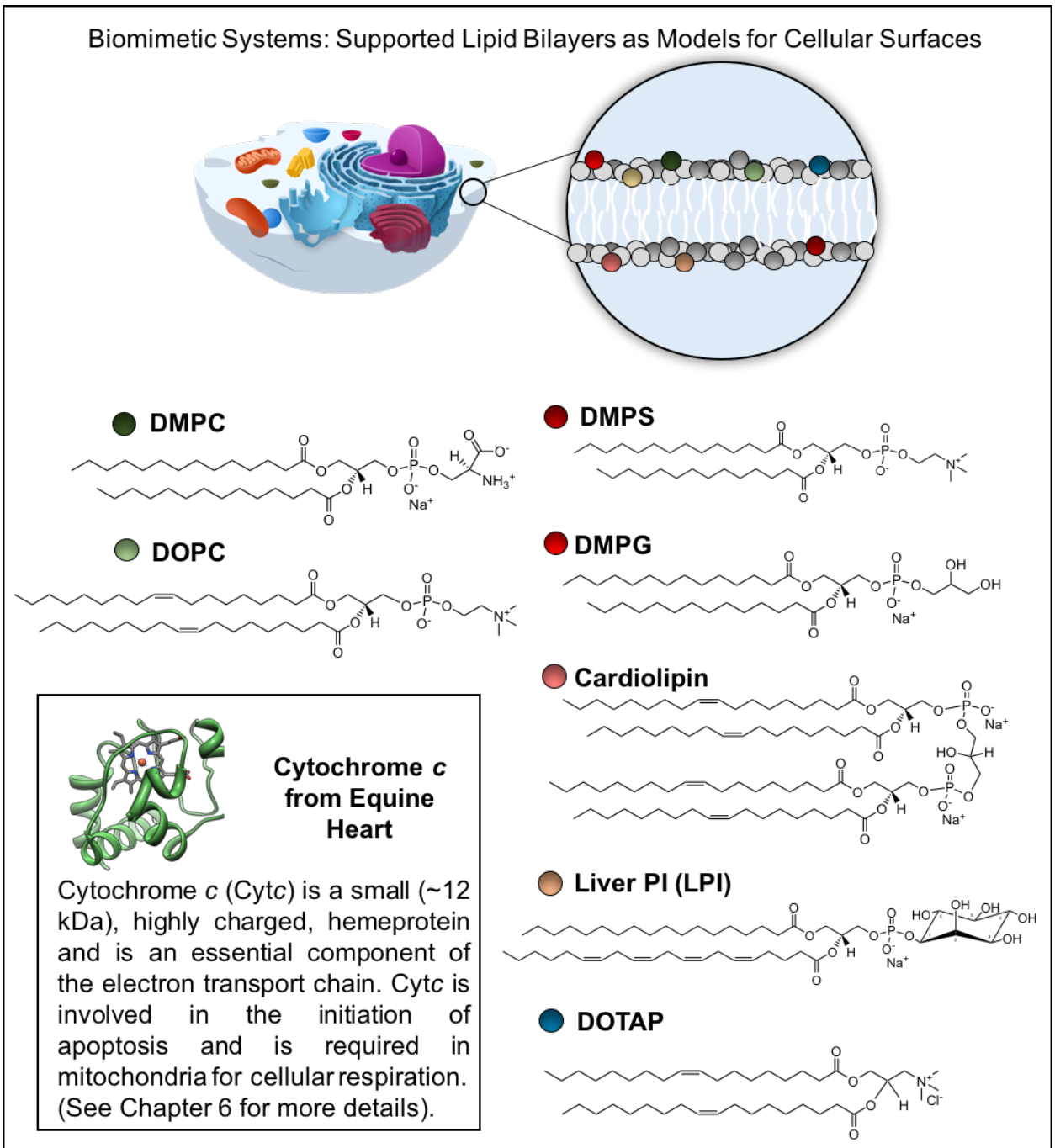

Scheme 1.1. Illustration of eukaryotic cell and model lipid bilayer (excludes other components (sterols, proteins, etc.), and summary of lipid chemical structures relevant to the studies discussed in this thesis. Supported lipid bilayers (SLBs) are used, herein, as models for cellular surfaces and are exclusively comprised of lipids. DMPC and DOPC are zwitterionic lipids, DMPS, DMPG, Cardiolipin, and Liver PI are anionic lipids, and DOTAP is a cationic lipid (typically used in transfection). Cytochrome c structure (https://commons.wikimedia.org/wiki/File:Cytochrome_c.png) and illustration of a eukaryotic cell (https://commons.wikimedia.org/wiki/File:Animal_Cell.svg#filelinks) are labeled for noncommercial reuse.

1.3.1. Surface Charge Density. Among the many tunable characteristics aspects of the nanoparticle surface are tunable, the surface charge can be easily modified through the use of coatings, ligands, polymers, and surface functionalization.[4,111,112] Through strategic modification of the surface charge and functionalization, some nanomaterials become less prone to aggregation,[113,114] demonstrate lower toxicity,[115] and become more photostable.[116] One of the most widely-studied cationic, linear polymers used for the functionalization of nanomaterials is poly(allylamine hydrochloride) (PAH).[33,35,40,117-126] Previous studies have shown that both PAH[127] and nanomaterials functionalized with PAH can be disruptive to model cellular membranes[35] and can be toxic to both bacteria[45,128,129] and whole organisms. Other studies comparing the toxicity of gold nanoparticles functionalized with PAH and another cationic polymer suggest that the chemical functionality of the ligand is also important in determining toxicity. Due to the importance of these physical properties, surface charge and charge density are motifs of this thesis, as we aim to not only understand the role of surface charge in driving these interactions, but also to quantify these important electrostatic parameters.

1.4. Tools for Probing Nanomaterials, Biological Surfaces, and the Nano/Bio Interface. The solid/water interface is difficult to access experimentally, mainly because traditional methods used to probe this interface do not provide molecular information, are not interface-specific, or are not sensitive enough to detect small numbers of oscillators on a surface, even at monolayer coverage.[130] As a result, the amount of reported molecular information regarding how nanoparticles interact with aqueous/solid interfaces, including biological membranes, is limited. Therefore, there exists therefore an urgent need to bridge this knowledge gap by probing the nano/bio interface with new tools.[49,130]

1.4.1 Fluorescence Techniques. Fluorescence microscopy is a powerful technique for the study of biological systems and nano/bio interactions because it is versatile and molecularly specific. One disadvantage of fluorescence-based approaches is that they often require the use of fluorescent labels which can increase the complexity of the system and interact differently with the surrounding environment than unlabeled lipids.[65,131,132] Yet, techniques such as fluorescence recovery after photobleaching (FRAP), fluorescence correlation spectroscopy, and experiments taking advantage of Förster resonance energy transfer,[133,134] have been invaluable in the study of interfacial processes[135,136] and elucidating the mechanism by which nanomaterials interact with biological systems.[137] Innately fluorescent nanomaterials, namely N_v-centered nanodiamond, carbon[65,138] and quantum dots, and gold nanoparticles, allow for a label-free method by which these interactions could be investigated, as well. In Chapter 4, we use the two-dimensional diffusion coefficients of SLBs determined in FRAP to assess their quality.

1.4.2. Optical and Acoustic Mass Sensors. Surface plasmon resonance (SPR) is a widely–used approach that reports on binding kinetics and thermodynamics, provides quantitative mass sensing, and does not require the use of electrochemical or spectroscopic labels.[130,139,140] SPR can also be done in real-time and with high sensitivity (~pg/mm^2).[139] Optical mass sensors based on localized surface plasmon resonance (LSPR) principles have been used to provide estimates for adsorbed analyte mass. Quartz-crystal microbalance with dissipation monitoring (QCM-D), is an acoustic mass sensor that is based on the piezoelectric properties of quartz crystals.[130] QCM-D, like SPR and LSPR, can be used to estimate not only the mass (hydrated mass which is the sum of the adsorbate mass and dynamically coupled solvent) associated with an adsorption event, but QCM-D also the viscoelastic properties of the adsorbing species. When QCM-D and LSPR are used in concert, both the mass of the adsorbate and degree of hydration can be estimated. Such an approach

is described in Chapter 5. For an in-depth discussion of other optical mass sensors see reference [130].

1.4.3. Other Spectroscopies/Microscopies. While probing the nano/bio interface is clearly an important part of understanding nano/bio interactions, understanding the characteristics of the nanoparticle surface is essential. X-ray photoelectron spectroscopy (XPS)[141,142] and Fourier transform infrared spectroscopy (FTIR)[142] have been used to report on the chemical composition and binding. Atomic force microscopy (AFM),[141] transmission[44,142-144] and scanning[145] electron microscopies yield information on the surface morphology and size of nanoparticles and provide insight into the nature of nano/bio interactions.[10,26] Secondarily, AFM has been useful in investigating nanomechanical properties of lipid bilayers,[89] as well as in the determination of surface charge and charge densities.[146-148]

1.5. Nonlinear Optical Spectroscopic Studies of Biological Interfaces. Nonlinear optical spectroscopy is a powerful tool for the investigation of biological interfaces.[130] Second harmonic generation (SHG) spectroscopy, as a surface-selective technique, has been used to investigate the interactions of nanomaterials, polymers, and proteins, with model and actual cellular surfaces. Specifically, SHG spectroscopy has been used to provide estimates for free energies of adsorption, charge densities, kinetic information, and even structural changes induced by adsorbing species.[149] Likewise, vibrational sum frequency generation (SFG) spectroscopy has also proven to be useful in investigating the same interactions,[56] providing information about the structural integrity of model membranes and structural and organizational changes that can occur as a consequence of these interactions.[150]

As no single approach can provide a detailed and complete picture of the nano/bio interface and nano/bio interactions, we employ a combinatorial approach that uses SHG spectroscopy,

vibrational SFG spectroscopy, and QCM-D. As demonstrated in this thesis, this multi-pronged approach allows us to provide estimates for charge densities, binding equilibrium constants, free energies of adsorption, the number of adsorbed species, and degree of ionization. Complementing the insights gained from a multi-faceted experimental approach with molecular dynamics simulations allows us to not only validate our models but also to establish a critical feedback loop through which our experiments and simulations can be refined, as discussed in Chapter 5.

1.6. Scope and Organization of Thesis. Broadly, this thesis focuses on understanding the fundamental interactions occurring between nanomaterials and polyelectrolytes which are commonly used to functionalize nanomaterials, and model cell membranes. Throughout this thesis, under a unifying motif of assessing the role of charge and charge density in nano/bio interactions, we apply SHG spectroscopy to the study of charged nanomaterials and free ligands for reasons outlined below. In addition to SHG, we employ a number of other analytical tools for the characterization of model membranes and nanoparticle surfaces, and towards building our understanding of nano/bio interactions.

This thesis specifically explores and addresses the following scientific questions:

1. Can we quantify, in terms of thermodynamics and electrostatics, the interactions occurring between carbon-based nanomaterials and model biological systems? Secondarily, how do the properties (composition, phase, etc.) of the model biological system and charge density of the material influence these interactions?
2. How can our experimental approach for evaluating nano/bio interactions be extended to polyelectrolytes (charged polymers) with various chemical functionalities?
3. How do the properties, primarily degree of ionization, of the polyelectrolyte change upon adsorption to model biological surfaces?

With these scientific questions in mind, this thesis is outlined as follows:

To facilitate the understanding of subsequent chapters, Chapter 2 provides a brief outline of the theory of SHG spectroscopy accompanied by a discussion of electrical double layer and adsorption models used in Chapters 3–5. Chapter 2 also includes experimental details and protocols that are common across Chapters 3–5. Building on the experimental foundation developed in Chapter 2, Chapters 3–6 discuss a combination of approaches for studying the interactions between nanoparticle and relevant-ligands and model biological interfaces as discussed further below.

Work discussed in Chapter 3 describes a combinatorial approach (SHG, QCM-D, and SFG) to investigate the role of surface charge in the interactions between oxidized multi-walled carbon nanotubes with varying degrees of oxidation, and SLBs. In Appendix 1, the application of SHG to the interactions of various carbon-based nanomaterials and SLBs is also presented.

Chapters 4 and 5 focus on extending on an approach used previously for PAH interacting with an SLB surface.[69] Given the important role that ligands can play in dictating the outcome of nano/bio interactions, a portion of this thesis focuses on specifically understanding the interplay between the uncoupled ligand (i.e. free polymer) and model biological surfaces. Chapter 4 discusses the quantification of a suite of polyelectrolytes with varying functionalities so as to explore 1) the robustness of this approach to describe a variety of polyelectrolytes and 2) the role of chemical functionality in the formation of more complex nanoarchitectures. Specifically, charge densities of cationic polymers adsorbed to lipid bilayers are estimated from SHG spectroscopy and QCM-D measurements.

Building on the insights developed in Chapter 5 we couple our previously established method with optical mass measurements from LSPR experiments and atomistic molecular

dynamics simulations. Through a strategic choice of oligomers of lysine and arginine, that exist within the length-scale accessible to our current computational framework, the insights gained in Chapter 5 are maximized by an overlap between experimental and computational insights. Further, minimizing the length-scale differences across experimental and computational studies aids in addressing the need to develop a feedback loop that informs on the modeling and simulation of experimental data and the interpretation of experimental results. Finally, Chapter 6 outlines our progress towards developing more representative and complex model biological systems. All of the work described in this thesis is in collaboration with the Center for Sustainable Nanotechnology, a National Science Foundation funded Center for Chemical Innovation.

CHAPTER 2

Theoretical Foundation of Second Harmonic Generation Spectroscopy Experiments

Portions of this chapter are reproduced with permission from the American Chemical Society and the Royal Society of Chemistry:

McGeachy, A. C.; Dalchand, N.; Caudill, E. R.; Li, T.; Dogangun, M.; Olenick, L. L.; Chang, H.; Pedersen, J. A.; Geiger, F. M., Interfacial Electrostatics of Poly(vinylamine hydrochloride), Poly(diallyldimethylammonium chloride), Poly-L-lysine, and Poly-L-Arginine Interacting with Lipid Bilayers. *Phys. Chem. Chem. Phys.* 2018, **20**, 10846-10856.

McGeachy, A. C.; Olenick, L. L.; Troiano, J. M.; Lankone, R. S.; Melby, E. S.; Kuech, T. R.; Ehimiaghe, E.; Fairbrother, D. H.; Pedersen, J. A.; Geiger, F. M., Resonantly Enhanced Nonlinear Optical Probes of Oxidized Multiwalled Carbon Nanotubes at Supported Lipid Bilayers. *J. Phys. Chem. B* 2017**, 121**, 1321-1329.

2.1. Second Harmonic Generation Spectroscopy (SHG) Theory. SHG is a coherent second-order nonlinear optical process in which two photons with frequency ω combine to form a single photon with frequency 2ω. As an even-order nonlinear optical process, and within the electric dipole approximation, SHG is forbidden in media in which the length of centrosymmetry extends further than the coherence length of the SHG process.[1-4] However, at the interface between two phases, inversion symmetry is broken, resulting in an observable SHG signal.[2,3] Consequently, SHG spectroscopy provides molecular-level resolution and surface selectivity.[4-9] As such, SHG spectroscopy is a particularly useful tool to study biological interfaces,[10-15] as the surface selectivity of the technique is higher than that of fluorescence or absorbance methods and can be conducted *in situ* and under ambient conditions that are biologically relevant.[8]

2.1.1. SHG: An Optical Voltmeter. The so-called $\chi^{(3)}$ method (or Eisenthal $\chi^{(3)}$ method)[16-18] is a non-resonant variant of SHG which has been used previously to probe interfacial adsorption processes of various species including ions,[6,11,19-22] proteins,[18,23,24] nanoparticles,[25-27] and polymers.[13,15] The SHG signal intensity, I_{SHG}, from charged interfaces is directly proportional to the electric field generated at the second harmonic as shown in Equation 2.1:

$$\sqrt{I_{SHG}} \propto E_{SHG} \propto \chi^{(2)} E_{\omega} E_{\omega} + \chi^{(3)} E_{\omega} E_{\omega} \int_{0}^{\infty} E_{dc}(z) e^{i\Delta k_z z} dz \qquad 2.1$$

where $\chi^{(2)}$ and $\chi^{(3)}$are the second- and third-order nonlinear susceptibility tensors, E_{SHG} is the electric field generated at the second harmonic, $E_{\omega}$is the incident electric field oscillating at the fundamental frequency (600 or 800 nm), E_{dc} is the z-(depth) dependent electric field produced by any interfacial charges,[28-30] and Δk_z is the inverse of the coherence length of the SHG process.[29,31-33] Integration yields the interfacial potential, Φ_0, making the method useful as what is now termed an "optical voltmeter" for label-free probing of charged interfaces.[4,5,16,17,34-40] As illustrated in

Equation 2.1, the $\chi^{(2)}$ term, which is attributable to the molecular hyperpolarizability of aligned species, is independent of the interfacial potential generated by the charged surface. The $\chi^{(3)}$ term is directly influenced by the interfacial potential and is related to the polarization and orientation of water molecules that align as a consequence of the electric field generated by the charged interface.[10,17,18]

Under some conditions, particularly in experiments with lower ionic strengths (< ~ 0.001 M), phase matching becomes important.[29] The increased importance of the phase matching term at lower ionic strengths is a consequence of the dispersion between the fundamental and second harmonic when the Debye length (κ^{-1}) is long compared to the wavevector mismatch[30] ($\Delta k = 2k_1 - k_2$) for the SHG process where k_1 and k_2 are wavevectors associated with the momenta of the fundamental and second harmonic fields.[41] In the reflection geometry employed here, and under the constant total electrolyte concentration of 0.1 M used here, Δk_z is of such a magnitude that the SHG signal is produced close to the interface, minimizing the effect of phase matching.[1,10,16,29] But, for a more rigorous discussion of the importance of phase matching under other experimental conditions, see references [16], [17], and [18].

As shown in Equation 2.1, and assuming that E_ω, $\chi^{(2)}$ and, $\chi^{(3)}$ remain constant, and Φ_0 is $\int_0^\infty E_{dc}(z)e^{i\Delta k_z z}dz$, Equation 2.1 can be rewritten as Equation 2.2 where E_{SHG} is proportional to Φ_0, A and B are constants specific to the system that contain the second- and third-order nonlinear susceptibility tensors, respectively, and the incident electric field oscillating at 600 or 800 nm.[10,15]

$$E_{SHG} \propto P_{2\omega} \propto A + B\Phi_0 \qquad 2.2$$

Equation 2.2. illustrates the utility of SHG spectroscopy as an optical voltmeter as our signal is clearly related to the interfacial potential. However, we cannot measure the interfacial potential

directly. As such, we employ models that can be used to estimate the surface charge density and potentials, as discussed below.

2.2. Resonantly Enhanced SHG Spectroscopy. Resonantly enhanced SHG, like the $\chi^{(3)}$ technique, occurs when two photons at frequency ω combine to form a single photon at twice the frequency. Resonance enhancement arises from the increased polarizability of interfacial species when the SHG or fundamental frequencies approach the resonant frequency of a molecular electronic transition. When an adsorbate has an accessible electronic transition, E_{SHG} is dependent on the second order nonlinear susceptibility, $\chi^{(2)}$, as shown in Equation 2.3.[8,19]

$$E_{SHG} \propto \sqrt{|\chi^{(2)} E_{\omega} E_{\omega}|^2} \tag{2.3}$$

The second order susceptibility is the sum of both resonant and nonresonant contributions as demonstrated in Equation 2.4.[8,19]

$$E_{SHG} \propto \sqrt{\left|\chi_{NR}^{(2)} + \chi_{R}^{(2)} e^{i\Delta\phi}\right|^2} \tag{2.4}$$

Here, $\chi_R^{(2)}$ and $\chi_{NR}^{(2)}$ represent the resonant and nonresonant components, respectively, with ϕ being the phase factor between the two contributions. The resonant contribution, $\chi_R^{(2)}$ relates directly to the number of interfacial species in resonance, N, and the second-order orientational average of the hyperpolarizability tensor, $\left\langle \ddot{\alpha}^{(2)} \right\rangle$ (Equation 2.5)[10]

$$\chi_R^{(2)} = N\langle \vec{\vec{\alpha}}^{(2)} \rangle \tag{2.5}$$

where

$$\overleftrightarrow{\alpha}^{(2)} \propto \frac{A}{\omega_{ca} - 2\omega + i\Gamma} \quad 2.6$$

and A is the oscillator strength, Γ is the spectral linewidth, and ω_{ca} is the resonant frequency of an electronic transition. As indicated by Equations 2.5 and 2.6, as the fundamental or SHG wavelengths (2ω) approach ω_{ca}, $\chi_R^{(2)}$ becomes larger.[42] Adding to the interfacial sensitivity of the SHG process, within the electric dipole approximation, only species oriented at the interface contribute to $\chi^{(2)}$.

2.3. Modeling Interfacial Adsorption Processes. As described extensively in the literature, second harmonic generation $\chi^{(3)}$ measurements can provide useful information about binding thermodynamics and electrostatics.[10,15,28,30,33] Combining surface complexation models (i.e., Gouy-Chapman or triple layer)[4,7] and adsorption models like the Langmuir or Hill isotherms (*vide infra*) allows us to quantify the interactions between adsorbates and supported lipid bilayers under investigation in this thesis. Specifically, the approach enables us to estimate charge densities, equilibrium constants, and ultimately free energies of adsorption.

2.3.1. Surface Complexation Models. The Gouy-Chapman (GC) model, mathematically described in Equation 2.7, is commonly used to describe the electrical double layer that forms as a consequence of a charged surface. (Figure 2.1).

$$\sigma = \sqrt{8\varepsilon_0\varepsilon_r IRT}\sinh\left(\frac{zF\Phi}{2RT}\right) \quad 2.7$$

Here, σ is the charge density with units of $\frac{C}{m^2}$, ε_0 is the permittivity in free space with units of $\frac{C^2}{Jm}$, ε_r is the relative permittivity which is unitless, I is the ionic strength with units of $\frac{mol}{L}$, R is the gas constant with units of $\frac{J}{mol\ K}$, T is the temperature with units in K, z is the valency of the screening

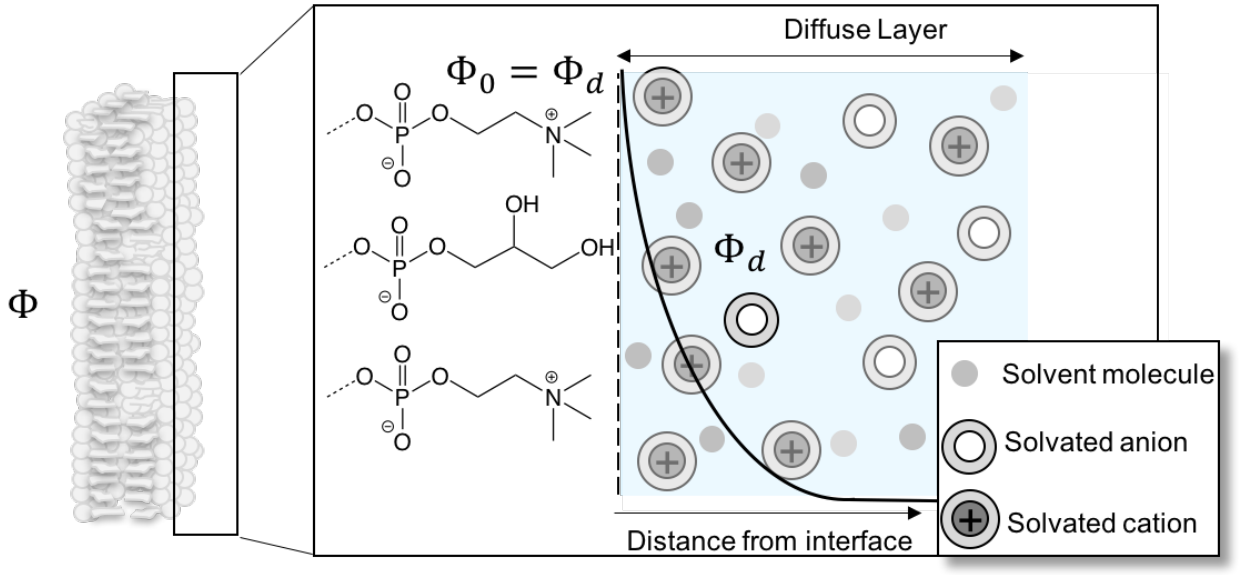

Figure 2.1. Illustration of Gouy-Chapman model. According to this model, the interfacial potential decreases exponentially from the surface out into the bulk. Further, the potential at the planes of the zero- and diffuse- planes are equal. Here, the supported lipid bilayer/SiO_2 surface carries a charge dictated by the chemistry of the phospholipid headgroups and environmental conditions.

ion (assuming a symmetric 1:1 electrolyte), and F is the Faraday constant with units of $\frac{C}{mol}$. Assuming the above constants (at T = 293 K) and a monovalent electrolyte, the known terms can all be combined to yield the following:[43,44]

$$\sigma = 0.1175\sqrt{I}\sinh(19.8\Phi) \quad 2.8$$

Rewriting Equation 2.8 and solving for Φ instead of σ yields:

$$\Phi = 0.0505\times \sinh^{-1}\left(\frac{8.5\sigma}{\sqrt{I}}\right) \quad 2.9$$

The interfacial region is generally considered to be comprised of three planes: the zero plane, the β-plane, and the diffuse plane. The zero plane is the surface of the supported lipid bilayer or silica substrate. The charge density at the zero plane, σ_0, and associated interfacial potential, Φ_0, are determined by the phospholipid composition (zwitterionic, anionic, and/or cationic, and degree of unsaturation) and environmental conditions (pH, temperature, ionic strength, etc.).[45] It should be noted that the charges associated with the lipid headgroups can be different distances from a given reference plane and as such, the surface is not exactly planar.[46] Thus this region is a planar approximation of the SLB surface charges. The β-plane is comprised of specifically adsorbed ions that counter the charge of the SLB and carries its own charge density, σ_β, and associated interfacial potential, Φ_β. Lastly, the diffuse plane contains counter-balancing ions that carries a charge density of σ_d and associated interfacial potential, Φ_d.

In the GC model it is assumed that the electrostatic potential is equivalent at the zero and diffuse planes ($\Phi_0 = \Phi_d$) and that Φ decreases exponentially into the bulk. In the diffuse layer, counterions (ions having the opposite charge than the charge of the surface) are held some distance away from the surface and the mobility of these ions is taken into account.[47] But the diffuse layer does not only contain counterions, co-ions are present as well. It is in the diffuse plane, then, where

the total potential drop occurs.[48] These assumptions are based on the idea that a subset of counterions will escape the attractive forces imposed by the charged interface, while a subset of co-ions will occupy a space closer to the charged surface, thereby balancing attractive and equilibrium forces. It is also assumed that these charged species that comprise the diffuse layer can be treated as point charges.

Equations 2.2 and 2.9 can be combined to yield Equation 2.10 which is used to relate SHG signal to surface charge density:

$$E_{SHG} \propto A + 0.0505 \times B \left\{ \sinh^{-1} \left((\sigma\theta) \left(\frac{8.5}{\sqrt{C_{elec}}} \right) \right) \right\} \qquad 2.10$$

where A and B are assumed constants related to the interface as discussed above, C_{elec} is the electrolyte concentration, including contributions from buffering agents and with units of molarity ($\frac{mol}{L}$), σ is the total charge density of the interface, and θ is the fractional surface coverage, the relevance of which is discussed below.

While the GC model has been used to describe the electrical double layer at charged interfaces, and at supported lipid bilayers in particular,[46,49-51] in Chapter 4, we also apply the triple layer model (or Gouy-Chapman-Stern model) to describe the electrical properties of the interface. Generally, the triple layer model is used because it is more versatile as it can be used over a broader range of ionic strengths and with a wider class of analytes.[52] In this model, the total charge is composed of two parts: the charge generated by ions held close to the surface and a diffuse layer. The ions held close to the charged surface are held by electrostatic forces and specific adsorption potential which is ion dependent. The latter is sometimes neglected.[48]

The electrical triple layer model can be summarized, mathematically, as shown in Equation 2.11:

$$\Phi_0 = \frac{\sigma_0}{C_1} + \frac{\sigma_\beta + \sigma_0}{C_2} + \Phi_d \quad 2.11$$

where $C_1$and $C_2$are the capacitances in the zero and β planes, σ_0 is the surface charge density of the zero plane, σ_β is the charge density at the β-plane, Φ_0 is the interfacial potential at the zero plane (surface), and Φ_d is the potential of the diffuse plane. It is assumed that Φ_d decays according to the Gouy-Chapman theory as discussed in the previous section (Figure 2.2). The charge densities sum to zero for charge neutrality.

In many studies of mineral surfaces, C_2, which is the capacitance of the diffuse layer, is typically assigned a value of 0.2 F/m^2.[7,52-54] We have previously shown in a study of trivalent metal cations adsorbing to fused silica that varying the value of C_2 by as much as 50% around 0.2 F/m^2 had no appreciable impact on model results.[20] Contextually, the width of the electrical double layer can be estimated from the differential capacitance which is defined as follows: $C = \frac{d\sigma}{d\Phi}$. At sufficiently small potentials, C can be approximated as $\frac{\varepsilon_0 \varepsilon_r}{\lambda_D}$ where $\lambda_D$is the Debye-Hückel screening length.[47,55] Following this approximation and assuming that there is a constant relative permittivity (ε_r) equaling that of bulk water (80.1), C_2 can vary from 0.07 F/m^2 at low ionic strengths (0.001 M) to 0.7 F/m^2 at biologically-relevant ionic strengths (~0.1 M). There are some shortcomings with the triple layer model as well, one of which is that the dielectric permittivity is constant throughout the entirety of the double layer.[56] Yet, the value of the dielectric permittivity close to the charged interface is lower than that of bulk water[57] and varies as a function of distance from the surface.[58] The implications of the permittivity constant used in estimating interfacial potential is discussed further in Chapter 5.

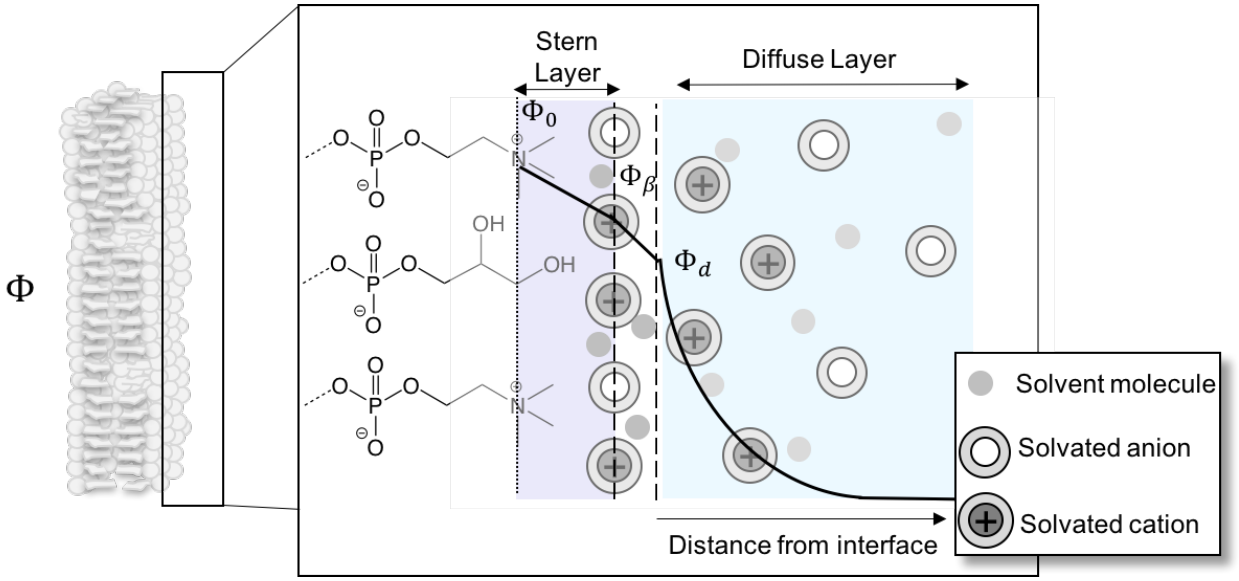

Figure 2.2. Illustration of triple layer model which consists of three planes: zero, β, and diffuse planes. Here, the supported lipid bilayer/SiO_2 surface carries a charge (σ_0) and interfacial potential, Φ_0 which are dictated by the lipid composition and experimental conditions. The β plane is comprised of specifically adsorbed ions with an interfacial potential of Φ_β and charge density, σ_β. The interfacial potential is described with a constant capacitance approach between the zero and β plane, and the β diffuse planes with capacitances of C_1 and C_2, respectively. Lastly, the outermost plane is the diffuse plane, Φ_d which decays exponentially in accordance with the Gouy-Chapman model.

Considering that the charge density is modulated by surface coverage, θ, we can combine Equations 2.2, 2.8, and 2.11 and arrive at a triple layer expression for the SHG response (Equation 2.12).

$$E_{SHG} \propto A + B\left\{\frac{\sigma_{ads}}{C_2}\theta + \frac{2k_BT}{ze}\sinh^{-1}\left((\sigma_0 + \sigma_{ads}\theta)\left(\frac{8.5\ M^{1/2}m^2C^{-1}}{\sqrt{M + C_{elec}}}\right)\right)\right\} \qquad 2.12$$

where $\sigma_0$is the charge density of the substrate, σ_{ads} is the charge density of the adsorbate at monolayer coverage, M is the bulk adsorbate concentration in $\frac{mol}{L}$, and C_{elec} is the background electrolyte concentration (which includes contributions from buffer (0.008 M for Tris or 0.003 M for HEPES) in $\frac{mol}{L}$.

2.3.2. Adsorption Models. As briefly discussed above, the surface charge density is modulated by surface coverage. Therefore, we need to introduce a model that can be used to relate surface coverage to adsorbate concentration. The Langmuir adsorption model describes the reversible adsorption of a species to a homogeneous, flat surface.[59,60] Additionally, it assumes that lateral interactions between adsorbed species occupying adjacent sites do not occur and that all binding sites are equivalent. The model takes the form of $\theta = \frac{K_{ads}M}{1+K_{ads}M}$ where θ represents the fractional surface coverage, K_{ads} is the apparent equilibrium constant of adsorption, and M is the bulk adsorbate concentration. In an extension of the Langmuir model, the Hill model[61] accounts for intramolecular coupling (i.e. change in binding affinity at one site in response to binding at another site). The Hill model takes the form $\theta = \frac{K_{ads}^n M^n}{1+K_{ads}^n M^n]}$.[61,62] The Hill-coefficient, n, describes cooperativity. If $n > 1$, the adsorption process is cooperative and as the concentration of adsorbate increases, the binding affinity increases. Conversely, when $n < 1$, the process is typically described

as being anti-cooperative, and increasing adsorbate concentrations at the interface reduces the binding affinity. The interpretation of cooperativity solely based on the experimentally determined Hill coefficients is problematic. For example, adsorption to heterogeneous surfaces can also result in artificially low n values[63,64] while electrostatics and reductions in dimensionality can explain high values for n.[62] When n is equal to unity, the Hill model reduces to the Langmuir model.

2.3.3. Estimating Thermodynamic Parameters from SHG Spectroscopy. Combining Equation 2.11 with the Hill equation, we arrive at Equation 2.13.

$$E_{SHG} \propto A + B \sinh^{-1}\left(\left(\sigma_0 + \sigma_{ads}\left(\frac{K_{ads}^n M^n}{1 + K_{ads}^n M^n}\right)\right)\left(\frac{8.5\, M^{1/2} m^2 C^{-1}}{\sqrt{M + C_{elec}}}\right)\right) \qquad 2.13$$

It is important to note that in our earlier work[15, 19, 25, 26] we incorrectly used a combination of cgs and SI units which is the reason that Equation 2.7 has been written with 30.2 instead of 8.44 used herein. These models are used in the analysis of SHG adsorption isotherms in Chapters 3-6. The apparent equilibrium constant, K_{ads}, can be used to calculate an apparent free energy of adsorption.

2.4. SHG Laser System and Procedures.

2.4.1. Laser System. SHG spectroscopy measurements discussed in Chapters 3-6 was conducted with the output from a Ti:sapphire laser system (Hurricane, Spectra-Physics, 800 nm, 120 fs pulses at a repetition rate of 80 MHz). The power is attenuated using a variable density filter down to 0.50 ± 0.05 W, and the beam is directed through a longpass filter to remove residual 400 nm light from the oscillator. The output beam from the oscillator is split, and part of the beam is used to continuously monitor the power over the course of the SHG experiment using a power meter (Newport 1917-R) to correct the SHG signal for any drifts in power. The transmitted 800 nm beam is focused on the fused silica/water interface at an incident angle of ~60° from the surface normal, less than the angle of total internal reflection. The fundamental 800 nm light is recollimated and

then filtered using a 400 nm bandpass filter (FBH400-40M ThorLabs, >90% peak transmission) and a monochromator tuned to the SHG wavelength (400 nm), as described earlier.[33] The SHG light is then directed into a photomultiplier tube where the signal is amplified and collected by a gated photon counter (Stanford Research Systems). The polarization combination used is *s*-in/all out.

In one set of experiments discussed in Chapter 3, a regeneratively amplified Ti:sapphire laser system (Hurricane, Spectra-Physics) provides 120 femtosecond pulses at a repetition rate of 1 kHz to an optical parametric amplifier (OPA-CF, Spectra-Physics) which is tuned to a fundamental wavelength between 570-610 nm. A variable density filter is used to attenuate the energy of the 120 femtosecond pulses to 0.40 ± 0.05 μJ/pulse, translating to a pump fluence of approximately 60 mJ/cm^2, to avoid thermal degradation of the sample and/or bilayer. The incident beam is focused to a 30 μm focal spot, at an angle just below the angle of total internal reflection, onto a silica/water interface containing an SLB. The reflected fundamental light is selectively filtered out through the use of a Schott filter and a monochromator tuned to the SHG wavelength. Here again the SHG light is then directed into a photomultiplier tube where the signal is amplified and collected by a gated photon counter.

2.4.2. Sample Cell, Flow System, and Substrate Preparation. SHG spectroscopy flow experiments were carried out using a home-built Teflon flow-cell and a fused silica hemispherical lens (ISP Optics, 1-in diameter, QU-HS-25-1) (Figure 2.3) that has been previously described.[12,15,25,26] The flow cell has an internal volume of ~3 mL. Our Teflon flow-cell, three-way valve, and all connected components, including tubing (PTFE tube (1/16”) and Swagelock fittings, were sonicated in methanol (~30 min) prior to each experiment. The flow-cell was then rinsed with copious volumes of Millipore water and then dried under nitrogen and oxygen plasma cleaned

(Harrick Plasma Cleaner, 18W, 300-500 mTorr) for 10 minutes. Prior to use, the tubing was flushed with Tris buffer solution. The PTFE-tubing was changed frequently to avoid contamination and cleaned with methanol, Millipore water (>18 MΩ), and buffer before reuse.

Hemispherical lenses were cleaned with Nochromix® for at least 1 hour and then rinsed with Millipore water. The hemispherical lenses were then transferred to a beaker containing fresh methanol and sonicated for 10 minutes, rinsed with Millipore water, and dried under N_2. Lastly, the hemispherical lenses were plasma cleaned for 10 minutes. As various methods were used for the formation of SLBs, the specific methods used for their formation is described in the respective chapters. All experiments, except where explicitly stated otherwise, are carried out under intermittent flow conditions as described in the subsequent chapters.

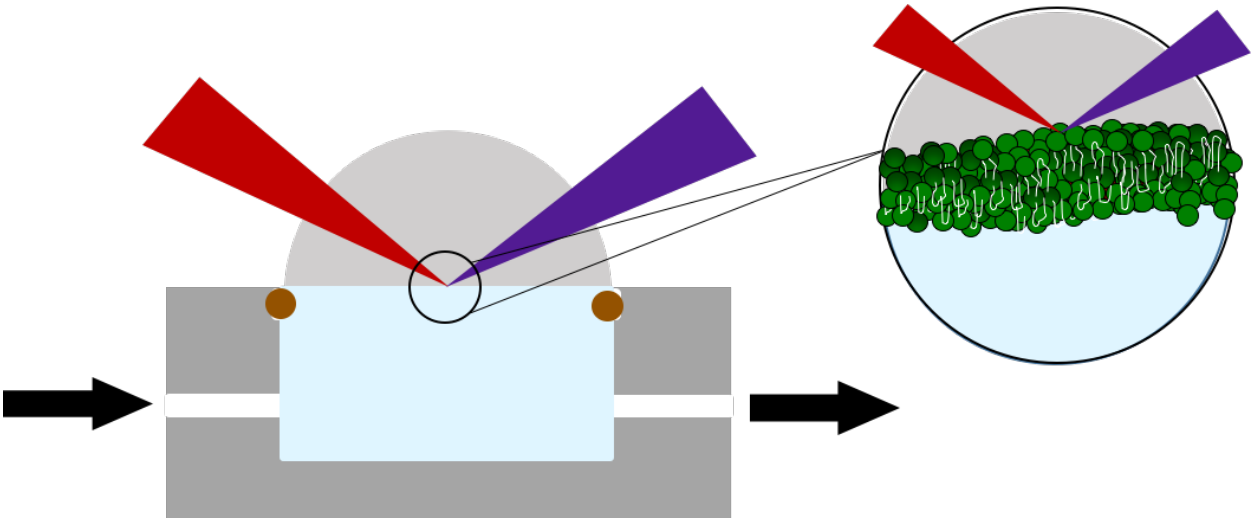

Figure 2.3. Cross-sectional view of the home-built Teflon flow cell used for second harmonic generation sepctroscopy experiments. Fundamental light is shown in red, while SHG is shown in purple. Arrows indicate flow into and out of the cell *via* PTFE tubing (omitted for clarity). The flow cell is capped with a fused silica hemispherical lens and a leak-tight seal is created with the use of an O-ring (shown in brown). (Inset) Zoomed in view of the solid/water interface where the supported lipid bilayer is formed.

CHAPTER 3

Resonantly Enhanced Nonlinear Optical Probes of Oxidized Multiwalled Carbon Nanotubes at Supported Lipid Bilayers

Portions of this chapter are reproduced with permission from the American Chemical Society:

McGeachy, A. C.; Olenick, L. L.; Troiano, J. M.; Lankone, R. S.; Melby, E. S.; Kuech, T. R.; Ehimiaghe, E.; Fairbrother, D. H.; Pedersen, J. A.; Geiger, F. M., Resonantly Enhanced Nonlinear Optical Probes of Oxidized Multiwalled Carbon Nanotubes at Supported Lipid Bilayers. *J. Phys. Chem. B,* 2017, **121**, 1321-1329.

3.1. Introduction. As a first test system for probing the nano-bio interface with nonlinear optics, we focused on carbon nanotubes (CNTs), as they have actual and proposed applications in consumer product areas including optics,[1,2] electronics,[3,4] biomedicine,[5] drug delivery,[6-9] environmental remediation[10-14] and energy technologies.[15,16] Applications and technologies that do not require specific chirality, diameters, or bandgaps often favor multiwalled CNTs (MWCNTs) over single walled carbon nanotubes because of the much lower cost and relative ease of production of MWCNTs.[17] The projected increase in the use of CNT-based nanomaterials, however, raises concern about the potential adverse impacts new technologies utilizing these materials may have on the environment.[18-26] Consequently, the possibility of environmental release of engineered nanomaterials in general,[19,27] and MWCNTs in particular, and their subsequent interaction with biological systems have motivated laboratory studies aimed at exploring how nanomaterials interact with biologically relevant systems of varying complexity,[26,28,29] including idealized model systems consisting of phospholipid membranes.[23,30-35] Several studies have indicated that CNTs may penetrate biological membranes, traverse the cell membrane, or may lead to alterations in cellular function, including death.[36-43]

In the environment, CNT surfaces are likely to contain oxygen-bearing functional groups.[44,45] Oxidized MWCNTs (O-MWCNTs) may thus represent a more realistic model system for studying the biogeochemical consequences of CNT release into the environment than pristine (unoxidized) CNTs.[46,47] Oxygen-containing functional groups are either grafted deliberately into the CNT sidewalls during covalent functionalization strategies or inadvertently as a result of exposure to oxidizing conditions.[48-50] The presence of oxygen-containing functional groups on CNTs increases their hydrophilicity[51,52] and stability in aqueous solutions.[44,53-55] Although concentrations of O-MWCNTs in the environment have yet to be determined, current

estimates based on a number of parameters including production rates suggest that CNT concentrations may be as high as several μg per kg of soil.[56] On the other hand, field experiments with natural benthic communities show that 2 mg of MWCNTs per kg aquatic sediment induced detectable changes in the structure of benthic organism communities.[57]

Given the difficulty in determining the concentration of CNTs in environmental settings and the uncertainty in current estimates of environmental concentrations, determining O-MWCNT concentrations that would be environmentally relevant in experimental laboratory model studies is challenging. Electrophysiological measurements conducted by Corredor *et al.* on suspended planar lipid bilayer membranes composed of 1,2-dioleoyl-*sn*-3-phosphotidylcholine (DOPC) suggest that O-MWCNTs at concentrations as low as 1.6 mg/L can induce transmembrane current fluxes and possibly traverse the lipid bilayer.[30] Yi and Chen explored the interactions between O-MWCNTs and DOPC under varying ionic strength and pH conditions using quartz crystal microbalance with dissipation monitoring (QCM-D). They reported no attachment of O-MWCNTs with surface oxygen concentrations of *ca*. 10% O to DOPC at 0.1 M NaCl at pH 7.4 (0.01 M HEPES) at O-MWCNT concentrations of 500 μg/L as detected by QCM-D.[33] Though significant progress has been made in exploring the impact of CNTs on biological systems, molecular-level insight into the interactions that occur between O-MWCNTs and biological systems remains limited.

Here, we apply a multi-pronged approach to investigate the interactions of O-MWCNTs in the ng/L to mg/L concentration range with supported lipid bilayers (SLBs), which have been used as model systems for probing the interaction of O-MWCNT with cellular membranes.[30,34,58,59] We employ, for the first time, second harmonic generation (SHG) to track the adsorption of nanotubes to the SLB and estimate binding equilibria and adsorption free

energies. We also report the first vibrational sum frequency generation (SFG) spectra of the carbon tail and headgroups within the lipids comprising the bilayer before, during, and after interaction with O-MWCNTs. Finally, we complement our spectroscopic measurements with mass measurements using QCM-D to estimate total mass attached. Our use of SLBs most likely prevents us from addressing possible experimental outcomes such as membrane piercing, and the formation of transmembrane channels, which molecular dynamics simulations[34,58,59] and experiments[30,37] indicate can occur under certain conditions. Instead, we focus on the initial step of attachment to the surface. We estimate the interaction free energies, and assess whether changes occur to the SLB structure before, during, and after interaction with the O-MWCNTs. Our results in the sub-ppb regime extend current molecular insights towards lower O-MWCNT concentrations than what had been available thus far, which may be of further relevance to biogeochemical conditions.

3.2. Experimental. As we discuss in Chapter 2, SHG and SFG spectroscopies are surface-general, label-free, and interface-specific techniques that allow interfacial processes to be monitored without the overwhelming contribution from bulk processes. When working with systems as complex as the nano/bio interface, we find that combining several techniques is advantageous in terms of facilitating data interpretation. Therefore, this work combines SHG and SFG spectroscopies and QCM-D measurements.

3.2.1. Laser System. Detailed descriptions of our SHG approach can be found elsewhere.[60-64] Here, we use incident wavelengths of 600 and 800 nm as described in detail in Chapter 2.

3.2.2. Flow Cell, Substrate, Solution, and Bilayer Preparation. The flow cell preparation procedures are outlined in Chapter 2. We note that concerns about the potential "stickiness" or adhesion of O-MWCNTs to the PTFE tubing we use in our flow cell prompted us to increase the

frequency with which we exchanged our tubing to once every other experiment. Before use, and between trials, the tubing was thoroughly rinsed with methanol, ultrapure water (≥ 18 MΩ·cm), and buffer solution. All buffers contained 0.01 M Tris adjusted to pH 7.4 using dilute HCl or NaOH as needed and are henceforth referred to as Tris buffer.

For most of the work described herein, we studied SLBs formed from 1,2-dimyristoyl-3-*sn*-glycerophosphatidylcholine (DMPC), as phospholipids bearing zwitterionic PC headgroup are the majority lipids in extracellular leaflet of eukaryotic cell membranes.[63] To prepare vesicle suspensions, 2 mg of 1,2-dimyristoyl-*sn*-glycero-3-phosphocholine (DMPC, Avanti Polar Lipids) in chloroform were dried under a gentle stream of N_2. The dried lipids were then placed in a vacuum desiccator overnight to remove any remaining organic solvent, and then stored in the freezer under nitrogen. Prior to use, the dried lipid vesicle films were rehydrated with a 0.1 M NaCl, 0.01 M Tris buffer, 0.005 M $CaCl_2$ solution buffered to pH 7.4 and gently warmed to a temperature above the chain melting temperature (T_m = 24 °C)[65] for approximately 1 h. Vortexing the solution produced a suspension of multilamellar lipid vesicles that was then mechanically extruded through a polycarbonate membrane with a pore size of 0.05 μm (Avanti Polar Lipids). The suspension was passed through the polycarbonate membrane 11 times, as suggested by the manufacturer. Bilayers composed of 1,2-dioleoyl-*sn*-glycero-3-phosphocholine (DOPC) and 1,2-dioleoyl-3-trimethylammonium-propane (DOTAP) were prepared in a similar fashion. The vesicle suspensions were stored in glass scintillation vials or polypropylene Falcon tubes until use. Vesicle-containing suspensions were used within 2 days of preparation. The vesicle fusion method is employed to form supported lipid bilayers.[66] In SHG and SFG experiments, the flow cell is first equilibrated with Tris buffer containing 0.1 M NaCl. After acquiring steady background signal, 4 mL of a 0.5 mg/mL vesicle-containing solution (0.1 M

NaCl, 0.01 M Tris buffer, 0.005 M $CaCl_2$, pH 7.4) is introduced into the flow cell. After allowing the SLB to form at the silica/water interface over the course of at least 20 minutes, the SLB is rinsed with $CaCl_2$-free Tris buffer (0.1 M NaCl) to remove remaining intact vesicles.

3.2.3. Preparation and Characterization of O-MWCNT Suspensions. A detailed procedure for the oxidation of MWCNTs is documented elsewhere.[46, 52] Briefly, pristine multiwall carbon nanotubes (MWCNTs) are purchased from NanoLab Inc. (Waltham, MA). The as-received MWCNTs are characterized by the manufacturer to have an outer diameter of 15 nm ± 5 nm, a length of 5-20 μm, and a carbon purity of > 95%. We use two different batches of oxidized MWCNTs that contain 12% and 7% surface oxygen, denoted below as 7% and 12% O-MWCNTs, using H_2SO_4/HNO_3. Uncertainties in surface oxygen contents are in the 1% range. The CNT purification procedure developed by Bitter *et al.* (2014)[46] was followed for all O-MWCNTs produced. Transmission electron microscopy (TEM, Philips CM 300) is used to examine the structure of the O-MWCNTs following the oxidation procedure. TEM samples are prepared by dipping a lacey-carbon grid into a colloidal suspension of O-MWCNTs in water; the sample is imaged at 300 kV and the images are collected with a CCD camera (Figure 3.1.A-B). Figure 3.1.A shows that the oxidation process leaves the MWCNTs structurally intact with approximately 10 walls and lengths on the order of several hundreds of nanometers. Dynamic light scattering (DLS) and laser Doppler micro-electrophoresis (Zetasizer Nano ZS, Malvern Instruments, 632.8 nm, 173° backscattering angle) are used to estimate changes in hydrodynamic diameter over time and to measure electrophoretic mobility (EPM) for assessing the stability of aqueous O-MWCNT-containing suspensions.

3.2.4. SHG Experiments. In SHG adsorption experiments, the O-MWCNT-containing suspensions are introduced into the cell at a given nanotube concentration using a flow rate of

2.5 mL/min for a total volume of approximately 8 mL. To avoid changes in SHG signal that could be attributable to changes in ionic strength or pH, the O-MWCNT solutions are prepared such that the conditions of the background electrolyte and pH remained constant (0.001 or 0.1 M NaCl, 0.01 mM Tris buffer, pH 7.4). Each suspension is vortexed for approximately 20 seconds immediately prior to introduction into the flow cell.

3.2.5. SFG Experiments. Following our previously described approach,[61,67] we tune the broadband IR output of an OPA to the C–H stretching region between 2800 cm^{-1} and 3000 cm^{-1}. SFG spectra are collected using near total internal reflection geometry and the *ssp* polarization combination, which probes components of the vibrational modes that are oriented perpendicular to the surface. Each SFG spectrum is composed of an average of

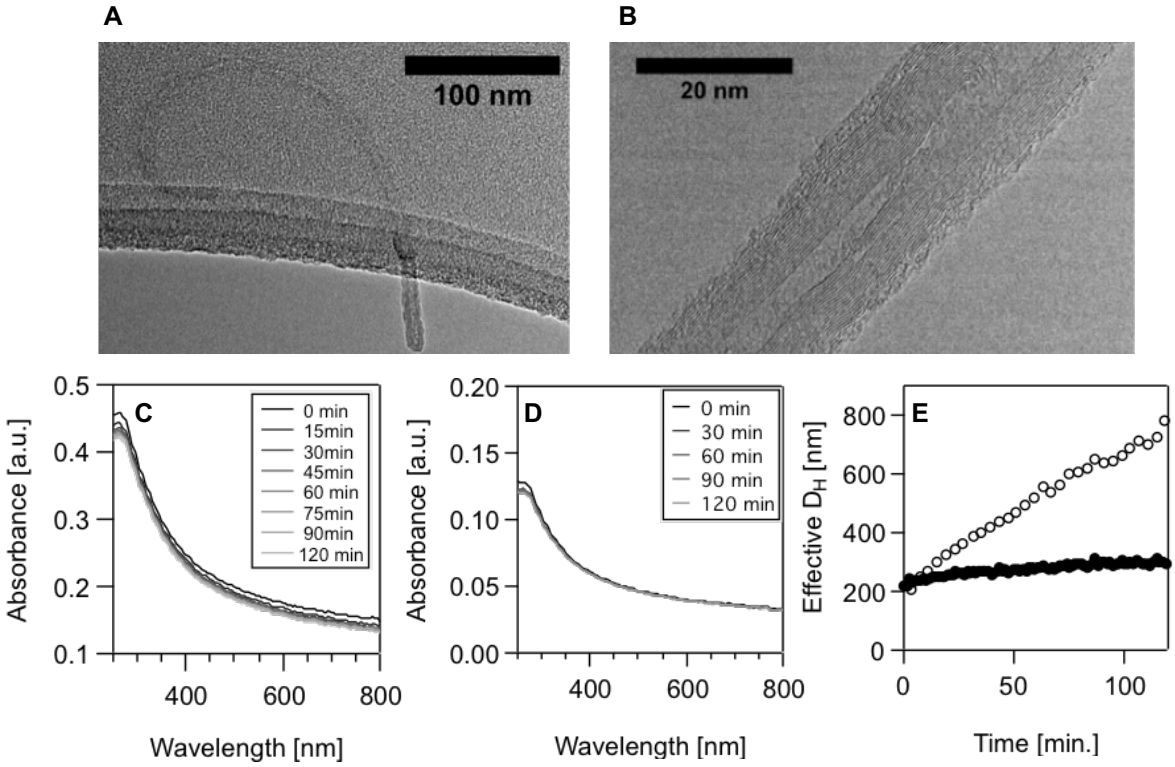

Figure 3.1. (A) Low- and (B) high-magnification TEM images of O-MWCNTs prepared by refluxing in 70% HNO_3. (C, D) UV-Vis absorbance spectra of 1 mg/L of (C) O-MWCNT (7% O) and (D) O-MWCNT (12% O) in 0.1 M NaCl, 0.01 M Tris buffer, pH 7.4 over the span of 2 hours. (E) Effective hydrodynamic diameter (D_H) of O-MWCNT with surface oxygen concentrations of 7% O (filled black circle) and 12% (open circle) O MWCNT suspensions at 1 mg/L, 0.1 M NaCl, 0.01 M Tris buffer, pH 7.4, as a function of time.

five acquisitions each integrated over 4 min. In SFG experiments the SLBs are rinsed with 30 mL of Tris buffer at a flow rate of 1.5 mL/min. SFG spectra of the SLBs before exposure to O-MWCNTs (Figure 3.2) agree well with our previous report,[63] and are consistent with the presence of well-formed bilayers.

3.2.6. QCM-D Experiments. QCM-D experiments are conducted using a modified version of our previously described procedures.[63] In these experiments, the particle attachment period was extended to 140 min, and the flow rate was reduced to 10 μL/min.

3.3. Results and Discussion.

3.3.1. Assessing the Stability of O-MWCNT Suspensions. Our DLS data indicates that some O-MWCNT aggregation occurs over the course of the SHG and SFG experiments, while UV-Vis data indicates the absence of settleable aggregates (Figure 3.1.C-D). Specifically, the UV-Vis data shown in Figure 3.1 indicates that the 7% O and 12% O MWCNTs are stable towards sedimentation over the timescale of the SHG and SFG experiments. Although DLS measurements (Figure 3.1.E) indicate some aggregation of the O-MWCNTs occurs over the time period of the optical experiments (two hours), the increase in the hydrodynamic diameter (D_H) of the 7% O-MWCNTs and 12% O-MWCNTs stabilizes after approximately 20 minutes at which point our SHG measurements are conducted. Comparable EPM values ($-6.1\ (\pm\ 2.9) \times 10^{-9}$ m^2/Vs and $-5.7\ (\pm\ 1.1) \times 10^{-9}$ m^2/Vs for O-MWCNTs with surface oxygen concentrations of 7% and 12% O respectively) were obtained despite the difference in the relative percentage of oxygen-containing functional groups. The lack of correlation between the atomic percent surface oxygen concentration and the measured electrophoretic mobilities at pH values higher than 6 has been observed in other studies of O-MWCNTs.[54] These various particle stability measurements

indicated that the SHG and SFG data are best described as representing the interactions of individual O-MWCNTs and small O-MWCNT aggregates with SLBs.

3.3.2. Attachment of O-MWCNTs to Supported Lipid Bilayers Prepared from DMPC. We have previously determined that after accounting for the interfacial potential contributed by the SiO_2 substrate, SLBs rich in phospholipids with phosphatidylcholine (PC) headgroups carry a negative interfacial potential at 0.1 M NaCl at pH 7.4,[63] which is important, given the negative surface potentials of the O-MWCNTs. Upon exposure to 1 mg/L O-MWCNTs in the presence of 0.1 M NaCl buffer, we observe a *ca*. 200 cm^{-1} broad contribution underneath the relatively sharp vibrational features observed prior to O-MWCNT exposure for 7% O-MWCNTs and 12% O-MWCNTs (Figure 3.2). We putatively attribute this broad spectral feature to the production of a non-resonant SFG response from the pool of polarizable free electrons associated with the π-electron system of the O-MWCNTs, reminiscent of the well-known nonresonant SFG response from polarizable metals.[68] Upon rinsing the bilayer with O-MWCNT-free solution, the SHG signal remains unchanged, indicating irreversible adsorption of O-MWCNTs to the SLBs over the timescale investigated.

The appearance of a non-resonant response, on top of which ride well-resolved vibrational features of the SLB, is observed in the majority of the experiments conducted across three O-MWCNT samples. Yet, we note that a subset of experiments conducted with 7% O-MWCNTs produced no change in the SFG signal (i.e., no increased non-resonant background develops), which we attribute to possible variation in aggregation

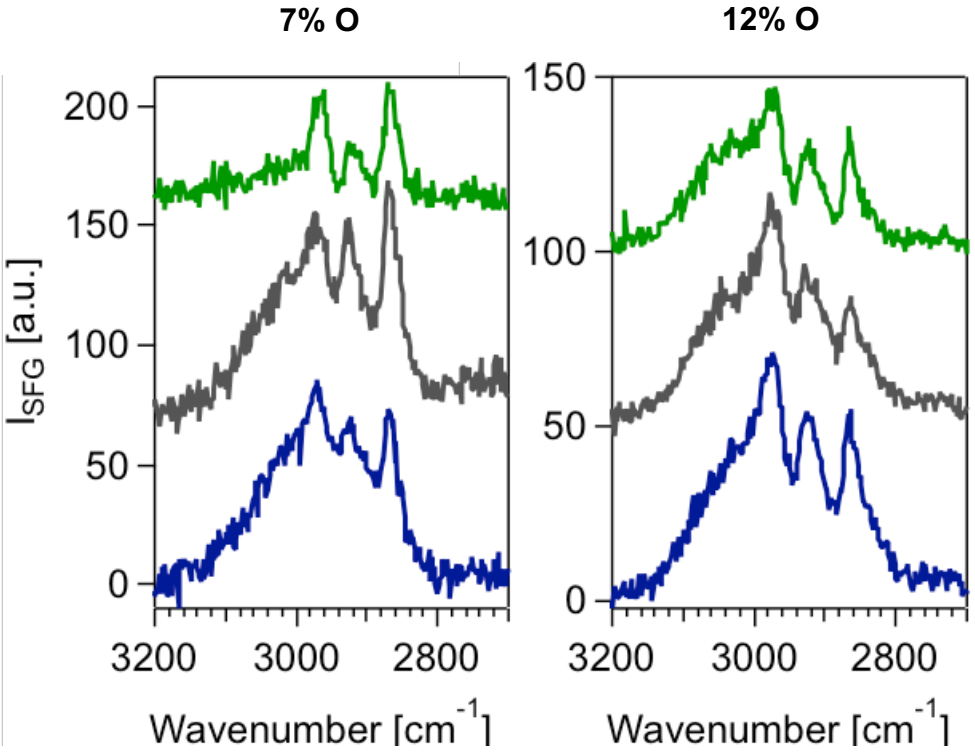

Figure 3.2. *ssp*-Polarized SFG spectra of SLBs formed from DMPC before (green) and after interaction with 1 mg/L O-MWCNT (gray), and after rinsing with 0.1 M NaCl buffer solution (blue) at 0.1 M NaCl. Three characteristic peaks at ~2960, ~2900, and ~2870 cm^{-1} are associated with C-H oscillators associated with the alkyl chains of the SLB formed from DMPC.

state or solution stability for the batch used in those specific experiments though these differences were not evident in UV-Vis and DLS measurements.

QCM-D studies conducted under conditions similar to those discussed in the SFG experiments (0.1 M NaCl buffer and 1 mg/L 7% O-MWCNTs) reveal a small but measurable frequency shift, $\Delta f = -0.57 \pm 0.16$ Hz. Upon rinsing the SLB formed from DMPC with buffer solution (i.e., no O-MWCNT present), the frequency shift increases to –0.33 ± 0.10 Hz (Figure 3.3). This observation is attributable to the removal of weakly bound carbon nanotubes, some portion of the bilayer, or both, along with loss of associated water and electrolyte. However, given that the SFG results do not indicate further bilayer alteration as shown in Figure 3.2, the rinsing likely leads to the loss of weakly bound 7% O-MWCNTs. QCM-D studies conducted under the same conditions with 12% O-MWCNTs yield larger frequency shifts of −3.5 ± 1.7 Hz, albeit with larger uncertainties of the point estimate (Figure 3.3) and no reversibility. The energy dissipation relative to the frequency changes for these systems ($\Delta D_5/(\Delta f_5/5) = 9.4\ (\pm\ 2.7) \times 10^{-7}$ Hz^{-1} and 8.3 (± 2.0) × 10^{-7} Hz^{-1} for the 7% and 12% O-MWCNTs, respectively) precludes application of the Sauerbrey equation to estimate the mass of O-MWCNTs on the SLBs.[69] Nevertheless, the small frequency shifts observed indicates that the surface coverages here are far below a monolayer.

3.3.3. SHG Control Studies. Given that these experiments are among the first to employ SHG to probe O-MWCNTs at liquid/solid interfaces, we briefly discuss outcomes from the control experiments we carried out to assess the validity and origin of the detected nonlinear optical signals. When compared to the bare SLB response at 0.1 M NaCl and 0.01 M Tris buffer (no O-MWCNTs present), we observed fractional SHG signal

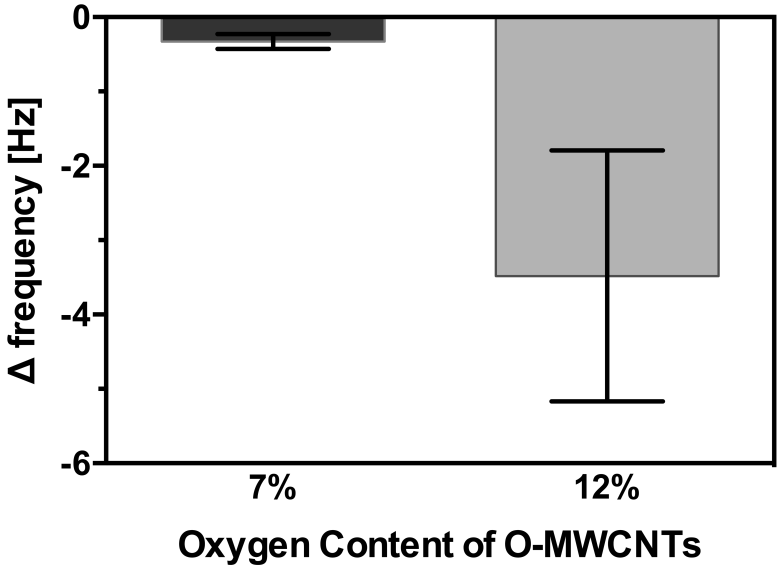

Figure 3.3. Attachment of O-MWCNTs (1 mg/L) to supported lipid bilayers formed from DMPC at 0.1 M NaCl (0.01 M Tris buffer, pH 7.4) as determined by QCM-D. Decreases in frequency correspond to increases in mass. Frequency data are reported for the 5th harmonic. Error bars represent one standard deviation (n = 3).

intensity increases as large as approximately 20% at λ_{SHG} = 300 nm (kHz amplifier laser source) for all of the O-MWCNTs studied. Adsorption of O-MWCNTs to bare silica (Figure 3.4) or defects in the SLB structure cannot be ruled out as a potential source for the observed SHG signal increases, given that adsorption isotherms for bare silica yield similar fractional increases in SHG intensity though adsorption to the underlying silica support is unlikely given that micron-scale defects in the SLB structure have not been observed. Based on QCM-D frequency shifts (24-26 Hz) and surface coverages (~3.4 to 4.1×10^{14} cm^{-2}), SFG spectroscopy (well-resolved spectra), AFM and fluorescence microscopy (diffusion coefficients of ~2 $\mu m^2/s$), forming supported lipid bilayers via the vesicle fusion method does result in the formation of fluid nearly complete supported lipid bilayers as was shown in our previously published work.[63] Given the QCM-D results indicating mass uptake upon introducing O-MWCNTs with surface oxygen concentrations of 7% and 12% to SLBs formed from DMPC, we interpret this SHG response to indicate nanotube attachment to the bilayer. Further, attachment of 7% O-MWCNTs to SLBs formed from DMPC, depends on ionic strength with no significant change in SHG signal intensity relative to the initial SLB is observed at 0.001 M NaCl (Figure 3.5.A), indicative of a repulsive electrostatic interaction between the O-MWCNTs and the SLBs. Similar trends in the adsorption of O-MWCNT under conditions of increasing ionic strength were also described in other work investigating the interactions of O-MWCNT and SLBs formed from DOPC.[33] To be clear, the term attachment here should not be taken to imply that covalent bonds are formed. Instead, the expectation is that the O-MWCNTs are physically adsorbed to the SLBs.

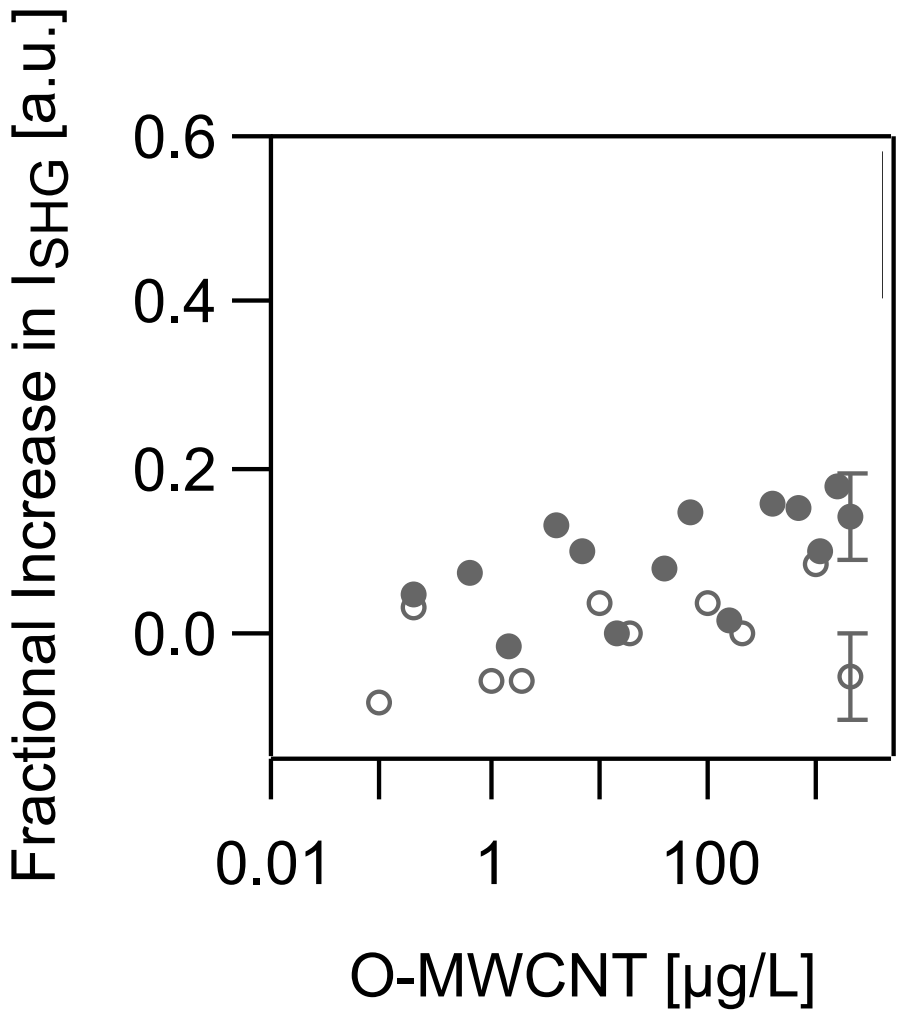

Figure 3.4. Fractional increase in SHG signal intensity as a function of O-MWCNT concentration, in µg/L, in the presence of bare fused silica substrate at both 0.001 M NaCl (open gray circle) and 0.1 M NaCl (filled gray circle). Error bars are generated from the standard deviation of all data points at a given ionic strength (shown on last for clarity).

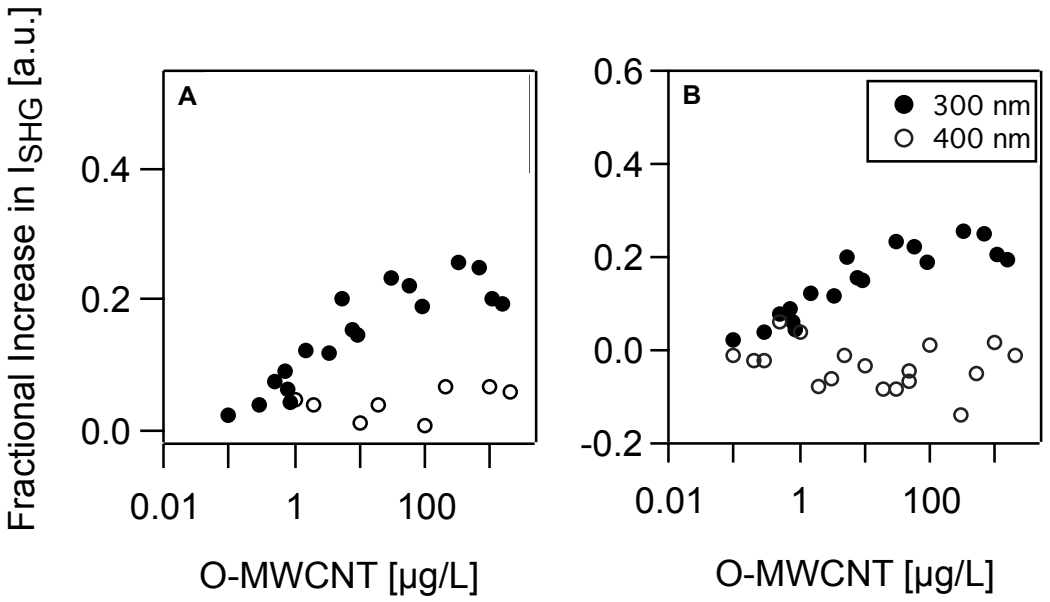

Figure 3.5. (A)Fractional increase in SHG signal intensity as a function of O-MWCNT concentration, in µg/L, in the presence of SLB formed from DMPC at both 0.001 M NaCl (open black circle) and 0.1 M NaCl (filled black circle). Error bars are generated from the standard deviation of all data points and is only showed on the last points for clarity. (B) Fractional increase in SHG signal intensity as a function of O-MWCNT concentration, in mg/L, in the presence of supported lipid bilayers formed from DMPC at 0.1 M NaCl, 0.01 M Tris buffer at pH 7.4 as monitored at 600 nm (λ_{SHG}=300 nm, filled circle) and 800 nm (λ_{SHG} = 400 nm, open circle) incident wavelengths.

To better understand the origin of our SHG signal gains, a second set of SHG experiments was conducted. At λ_{SHG} = 400 nm (MHz oscillator laser source) we observe no change in SHG signal intensity upon interaction of SLBs formed from DMPC with O-MWCNTs (Figure 3.5.B). The finding of significant increases in the SHG response at 300 nm that coincide with O-MWCNT addition and a lack of signal increase at 400 nm indicates that SHG resonance enhancement, which can substantially boost signal intensities when the SHG wavelength matches an electronic transition in the surface-bound species,[70-72] may be an important contributor to the SHG signals recorded here. Indeed, given the optical absorbance features of the O-MWCNTs towards the shorter wavelengths (Figure 3.1), it is likely that our experiments are approaching electronic two-photon resonance with the $\pi \rightarrow \pi^*$ transitions of the nanotubes. Yet, further experiments using SHG spectroscopy with varying incident and SHG wavelengths are needed to unambiguously assess the role of resonance enhancement here.

To determine the damage threshold of the SLB systems and the bare silica substrate in the presence of 2 mg/L O-MWCNT, we introduced, in two separate experiments, two concentrations (1 and 2 mg/L) of O-MWCNTs in 100 mM NaCl buffer to the flow cell and increased the incident visible pulse energy in increments of 0.05 μJ up to 0.5 μJ. Fits of a power function to the SHG intensity as a function of pulse energy yield a quadratic dependence at a concentration of 1 mg/L (Figure 3.6.A) but deviate somewhat (P = 2.6) at a concentration of 2 mg/L (Figure 3.6.B). Departures from the expected quadratic dependence indicate optical breakdown, optical processes other than SHG, or sample damage, which may be attributable to nanotube aggregation specifically

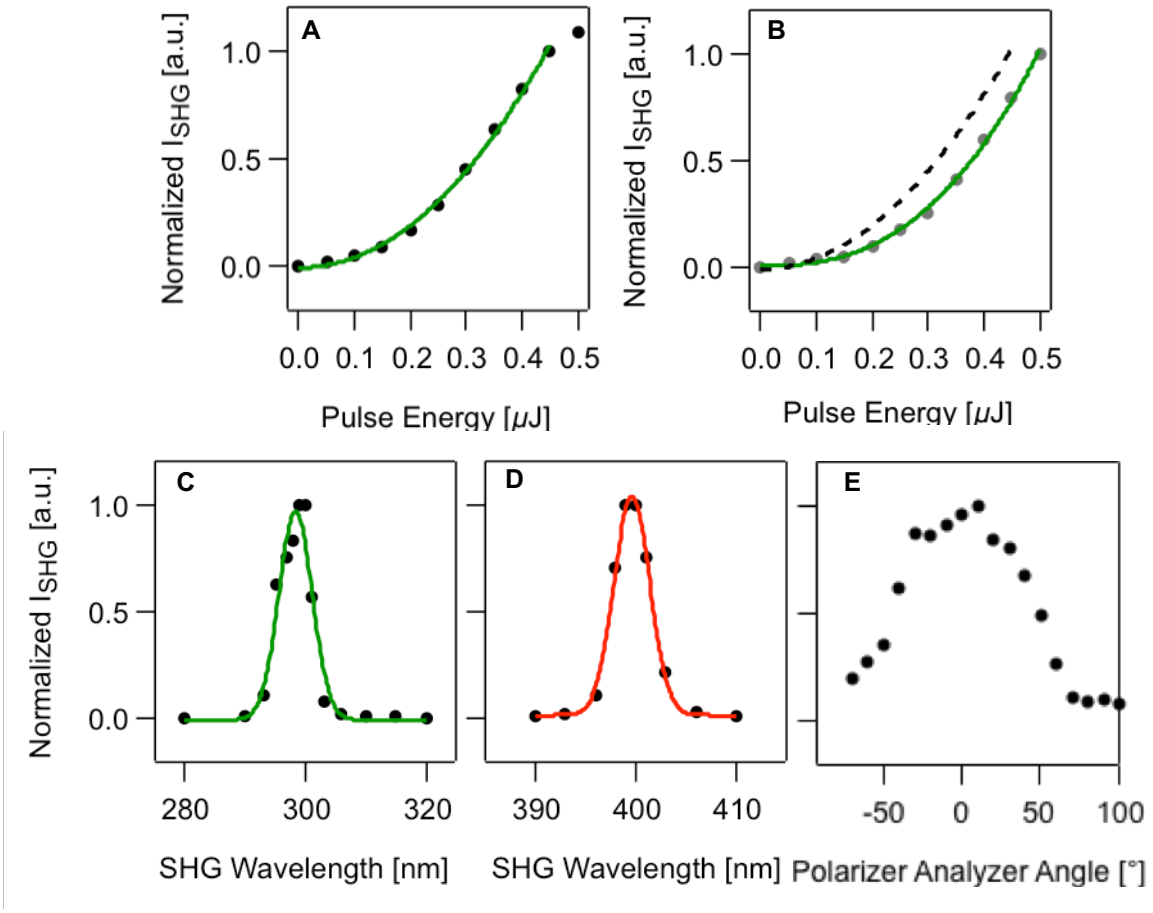

Figure 3.6. (A) Normalized SHG intensity as a function of pulse energy at 600 nm fundamental light field for 1 mg/L O-MWCNT interacting with an SLB formed from DMPC at 0.1 M NaCl. Green curve is a power function of the form $y = A + Bx^p$, where p = 2.1 ± 0.1. (B) Normalized SHG intensity as a function of pulse energy at 600 nm fundamental light field for 2 mg/L O-MWCNT interacting with an SLB formed from DMPC at 0.1 M NaCl. The green curve is a power function of the form $y = A + Bx^p$, where p = 2.6 ± 0.1. The black dashed line is a representative quadratic curve with a power of 2. (C) SHG intensity with the fundamental beam at 600 nm collected as a function of monochromator wavelength and Gaussian fit (solid green line) resulting in 3.9 ± 0.4 nm bandwidth for 2 mg/L concentration of O-MWCNT interacting with an SLB formed from DMPC at 0.1 M NaCl, (D) SHG intensity with the fundamental beam at 800 nm collected as a function of monochromator wavelength and Gaussian fit (solid red line) resulting in 2.5 ± 0.1 nm bandwidth for 2 mg/L concentration of O-MWCNT interacting with an SLB formed from DMPC at 0.1 M NaCl, (E) SHG intensity as a function of output polarization angle aligned with surface normal while probing with *p*-polarized fundamental light field for 2 mg/L O-MWCNT interacting with a SLB formed from DMPC at 0.1 M NaCl.

at the interface, as opposed to the bulk aqueous solution, and strong absorbance at this high concentration and pulse energy. Given the data shown in Figure 3.6.A and 3.6.B, all SHG experiments were carried out using nanotube concentrations ≤ 1 mg/L, and incident pulse energies of 0.40 ± 0.05 μJ so as to remain within the regime of well-behaved SHG responses.

Additional SHG bandwidth studies show that SHG signals recorded at λ_{SHG} of 300 and 400 nm (Figure 3.6.C, 3.6.D respectively) are well behaved, showing no evidence of fluorescence or radiation other than SHG entering the photomultiplier tube. Finally, SHG polarization studies carried out with *p*-polarized incident light and at λ_{SHG} = 300 nm show that the SHG signal is well polarized along the surface normal (Figure 3.6.E).

3.3.4. SHG Adsorption Isotherm Measurements. Having verified that the nonlinear signal response was indeed due to SHG, we proceeded to record the SHG response as a function of O-MWCNT (7% O) concentration. Figure 3.7 shows the average of 18 individual adsorption isotherm measurements, each time using newly formed SLBs and newly prepared O-MWCNT (7% O) suspension. We find that the SHG response increases with O-MWCNT (7% O) concentration and begins to plateau at approximately 10 μg/L in the case of all O-MWCNTs investigated here, regardless of surface oxygen concentration. This plateau indicates some limiting surface coverage has been reached.

To provide an estimate for the interaction energy, we fit the Langmuir adsorption model[73-75] to the SHG adsorption isotherms. The Langmuir fit yielded an apparent equilibrium constant, K_L^{app}, of 1.2 ± 0.2 L/μg and 2.0 ± 0.4 L/μg for 100 mM NaCl buffer, corresponding to adsorption free energy estimates of −52 ± 0.4 kJ/mol$_C$ and −53 ± 0.8

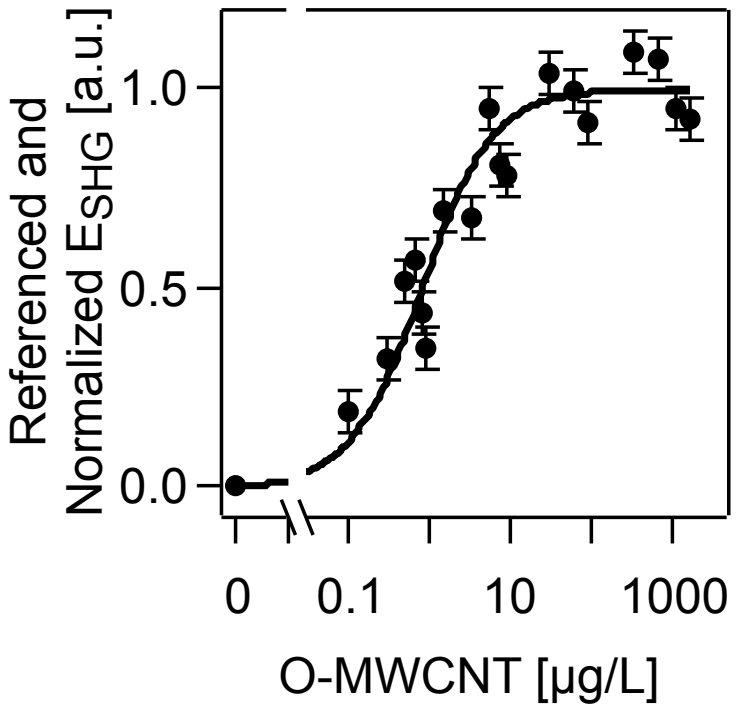

Figure 3.7. SHG *E*-fields as a function of O-MWCNT concentration (7% O), in μg/L, collected at 300 nm, normalized to maximum *E*-field at high O-MWCNT concentration recorded at 0.1 M NaCl, pH 7.4 in the presence of a SLB formed from DMPC at 0.1 M NaCl and referenced to the SHG signal from an SLB formed from DMPC at the silica/water interface (filled circles). The black solid line is a fit of the Langmuir adsorption model to the experimental data collected at 0.1 M NaCl in the presence of a SLB formed from DMPC, specifically of the form $\theta = K_L^{app} C/(1+K_L^{app} C)$, where K_L^{app} is the apparent equilibrium attachment constant, C is the concentration of O-MWCNT in μg/L, and θ is the relative SHG E-field. Error bars are generated from the standard deviation of data points collected at high particle concentration.

for the O-MWCNTs with surface oxygen concentrations of 7% and 12% respectively. In this analysis, we used the 55.5 molar (or 10^9 μg/L) concentration of water as a standard state for adsorption from solution.[76] Departures from the Langmuir model could be attributable to the lack of reversibility, (direct or indirect) particle-particle interactions (e.g., O-MWCNT aggregation), and the heterogeneous nature of O-MWCNTs, and are likely to be masked by the uncertainty in the reported point estimate.

3.3.5. O-MWCNT Adsorption to SLBs Prepared from DOPC and DOPC/DOTAP. O-MWCNT with surface oxygen concentrations of 8% O also adsorbed to SLBs composed of zwitterionic DOPC and DOPC bilayers containing cationic 1,2-dioleoyl-3-trimethylammoniumpropane (DOTAP) (Figure 3.8). (The batch of O-MWCNTs used in these experiments had a surface oxygen concentration of 8%, while those described in the previous sections had 7% O.) While we hypothesized that the adsorption of these negatively charged O-MWCNT particles would be higher in the presence of DOTAP, a cationic lipid, our SHG signals were comparable across SLBs formed from DOPC, DMPC, and 9:1 DOPC/DOTAP (Figure 3.8). Given that the surface charge of the pure SLB formed from DOPC and 9:1 DOPC/DOTAP are comparable,[63] the lack of significant difference in the adsorption behavior for these two bilayer systems is not surprising.

3.4. Possible Interaction Mechanism and Conclusions. The results from our SHG, SFG and QCM-D studies show that O-MWCNTs attach to the SLB probed here at 0.1 M NaCl to a small extent. Adsorption of the CNTs to the SLBs likely does not cause significant disruption or displacement of the SLB as indicated by the retention of the characteristic SFG spectral features associated with DMPC, despite the development of a strong non-

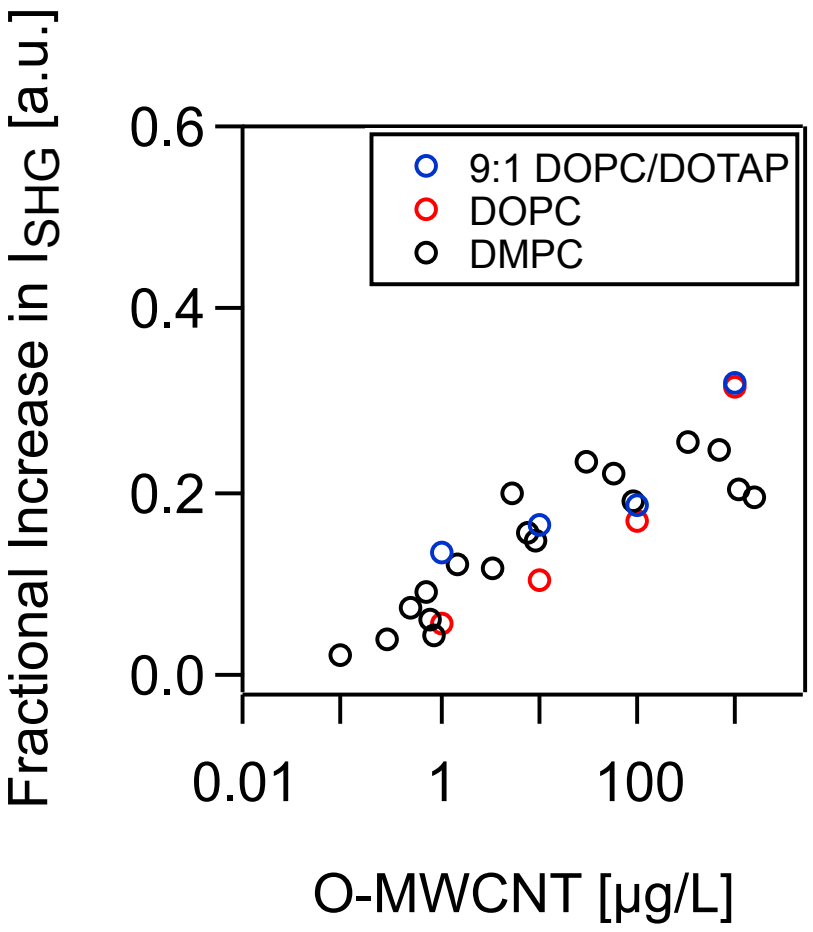

Figure 3.8. Fractional increase in SHG signal intensity as a function of O-MWCNT concentration, in µg/L, in the presence of supported lipid bilayers formed from 9:1 DOPC/DOTAP (blue open circle), DOPC (red open circle), and DMPC (black open circle) at 0.1 M NaCl, 0.01 M Tris buffer at pH 7.4. For both the DOPC and 9:1 DOPC/DOTAP SLBs, the O-MWCNT used have surface oxygen concentrations of 8% while for the interaction studies involving DMPC, the concentration is 7% O.

resonant background. Yi and Chen[33] previously reported no attachment of O-MWCNTs (10.6% oxygen) to SLBs composed of DOPC below a NaCl concentration of 200 mM at pH 7.3 (0.2 mM $NaHCO_3$) at 37 °C. The two studies differed with respect to lipids used to form SLBs (DOPC vs. DMPC), O-MWCNT concentration, the nature and concentration of the buffer, flow rate, and, likely most importantly, temperature. Nonetheless, similar to the results of Yi and Chen,[33] we observe more attachment to SLBs formed from DMPC or DOPC at higher ionic strength and no attachment at lower ionic strength (0.001 M NaCl).

As the O-MWCNT carry small negative zeta potentials under the conditions of the experiments,[33,54,55] and given that SLBs composed of lipids having zwitterionic headgroups carry negative interfacial potentials,[56] the mechanism by which O-MWCNTs adsorb to SLBs formed from DMPC and DOPC likely involves sizeable entropy gains as water molecules and electrolyte ions are displaced upon attachment of the nanotubes. Coulomb repulsion between the like-charged O-MWCNTs and the SLBs are thus overcome. Indeed, SHG experiments using bilayers prepared from 9:1 mixtures of DOPC/DOTAP, which are also associated with a negative interfacial potential under the experimental conditions,[63] yield comparable fractional increases in SHG intensity upon exposure to O-MWCNTs as that of DOPC and DMPC further supporting our conclusion.

In summary, we have employed SHG and SFG spectroscopy to directly probe O-MWCNTs interacting with supported lipid bilayers. We showed that O-MWCNT adsorb to SLBs rich in PC lipids at 0.1 M NaCl under the conditions explored in this study and at concentration in the sub-ng/L range. Resonantly enhanced SHG spectroscopy served as a chemically specific probe and is demonstrated to provide higher sensitivity to sub-μg/L O-MWCNT adsorption processes than QCM-D. We also showed that adsorption of O-MWCNTs to SLBs does not result in significant

disruption or displacement of the lipid bilayer as indicated by SFG spectroscopy. We cannot, however, rule out the formation of pores or assess the extent of local disruption to the bilayer.

In Chapter 4, we build on the toolbox of techniques employed here to investigate the role of charge in the interactions of polyelectrolytes with SLBs. Similar to the distribution of various functional groups along the backbone of the CNT structure, polyelectrolytes carry a number of groups along their main chains. Using polyelectrolytes allows us to understand how this multi-technique approach can be applied to the quantification of surface charge and charge density in systems with more flexibility than that exhibited by the CNTs described herein.

CHAPTER 4

Interfacial Electrostatics of Poly(vinylamine hydrochloride), Poly(diallyldimethylammonium chloride), Poly-L-lysine, and Poly-L-arginine Interacting with Lipid Bilayers

Portions of this chapter are reproduced with permission from the Royal Society of Chemistry:

McGeachy, A. C.; Dalchand, N.; Caudill, E. R.; Li, T.; Dogangun, M.; Olenick, L. L.; Chang, H.; Pedersen, J. A.; Geiger, F. M., Interfacial Electrostatics of Poly(vinylamine hydrochloride), Poly(diallyldimethylammonium chloride), Poly-L-lysine, and Poly-L-Arginine Interacting with Lipid Bilayers. *Phys. Chem. Chem. Phys.* 2018, **20**, 10846-10856.

4.1. Introduction. Nanoscale carbon-based and polymeric materials constitute two classes of nanomaterials having the largest market volumes, highest risks of industrial impact and public exposure, and both are identified as priority materials in need of regulatory consideration.[1] In Chapter 3, we explore the interactions of oxidized multiwalled carbon nanotubes with supported lipid bilayers (SLBs). There we find that negatively charged carbon nanotubes adsorb to the surface of the SLB in a non-destructive manner. Here, we proceed to extend on the insights gained in the previous chapter through the investigation of cationic charged groups on polymers. The motivation for this work is two-fold. As discussed in Chapter 1, nanoparticles are commonly functionalized with polymers or peptides to impart specific attributes for increased stability or functionality, for example. Often, nanoparticles are prepared in an excess of the desired polymer, and insufficient or incomplete purification strategies can leave a sometimes unknown concentration of polymer in solution with the functionalized nanoparticle.[2,3] Indeed, our experience with various purification strategies for the removal of excess poly(allylamine hydrochloride) (PAH) polymer from gold nanoparticle suspensions, has motivated a series of control studies which have developed into a highly informative project of its own. PAH, as an example, is known to disrupt model and actual[4] biological systems when bound to nanoparticles or free in solution. Unfortunately, this coexistence of sometimes large, and unaccounted for, concentrations of polymer in solution with nanoparticles can make it difficult to elucidate the toxicity mechanism as both the nanoparticle and/or free ligand can be responsible.[2,3] In addition to the motivation to understand the propensity of free ligands to disrupt model cellular surfaces and to quantify these interactions, polymers and polymeric particles represent an importance class of materials as discussed in more detail below.

Widespread interest in and utility of antimicrobial polymers, cell-penetrating peptides, bioelectrodes, and biosensors has driven many experimental and theoretical studies devoted to elucidating the interactions of polymers with cell surfaces[5-12] and model systems.[13-22] Outstanding questions in this field pertain to surface charge and charge density,[5,9,10,22-24] particularly for polyelectrolytes in spherical nucleic acids,[25-27] antimicrobial surfaces,[5,9] nonviral vectors,[10] as well as films[28] and gels.[24] So far, experimental approaches providing answers to how many charges a polycation carries upon attachment to a surface or interface are scarce, if not absent, especially when considering those that require no external labels. Importantly, an accurate description of how polycations interact with surfaces or interfaces is also a key requirement for modeling their interaction kinetics. Reaction rates, being proportional to absolute surface coverages, require knowledge of said absolute coverages, especially when it comes to heterogeneous redox reaction. Another example where knowledge of the absolute number of charges on adsorbed species is paramount is the heterogeneous kinetic salt effect, in which reaction rates increase or decrease with said number, depending on the ionic strength.[29]

Interfacial charge density estimates from experiments are important, as molecular dynamic (MD) simulations suggest that some linear polycations such as poly(vinylamine) and polyethylenimine (PEI) can accumulate, through electrostatic interactions, phosphatidylglycerol (PG) lipids present in simulated bacterial membranes,[30] a result also reported for polybetaines.[19] PAH is another widely investigated polycation under exploration for use in thin films,[5,31-33] drug delivery,[34] and cell encapsulation.[35] As a weak polyelectrolyte, PAH has been reported to shift its ammonium pK_a in multilayer films[28,36,37] and at model biological interfaces,[38] a result not expected with polyelectrolytes containing quaternary amines, such as poly(diallyldimethylammonium chloride). In addition to charge density, the structure of the

charged functionality can significantly influence the interactions of the polymer with lipids and macromolecules and have biological consequences. For instance, atomistic simulations of PAH, PEI, poly(vinylamine), and poly-L-lysine (PLL) interactions with DNA reveal that two different binding behaviors lead to the formation of polyplexes.[39] Of the polymers explored, only poly(vinylamine) embeds into the DNA major groove, a behavior not observed even with poly(allylamine) despite both polymers having similar functionalities. The authors hypothesized that the length of the pendant chains is responsible for this observation, as the amine group of poly(vinylamine) is one methylene shorter relative to poly(allylamine) (Figure 4.1). Further, in studies exploring the antimicrobial activity of copolymers with various cationic functional groups against *Escherichia coli*, polymers containing primary amines demonstrated a higher degree of antimicrobial activity relative to those bearing quaternary ammonium groups.[40]

With the importance of polyelectrolyte charge density in mind, we explore here the quantification of charge density and the ultimate role that charge density plays in the interactions that occur between polyelectrolytes having varying functionalization and SLBs as models for biological membranes. To this end, we have published an approach to estimate charge density on adsorbed entities that pairs surface-sensitive nonlinear optical spectroscopies, namely second harmonic generation (SHG) and vibrational sum frequency generation (SFG) spectroscopies, with acoustic mass measurements from quartz crystal microbalance with dissipation monitoring (QCM-D) as well as coarse-grained and molecular dynamic simulations.[38] We are further motivated by a previous study[41] exploring the role of chemical functionality, size, and charge in the disruption of SLBs. Generation 7 (G7) amine-terminated PAMAM dendrimers were shown to form and exacerbate membrane defects whereas this effect was reduced (G5) or eliminated (G3) in lower generation dendrimers. Moreover, replacing the terminal amine groups with

acetamide, reduced the propensity even further for G5 dendrimers to produce holes in the SLB. While this study and others highlight the important role that size, charge, chemical functionality, and molecular mass can play in the interactions that polymers have with model and actual cellular surfaces, these studies do not provide a quantitative measure for the surface charge of the dendrimers, SLB, or the adsorbed polymer layer. In a comparative study exploring the interactions of PLL and PLR nonamers with lipid bilayers composed from mixtures of anionic PG and zwitterionic phosphatidylcholine (PC) lipids, PLR was found to bind more favorably to lipid bilayers than PLL.[15] Although a pH-sensitive sensor composed of ortho-rhodamine B conjugated with the free amine of (1-hexadecanoyl-2-(9Z-octadecenoyl)-*sn*-glycero-3-phosphoethanolamine) was used to monitor changes in interfacial potential, no values for charge density or interfacial polymer concentration were reported due to stated limitations in the capabilities of the binding assay used.[15]

Our present work explores a suite of linear cationic polymers differing in chemical structures (Figure 4.1) that includes poly(vinylamine hydrochloride) (PVAm), poly(diallyldimethylammonium chloride) (PDADMAC), poly-L-lysine hydrobromide (PLL) and poly-L-arginine hydrochloride (PLR). This suite of polymers consists of various cationic groups including primary amines (PVAm and PLL), a quaternary ammonium (PDADMAC), and a guanidinium group (PLR). Given the diversity of the interactions that can occur between polycationic polymers, with varying chemical functionalities,[30,42] and biological interfaces, this suite of polymers allows us to explore the applicability of our quantitative approach for estimating charge densities. Here, we use a label-free method for estimating polymer-bilayer interactions to aid in the interpretation of such results and in understanding the molecular-level mechanisms by which polymers interact with biological surfaces. Specifically, we estimate

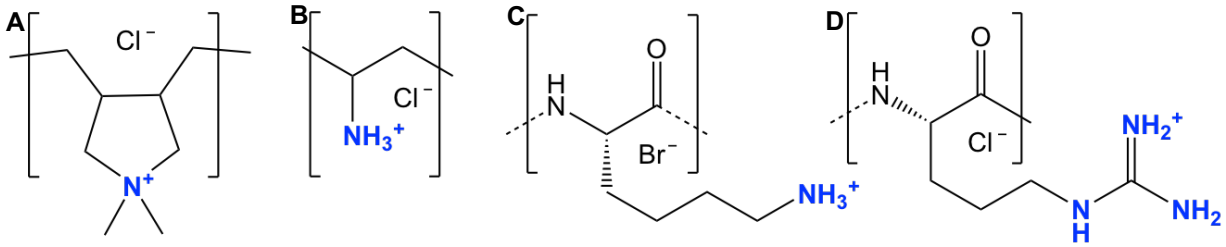

Figure 4.1. Structures of the polycations studied herein: (A) poly(diallyldimethyl ammonium chloride) (PDADMAC), (B) poly(vinylamine hydrochloride) (PVAm), (C) poly-L-lysine hydrobromide (PLL), and (D) poly-L-arginine hydrochloride (PLR).

interfacial charge densities from nonresonant second harmonic measurements that we pair with acoustic mass (polymer mass plus hydrodynamically coupled water) estimates from QCM-D measurements. This approach provides the lower bounds of charge per attached polycation, because (1) not all charges associated with the polycation may be located within the SHG active interfacial region and (2) the water content contributing to the mass estimates is not known quantitatively unless another technique such as nanoplasmonic sensing or optical waveguide lightmode spectroscopy is used, which is not the case here.

4.2. Experimental Methods.

4.2.1. Vesicle and SLB Preparation. Two-milligram vesicle suspensions of 9:1 molar ratios of 1,2-dimyristoyl-*sn*-glycero-3-phosphocholine (DMPC, Avanti Polar Lipids) and 1,2-dimyristoyl-*sn*-glycero-3-phospho-(1'*rac*-glycerol) (sodium salt) (DMPG, Avanti Polar Lipids) were dried under a gentle stream of N_2 and placed in a vacuum desiccator for at least 3 hours. As multiple methods for reconstituting and forming supported lipid bilayers exist, we used two methods somewhat interchangeably in order to evaluate the reproducibility and transferability of the results that we observe in our SHG measurements. Both methods produce similar outcomes in SHG experiments probing the interaction of polyelectrolytes with SLBs. The concentration of Tris buffer (0.01 M) adjusted to pH 7.4 is constant throughout and henceforth will be omitted. The bilayers prepared are well formed, as characterized in detail in our previous reports.[43,44]

The procedure for drying lipid films is consistent across Methods 1 and 2. Details of each method are outlined below:

Method 1. Lipid vesicle films were reconstituted with 0.1 M NaCl, 0.005 M $CaCl_2$ Tris buffer and gently warmed for 30 minutes. The reconstituted lipids were mechanically extruded through a polycarbonate membrane with a pore size of 0.05 μm at a lipid concentration of 2 mg/mL

(Avanti Polar Lipids). The vesicle solutions were diluted to a final concentration of 0.5 mg/mL at 0.1 M NaCl, 0.005 M $CaCl_2$ Tris buffer and stored in a 5-mL polypropylene round bottom Falcon tubes at 4 °C (Method 1). The addition of divalent salts has been shown to facilitate the formation of lipid bilayers from vesicle containing solutions onto supportive substrates such as fused silica. However, addition of $CaCl_2$ to vesicles containing large amounts of anionic lipids has been shown to result in vesicle aggregation. We have previously shown that there is no noticeable aggregation of vesicles using Method 1.[44] The majority of experiments involving PVAm and PDADMAC (400-500 kDa) were performed using Method 1. In experiments performed with this method, the cell was equilibrated with 0.1 M NaCl Tris buffer adjusted to pH 7.4. The vesicle containing solutions was then introduced into the flow cell at a flow rate of approximately 2 mL/min. After allowing the bilayer to form over at least 15 minutes, the flow cell is then flushed with 20 mL of 0.1 M NaCl Tris buffer. All experiments are performed at room temperature (~20 °C). Fluorescence recovery after photobleaching (FRAP) has shown that this method produces well-formed bilayers.[43]

Method 2. We also conducted a subset of experiments with lipids that were reconstituted instead with 0.001 M NaCl Tris buffer, vortexed, and transferred to 2-mL microcentrifuge tubes. After vortexing, the lipids were sonicated (bath sonicator for 30 minutes) and then subjected to 3 freeze-thaw cycles (5-minute liquid N_2 and 5-minute thaw in bath sonicator) (Method 2). Method 2 for vesicle preparation was also used primarily for SHG experiments with PDADMAC (100 kDa), PLL, and PLR. However, control experiments using this method for PVAm and PDADMAC (400 kDa) were also conducted. The vesicles were stored in a 2-mL microcentrifuge tube at 4 °C and diluted to a final concentration of 0.5 mg/mL at 0.15 M NaCl, 0.01 M Tris, 0.005 M $CaCl_2$ immediately before use for SHG experiments. In SHG experiments performed

with this method, the SHG flow cell was equilibrated with 0.15 M NaCl, Tris buffer, 0.005 M $CaCl_2$ Tris buffer and then lipid suspensions were injected at a flow rate of 2 mL/min. After allowing the bilayer to form over at least 15 minutes, the flow cell was flushed with 10 mL of 0.15 M NaCl Tris buffer, 0.005 M $CaCl_2$, 10 mL of 0.15 M NaCl Tris buffer, and finally 20 mL of 0.1 M NaCl Tris buffer. All experiments are performed at room temperature (~20 °C).

4.2.2. Polymer Solution Preparation. Poly(diallyldimethylammonium chloride) (PDADMAC, 400-500 kDa, 20 % wt. in H_2O), poly-L-lysine hydrobromide (PLL, 4-15 kDa), and poly-L-arginine hydrochloride (PLR, 5-15 kDa) are purchased from Sigma Aldrich and used without further purification. Poly(vinylamine hydrochloride (PVAm, 25 kDa) was purchased from Polysciences and used without further purification. All polymer solutions, with the exception of PDADMAC, were prepared and stored in 0.001 M NaCl. Poly(vinyl alcohol) with molecular weights of 9 kDa (Product Number 360627) and 85 kDa (Product Number 363081) (PVA), and poly(acrylic acid) (PAA, Product Number 416037) were also purchased from Sigma Aldrich. Polymer concentrations were determined based on the average molecular mass of the polymer, and the average number of repeat units was determined by dividing the average polymer molecular mass by the molar mass of one monomer, including the counterion mass.

4.2.3. Fluorescence Recovery after Photobleaching (FRAP) Measurements. FRAP is a fluorescence technique that is used here to provide insight into lipid surface coverage and the two-dimensional lateral mobility of lipids within the silica-supported lipid bilayer. Diffusion coefficients, determined through FRAP measurements, have been used previously as a method for evaluating the quality of supported lipid bilayers.[43-45] Here, FRAP measurements were carried out in a manner consistent with our previously published work.[43] Specifically, we used a Leica Spinning Disk Microscope (Leica DMI6000 inverted microscope equipped with a

Yokogawa CSU-X1 Spinning Disk module) with either a 40X or 63X oil immersion objective. The samples are visualized by a Photometrics Evolve Delta512 camera (60fps at 512 × 512 chip camera, 16 μm pixel size, backthinned electron multiplying charge coupled device). Photobleaching was carried out using an iLas^2 attachment from Roper Scientific which is mounted onto the microscope (401 nm 50 mW; 50-100% of laser power). Images were collected with the Green ET525/50M emission filter and 488 nm, 50 mW laser at 10-15% power. Metamorph was used for data collection and ImageJ was used for data processing. The simFRAP plugin for ImageJ was used to extract lateral diffusion coefficients.[46]

For these experiments, the vesicles were doped with 0.1 mol% TopFluor PC® (Avanti Polar Lipids, 810281). Experiments were carried out in a similar manner as briefly described in Chapter 2. Specifically, we used a homebuilt Teflon flow cell and a 1-inch diameter UV grade fused silica window (ISP Optics, QU-W-25-1) marked on the edge with marker (to facilitate aligning) and either Method 1 or Method 2 for vesicle preparation (T = 20-22°C). After forming the SLB in the Teflon flow cell at the silica/water interface, the SLB was rinsed with 20 mL of 0.1 M NaCl, 0.01 M Tris buffer solution adjusted to pH 7.4. The window was carefully removed and mounted into a modified closed cultivation cell (Pecon, POC-R2). To avoid disrupting the bilayer, the window is separated from the imaging window by a thin layer of silicone grease and a small reservoir of 0.1 M NaCl buffer (Figure 4.2).

For SLBs produced with Method 1, which did not employ the freeze-thaw pretreatment, we find an average diffusion coefficient of 0.6 ± 0.3 μm^2/s (18 replicates over 6 individual samples). SLBs formed from Method 2 have an average diffusion coefficient of 1.4 ± 0.3 μm^2/s (18 replicates over 2 individual samples). We also find that both methods discussed above produce SLBs with mixtures of liquid-crystalline and gel phase domains. As such, we find

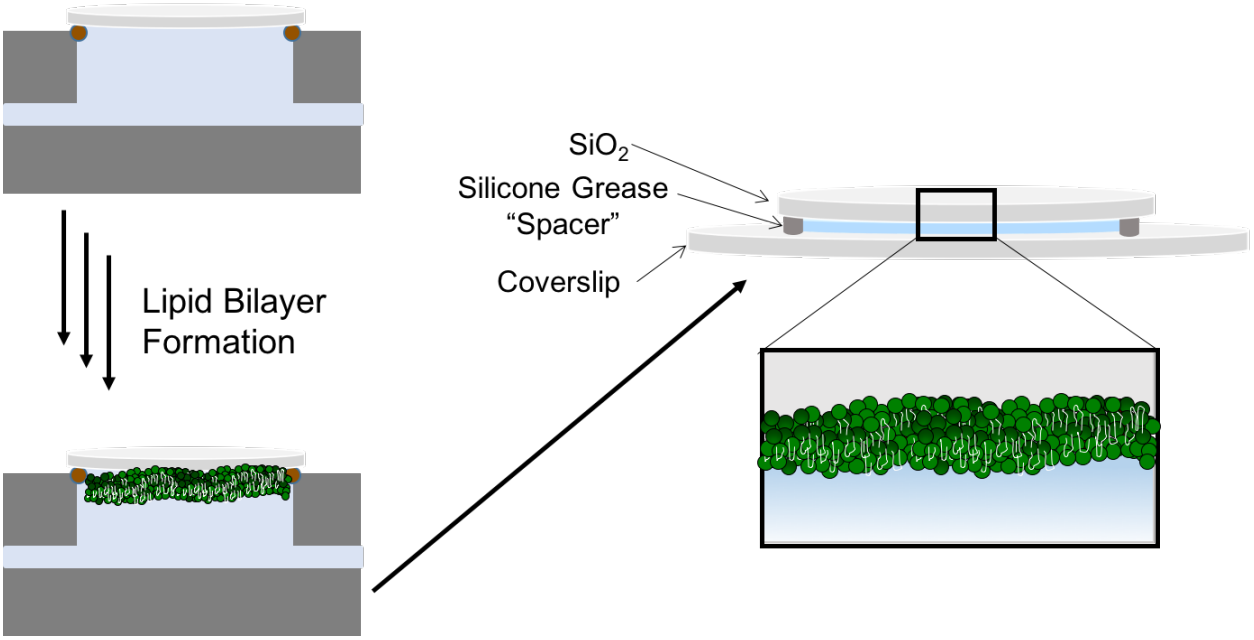

Figure 4.2. Illustration of FRAP experimental setup. The flow cell and method for forming SLBs is consistent with the procedure used in our SHG experiments. After allowing the SLB to form and rinsing away excess vesicles, the optical window was removed from the SHG flow cell. The optical window was then mounted into a modified closed cultivation cell (omitted for clarity). Four silicone grease "spacers" were placed onto a glass coverslip and excess grease was removed. The window was separated from the glass coverslip by these spacers and a pool of hydrating buffer to ensure that the bilayer has minimal contact with air.

diffusion coefficients on the order of ~1 and ~0.01 $\mu m^2/s$ which corresponds to the liquid-crystalline and gel phase supported lipid bilayers, respectively. The diffusion coefficients reported here agree well with our previously reported estimates for diffusion coefficients of SLBs formed via Method 1.[43] Representative traces are shown in Figure 4.3. The error associated with the average diffusion coefficient is the standard error determined by dividing the standard deviation of the diffusion coefficients over all of the sample replicates by the square root of the number of replicates.

4.2.4. SHG Adsorption Experiments. The flow cell was equilibrated with 0.1 M NaCl buffer (Method 1) or 0.15 M NaCl and 0.005 M $CaCl_2$ (Method 2), and the SHG signal was monitored for at least 10 minutes to obtain a stable baseline. Vesicle-containing solutions were then introduced into the Teflon flow cell *via* the three-way valve at a rate of approximately 2 mL/min. Supported lipid bilayers formed over the course of at least 15 minutes *via* the vesicle fusion method.[38,43-45] The resulting 9:1 DMPC/DMPG bilayer was then rinsed at the same flow rate with (1) 20 mL of 0.1 M NaCl Tris buffer (Method 1) or (2) 10 mL of 0.15 M NaCl and 0.005 M $CaCl_2$ Tris buffer, 10 mL of 0.15 M NaCl Tris buffer, and 20 mL of 0.1 M NaCl Tris buffer (Method 2) to remove any excess vesicles, and the SHG signal was monitored for at least 20 minutes or until stable. The SHG signal recorded prior to polymer solution introduction serves as the baseline signal to which the data are normalized. To generate SHG adsorption isotherms, sequentially higher concentrations of polymer were introduced into the flow cell (20 mL at 2 mL/min), and the SHG signal was allowed to stabilize (~30 minutes). The average SHG signal over the last 10-15 minutes was used.

Single-exposure experiments were also performed to assess reversibility. In these single exposure experiments, referred to herein as on/off experiments, the SHG baseline signal from a

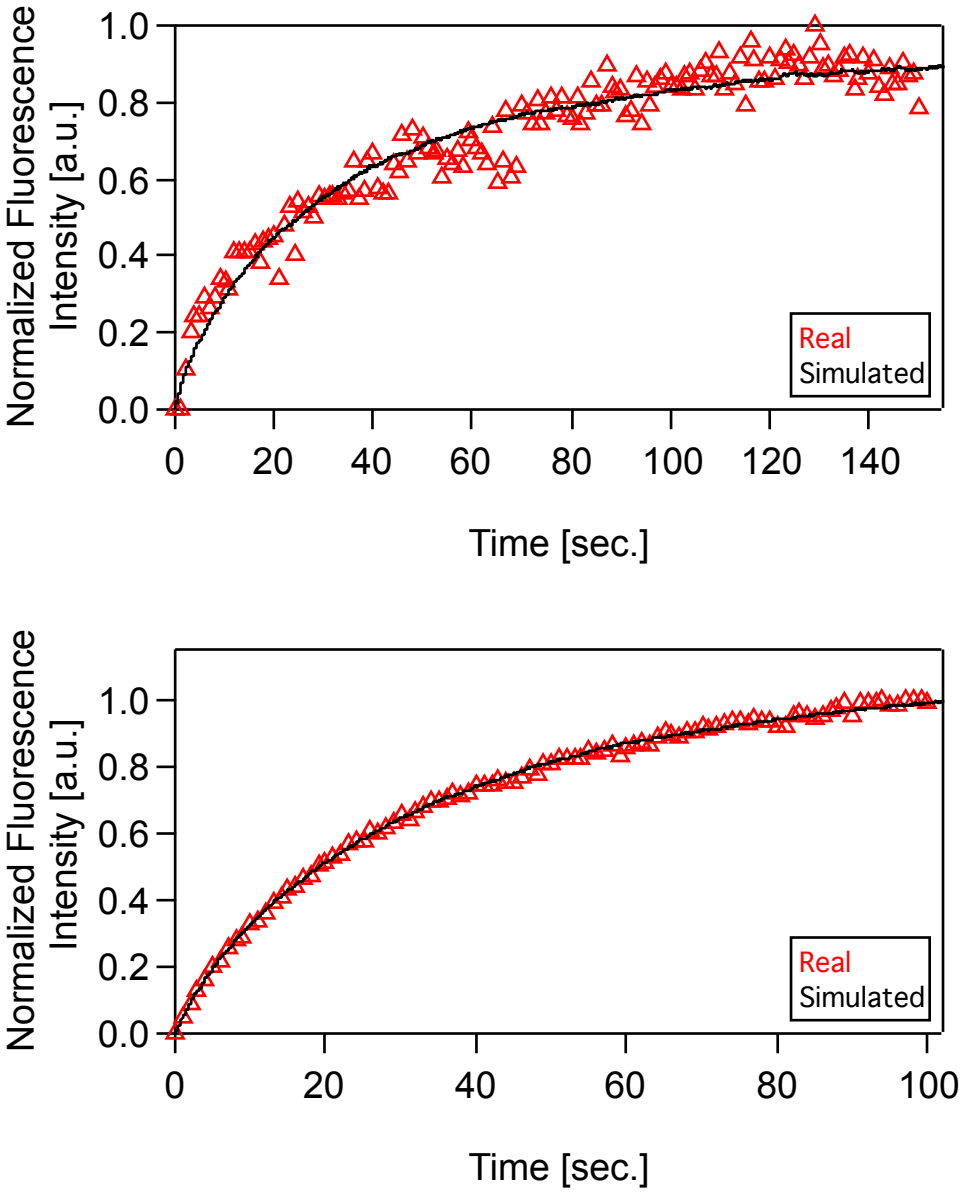

Figure 4.3. Representative simFRAP plots of normalized fluorescence intensity as a function of time for SLBs formed from 9:1 DMPC/DMPG for Method 1 (top) and Method 2 (bottom). The diffusion coefficients are consistent with a bilayer undergoing a gel-to-liquid phase transition.

SLB formed from 9:1 DMPC/DMPG at 0.1 M NaCl was collected for at least ~45 minutes. Then, 20 mL of solution at the desired polymer concentration was introduced into the flow cell, maintaining the same background electrolyte concentration (0.1 M NaCl), and the SHG signal was monitored for 70 minutes before rinsing with 20 mL of a polymer-free solution at 0.1 M NaCl. In experiments conducted at lower ionic strengths (0.01 M), where the only contribution to ionic strength was the Tris buffer (i.e., no added NaCl), the initial rinse with 0.1 M NaCl after bilayer formation, was followed by a rinse with 20 mL Tris buffer (no NaCl present). The adsorption isotherms and on/off experiments were then carried out in the same manner using salt-free buffer. All experiments were carried out at room temperature (20-21°C) which is just below the temperature at which the lipids transition from an ordered gel phase to a disordered liquid crystalline phase of DMPC and DMPG (T_m 24 and 23°C respectively).

4.3. Results and Discussion.

4.3.1. Polycation Adsorption to Supported Lipid Bilayers. The adsorption of polycationic polymers to membranes is driven, in part, by short-range electrostatic interactions, although some studies have suggested that hydrophobic interactions and hydrogen bonding are also important in these interactions.[30,47] While PLR and PVAm adsorb to lipid bilayers formed from pure zwitterionic DMPC and a 9:1 mixture of DMPC/DMPG, as evidenced by the decrease in SHG signal upon introduction of polymer solution, PLL and PDADMAC do not change the observed SHG signal considerably upon interaction with SLBs formed from DMPC (Figure 4.4). These results suggest that, as expected, PLL and PLR adsorption to SLBs containing PG-lipids is driven, at least in part, by electrostatics. These qualitative outcomes are similar to what has been reported elsewhere.[15,48]

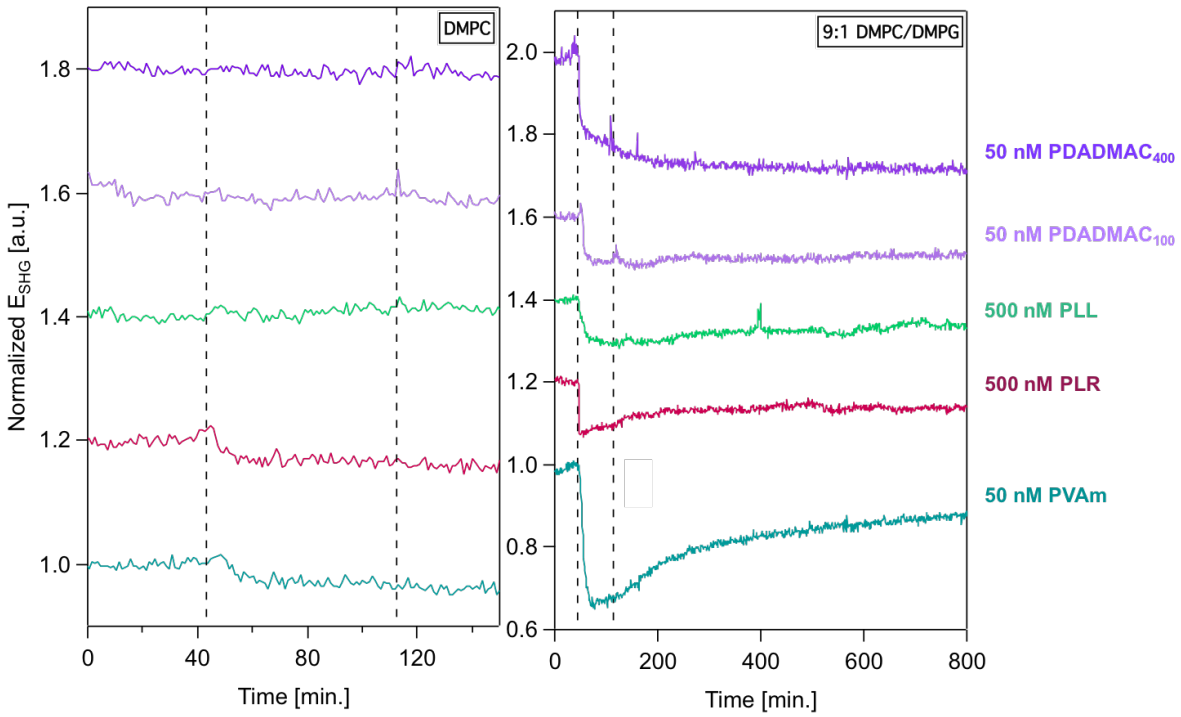

Figure 4.4. Normalized SHG *E*-field as a function of time in the presence SLBs formed from (left) DMPC or (right) 9:1 DMPC/DMPG for 50 nM $PDADMAC_{400}$ (dark purple), 50 nM $PDADMAC_{100}$ (light purple), 500 nM PLL (light green), 500 nM PLR (red), and 50 nM PVAm (teal) at 0.1 M NaCl, 0.01 M Tris buffer, pH 7.4. At t = 0, the supported lipid bilayer is unperturbed and the SHG signal is monitored at 0.1 M NaCl. At t = 43 min, polymer solution is introduced into the flow cell and at t = 112 min the flow cell is rinsed with polymer-free solution composed of 0.1 M NaCl, 0.01 M Tris, pH 7.4.

4.3.2. Reversibility and Timescales. SHG and QCM-D were also used to investigate the reversibility of polycation binding to the SLBs. In these experiments, SLBs were exposed to 50 nM concentrations of PVAm or PDADMAC or to 0.5 μM of PLL or PLR, at 0.1 M NaCl. These polymer concentrations correspond to saturation coverage as determined by SHG, as discussed later from our adsorption isotherm measurements.

PLL, PLR, and PVAm interacting with SLBs formed from 9:1 DMPC/DMPG all show partial to complete reversibility upon rinsing with 0.1 M NaCl polymer-free buffer solutions (Figure 4.2B), albeit over long timescales (>8 hours). PLL, PLR, and PVAm interacting with SLBs formed from 9:1 DMPC/DMPG all show partial to complete reversibility upon rinsing with 0.1 M NaCl polymer-free buffer solutions (Figure 4.4), albeit over long timescales (>8 hours). We note here that such long timescales are generally not probed using nonlinear optics or quartz crystal microbalances, as drifts in the signal due to a variety of exogenous signal variations typically prevent one from making such "long-term" measurements. Indeed, Fig. 4.4B shows that had the measurements ceased after two hours, already an impressive feat in probing surface processes at buried interfaces using ultrafast lasers, the varying extent of reversible binding for PVAm, PLR, PLL, and $PDADMAC_{100}$ would not have been identified. An important part to overcoming the difficulty of long-term surface interaction tracking is due to the low long-term drift of our Ti:S oscillator (0.5% drift in power over two hours.

PDADMAC, regardless of molecular mass, remains adsorbed to the SLB surface as evidenced by the continued suppression of the SHG signal after rinsing, as compared to the SHG signal of the bare SLB prior to exposure. These results might be explained by the significantly larger molecular mass of the PDADMAC polymers, as compared to the (reversibly bound) much lower molecular mass polymers (PVAm, PLL, and PLR). While QCM-D reversibility studies do

not indicate that the adsorption process demonstrates reversibility over 20 minutes of rinsing, the longer-term SHG studies indicate that polymer adsorption is indeed reversible over longer timescales (>8 hours). Indeed, close to full reversibility is observed in the case of PVAm over these timescales. We therefore apply Langmuir model-based adsorption isotherms to describe the adsorption behavior of the various polyelectrolytes studied herein. Note that neither SHG spectroscopy nor QCM-D can independently distinguish between removal of lipids, polymer, or a combination thereof. However, vibrational sum frequency generation spectroscopy experiments show only negligible changes in the spectral features from the SLBs studied here before and after they have been exposed to the polycations.

4.3.3. Comparable Binding Free Energies Across All Polymers Despite Differences in Molecular Structure and Mass. Recently, the Hill adsorption model was applied to the adsorption of PLL and PLR to lipid bilayers formed from 1-palmitoyl-2-oleoyl-*sn*-glycero-3-phospho-(1'*rac*-glycerol) (sodium salt) (POPG) and 1-palmitoyl-2-oleoyl-*sn*-glycero-3-phosphocholine (POPC).[15] As reported by Cremer and co-workers, using a simple Langmuir model to describe the adsorption of PLL and PLR to SLBs is difficult. These studies revealed that PLR nonamers adsorbed more cooperatively to SLBs than did PLL nonamers, although binding of PLR and PLL was largely anti-cooperative under most conditions explored.[8] Given that some cooperative binding is expected in the adsorption of PLL and PLR specifically in these systems, we opted to use the Hill model, which provides better fits with the experimental data presented here.

Using our previously published approach,[38] we estimate charge densities, equilibrium constants, mass uptake, degree of ionization, and free energies of adsorption for the polycation/bilayer systems studied in this work (Table 4.1). Figure 4.5 shows that with

Table 4.1. Summary of experimental data for polycations adsorbing to SLBs formed from 9:1 DMPC/DMPG at 0.1 M NaCl

	binding constant	adsorption free energy	surface charge density[a]	Hill coefficient	acoustic surface mass density	number density[b]
	K_{app} [M^{-1}]	ΔG [kJ/mol]	σ [C/m^2]	n	$\Gamma_{QCM\text{-}D}$ [ng/cm^2]	N_{ads} [cm^{-2}]
$PDADMAC_{400}$	$9.5 (\pm 6.1) \times 10^8$	-61 ± 1.6	0.30 ± 0.15	0.93 ± 0.09	460 ± 5	$4.23 (\pm 0.05) \times 10^{11}$
$PDADMAC_{100}$	$2.3 (\pm 2.1) \times 10^8$	-58 ± 2.2	0.27 ± 0.18	0.92 ± 0.14	290 ± 18	$1.22 (\pm 0.07) \times 10^{12}$
PVAm	$1.4 (\pm 0.5) \times 10^8$	-56 ± 0.8	0.16 ± 0.16	3.3 ± 1.5	270 ± 12	$4.48 (\pm 0.2) \times 10^{12}$
PLL	$2.6 (\pm 2.1) \times 10^7$	-52 ± 2.2	0.18 ± 0.20	1.6 ± 0.77	250 ± 15	$1.04 (\pm 0.06) \times 10^{13}$
PLR	$2.8 (\pm 1.4) \times 10^7$	-52 ± 1.2	0.24 ± 0.08	0.89 ± 0.08	240 ± 31	$9.90 (\pm 1.3) \times 10^{12}$

[a]Surface charge density of adsorbed polymer layer (not including charge density of 9:1 DMPC/DMPG bilayer. [b]assuming that ~30% of the acoustic surface mass density is attributable to hydrodynamically coupled water.

increasing polymer concentration, the SHG signal intensity decreases as the bilayer surface charge decreases in magnitude due to polycation attachment. Control SHG experiments using (uncharged) polyalcohols show negligible binding ("PVOH" in Figure 4.5A, 4.5B).

Dividing the average molecular mass of the polymer by the molar mass of the corresponding monomer (including the mass contributions from the counterion), we now account for molar mass differences across the various polycations we studied (Figure 4.5B). Plotting the SHG response after normalizing it to the zero-polycation concentration case and referencing to the response obtained for the highest polycation concentration reveals that the individual adsorption isotherms of all the polycations converge on a single curve, with an inflection point corresponding to 10^{-6} mol/L of cations in solution (Figure 4.5C). Our approach is similar to an exploration of the binding activity of polycations with pendent biguanide or quaternary ammonium functional groups,[6,7] in which accounting for molecular mass differences between the two polymers led to comparable antimicrobial activity.

Here we apply a combined Gouy-Chapman and Hill model to describe the binding of these polymers to the bilayer surface. When referenced to the molarity of water (55.5 M), the apparent equilibrium constants determined from SHG isotherms correspond to apparent adsorption free energies of –61 ± 2, –58 ± 2, –57 ± 1, –52 ± 2, –52 ± 1 kJ/mol for $PDADMAC_{400}$, $PDADMAC_{100}$, PVAm, PLL, and PLR, respectively (Table 4.1). Comparable free energies associated with the adsorption of PDADMAC to that of the polymers explored herein are somewhat surprising since PDADMAC is expected to only weakly interact with lipids, given the charge shielding in the quaternary ammonium groups. The nuances of the binding behavior of the polycations studied here are likely to manifest themselves in their binding entropies and enthalpies. For instance, given differences in the molecular weights and the

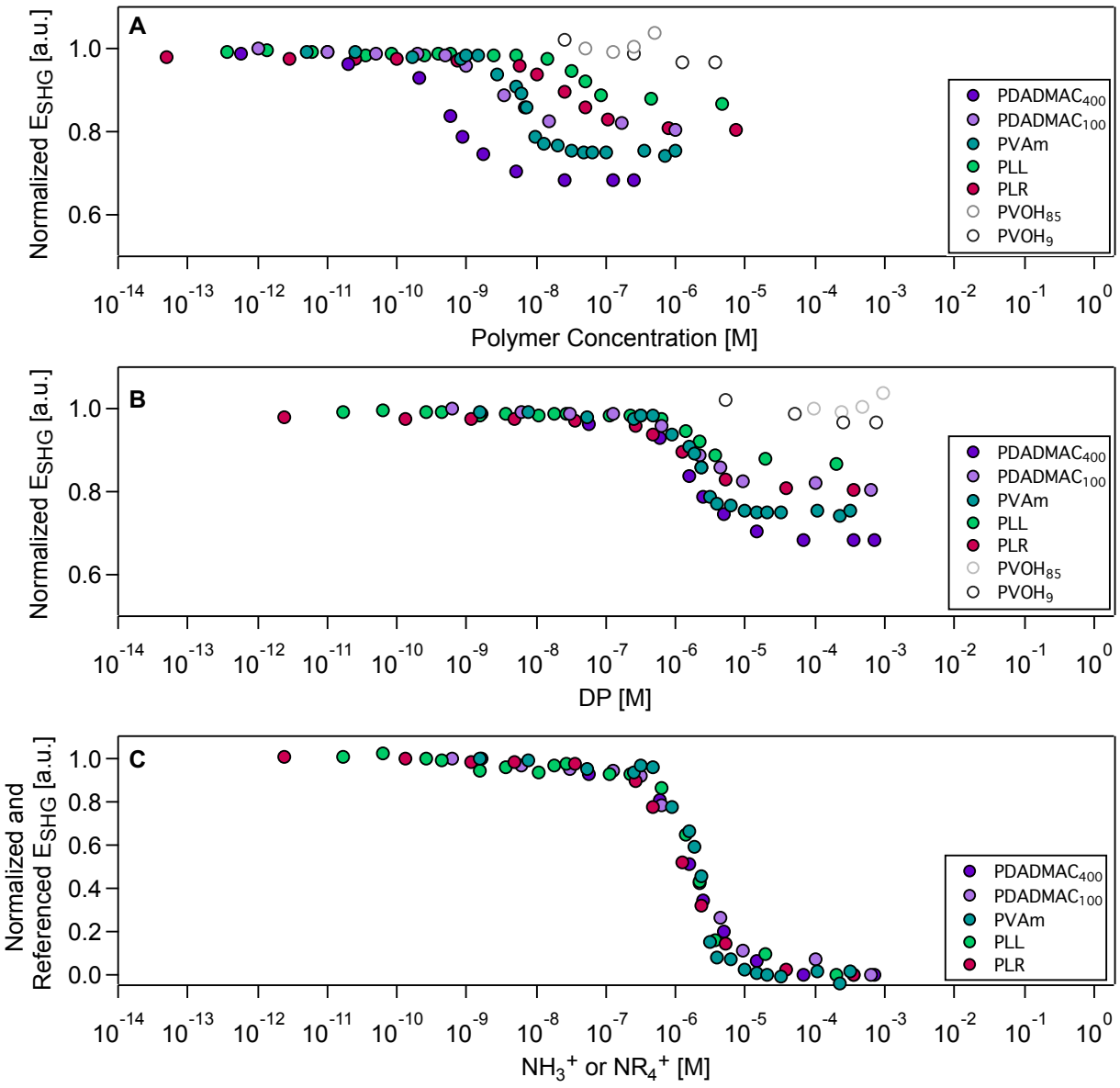

Figure 4.5. Normalized SHG *E*-field as a function of (A) polymer molar concentration, (B) the number of repeat units (degree of polymerization, DP), in molarity, and (C) amount of positive charge (molar units) at 0.1 M NaCl Tris buffer at pH 7.4. In (B) the concentration on the basis of repeat units is determined by multiplying the polymer concentration, in molarity, by the number of repeat units. In (C) the concentration of positive charges is determined by multiplying the polymer concentration, in molarity, by the number of repeat units. Each polymer data set is independently normalized and referenced. The SHG *E*-field displayed is normalized to the SHG *E*-field associated with the supported lipid bilayer formed from 9:1 DMPC/DMPG prior to exposure to polymer.

differing propensities of the polycations described here to reorient or release water and counterions from the bilayer surface upon adsorption, and to perturb local lipid ordering,[30] it is conceivable that the entropic contributions to the free energies vary significantly across polymers. A comparison of the results derived from combinations of two surface complexation models (triple-Layer and Gouy-Chapman), and Langmuir and Hill models is provided in the below (Table 4.2). Future experiments will address this point through the use of temperature-controlled experiments, an aim beyond the scope of this current work.

In addition to providing estimates for charge densities, the approach described herein also allows us to explore the cooperative nature, or the lack thereof, of polyelectrolyte adsorption to lipid bilayers. Atomistic-scale MD simulations suggest that strong interactions between PVAm and the headgroups of PG-lipids results in competitive binding between two different PVAm polymer chains.[30] With a Hill coefficient of 2.3, we find that the adsorption of PVAm to 9:1 DMPC/DMPG bilayers is more positively cooperative than any of the other polymers explored herein. In fact, none of the other polymers demonstrate positive or negative cooperativity based on their estimated Hill coefficients, which are close to unity. Unlike PLL and PLR, two other relatively weak polyelectrolytes, PVAm is subject to the polyelectrolyte effect. Specifically, the relative distance between neighboring amine groups gives rise to a unique ionization behavior that allows PVAm to maintain partially ionized over most of the pH scale.[49] Our previous report on PAH showed that the pK_a shift associated with PAH adsorption to 9:1 DMPC/DMPG could be substantial.[38] Here, we expect this shift to be even larger given the unique relationship between neighboring amine groups associated with PVAm.

4.3.4. Charge Densities of Polycations Attached to SLBs. Previous work indicates that SLBs formed from 9:1 mixtures of DMPC and DMPG are associated with a negative charge density

Table 4.2. Summary of Estimates for Charge Densities (σ) and Apparent Equilibrium Constants Yielded from Different Adsorption Models

		GC+Langmuir	GC+Hill	TL+Langmuir[a]	TL+Hill[a]
$PDADMAC_{400}$	K [M^{-1}]	1.3 (± 0.5) × 10^9	9.5 (± 6.1) × 10^8	2.6 (± 0.4) × 10^9	2.3 (± 0.6) × 10^9
	σ [C/m^2]	0.25 ± 0.09	0.30 ± 0.15	0.32 ± 0.19	0.24 ± 0.23
	n	–	0.92 ± 0.09	–	1.24 ± 0.22
	χ^2	2.49 × 10^{-4}	2.20 × 10^{-4}	6.28 × 10^{-4}	6.27 × 10^{-4}
$PDADMAC_{100}$	K [M^{-1}]	3.5 (± 1.3) × 10^8	2.3 (± 2.1) × 10^8	6.4 (± 0.7) × 10^8	5.7 (± 1.2) × 10^8
	σ [C/m^2]	0.20 ± 0.06	0.28 ± 0.18	0.24 ± 0.05	0.20 ± 0.08
	n	–	0.92 ± 0.14	–	1.1 ± 0.16
	χ^2	2.00 × 10^{-4}	1.96 × 10^{-4}	2.12 × 10^{-4}	1.65 × 10^{-4}
PVAm	K [M^{-1}]	9.6 (± 49) × 10^7	1.7 (± 0.7) × 10^8	2.8 (± 0.6) × 10^8	1.8 (± 0.1) × 10^8
	σ [C/m^2]	0.11 ± 1.0	0.16 ± 0.15	0.47 ± 0.27	0.30 ± 0.05
	n	–	2.3 ± 1.0	–	2.9 ± 0.3
	χ^2	9.9× 10^{-3}	1.74 × 10^{-3}	7.69× 10^{-3}	1.17 × 10^{-3}
PLL	K [M^{-1}]	1.2 (± 1.3) × 10^7	2.6 (± 2.1) × 10^7	1.6 (± 0.7) × 10^7	2.8 (± 2.1) × 10^7
	σ [C/m^2]	0.35 ± 0.35	0.18 ± 0.20	0.17 ± 0.42	0.08 ± 0.34
	n	–	1.6 ± 0.76	–	2.2 ± 1.3
	χ^2	3.54 × 10^{-4}	2.52 × 10^{-4}	8.21 × 10^{-4}	2.78 × 10^{-4}
PLR	K [M^{-1}]	4.4 (± 0.5) × 10^7	2.8 (± 1.4) × 10^7	3.4 (± 0.8) × 10^7	3.6 (± 0.3) × 10^7
	σ [C/m^2]	0.17 ± 0.02	0.24 ± 0.08	0.23 ± 0.26	0.24 ± 0.20
	n	–	0.89 ± 0.08	–	1.28 ± 0.05
	χ^2	4.08 × 10^{-5}	4.40 × 10^{-5}	2.00 × 10^{-4}	3.00 × 10^{-5}

[a] C_2 assigned a value of 0.2 F/m^2

(-0.11 ± 0.06 C/m^2).[38] Accounting for this charge density, and using Equation 2.13, we estimate the total interfacial charge densities listed in Table 4.1 (Figure 4.6). Specifically, the charge densities reported in Table 4.1 are the charge densities for the adlayers after accounting for the charge density of the SLB (σ_{ads} in Equation 2.13). PDADMAC (Figure 4.6A, 4.6B) and PLR (Figure 4.6E) appear to bind to a large extent, reversing the surface charge of the lipid bilayer. Unfortunately, considerably large errors on the estimated charge densities of PLL (Figure 4.6D) and PVAm (Figure 4.6C) prevent us from drawing further conclusions on whether adsorption to SLBs formed from 9:1 DMPC/DMPG results merely in charge neutralization or if the surface charge is indeed reversed. These results are in line, at least in part, with previously published studies employing atomistic-level MD simulations which show that some polycations neutralize or cause overcharging of lipid bilayers composed from 4:1 mixtures of phosphatidylethanolamine and PG lipids.[30] In these simulations, accumulation of chloride ions at the Helmholtz plane suggests that poly(vinylamine), PEI, and PLL overcharge the membrane surface upon adsorption. Further, adsorption of poly(vinylamine) to PG-containing phospholipid bilayers can (1) cooperatively accumulate Na^+ ions and (2) induce the reorientation of water molecules at the membrane surface.[30]

We assume that $\chi^{(3)}$, which accounts for the net orientation of water molecules polarized due to the presence of a charged interface, remains constant over the course of our experiments. Given that SHG signal intensity is proportional to the square modulus of the SHG *E*-field, and the number of water molecules present remains constant throughout, the reorientation of water molecules upon interfacial overcharging is not captured in these measurements.

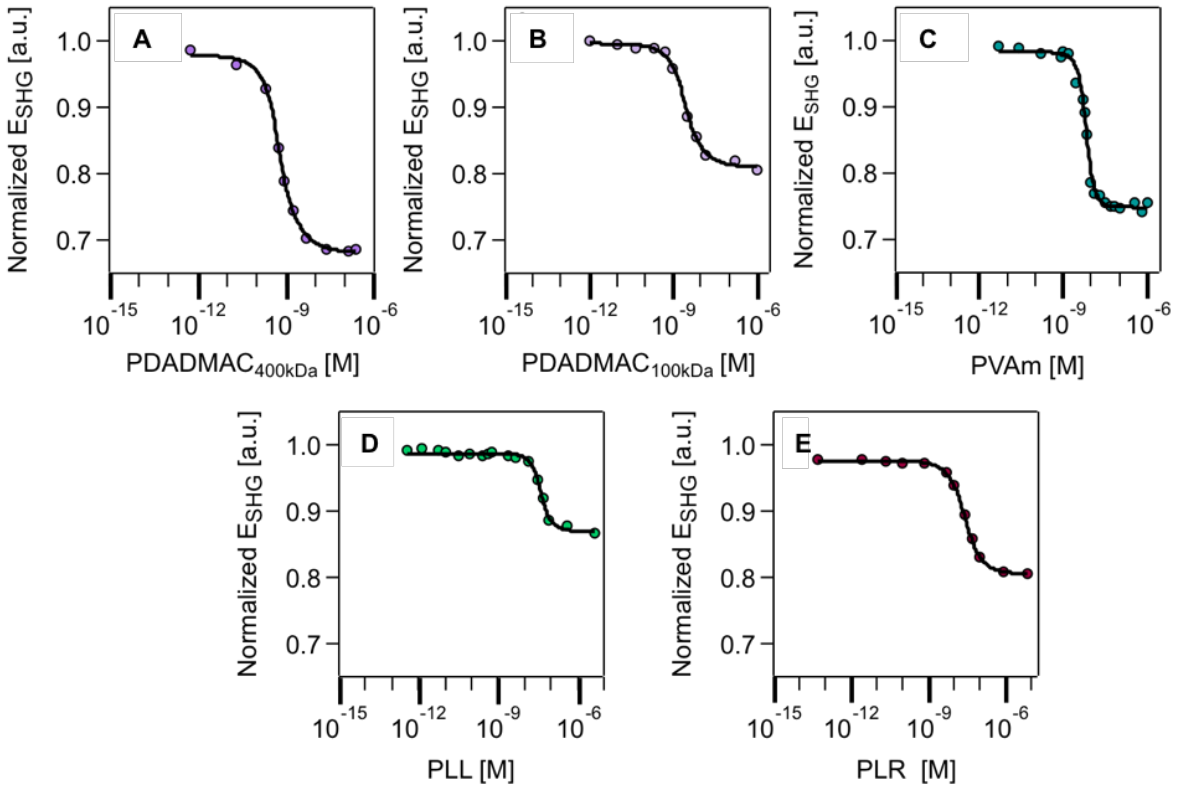

Figure 4.6. Normalized SHG *E*-field as a function of polymer concentration, in molarity, at 0.1 M NaCl, 0.01 M Tris, pH 7.4 for (A) $PDADMAC_{400}$, (B) $PDADMAC_{100}$, (C) PVAm, (D) PLL, and (E) PLR. SHG *E*-field is normalized to the SHG *E*-field associated with the supported lipid bilayer formed from 9:1 DMPC/DMPG prior to exposure to polymer. Each individual adsorption isotherm is shown with the corresponding fit with the combined Hill/Gouy-Chapman equation (black solid line).

As a complement to the charge densities, and to provide additional insight into the adsorption properties of the polycations explored herein, QCM-D experiments were conducted under the same experimental conditions (0.1 M NaCl, 0.01 M Tris buffer, pH 7.4). QCM-D mass measurements yield the acoustic mass associated with polymer adsorption (which contains dynamically coupled solvent) to SLBs from which we estimate the number of polymer chains associated with the bilayer and the degree of ionization. Using the acoustic mass data from QCM-D measurements, and assuming that 30% of the sensed mass adsorbed is due to mass contributions from coupled water molecules,[50] we estimate number densities (in terms of polymer density per square centimeter) on the order of 10^{11}–10^{13} polymers/cm^2 corresponding to approximately 10^{14} charges/cm^2 (Table 4.1), again given the caveat that not all charges associated with the adsorbed polycations may be captured in the SHG-active interfacial region. Previous studies using colorimetric assays have reported a minimum surface charge density on the order of 10^{15}–10^{16} positive charges per square centimeter required for effective antibacterial activity.[9] Here, our adsorbed film charge densities are just below those values.

Combining the charge densities from our SHG experiments with the estimates for polymer mass density from the QCM-D measurements, and assuming again that ~30% of the associated mass is attributed to water molecules associated with the adsorbed polymer, we find that 7%, 20%, 30% of the ionizable groups of PVAm, PLL, and PLR are charged, respectively, under the conditions of our experiments, provided that each amine group is available to participate in binding to the membrane surface and is sensed in the SHG active interfacial region. These results show that PVAm is associated with the lowest degree of ionization of any of the polymers explored herein. At pH 7.4, PVAm is expected to be approximately 50–70% ionized[51] but ionization depends strongly on the extent of hydrolysis.[52] Given the previously discussed

caveats, and the uncertainty in the percent of acoustic mass attributable to polymer alone (i.e. excluding contributions from hydryodynamically coupled water molecules), we have also provided estimates for percent ionization and polymer number density with water contents ranging from 1-70% of the acoustic mass. (Figure 4.7)

In addition to the result regarding PVAm discussed above, PDADMAC also appears to have a smaller fraction of charged groups than expected. This result is consistent with reports that polymers containing quaternary ammonium functional groups interact only weakly with lipid membranes[42] and points towards the special role that contact ion pairing, or counter ion condensation, may play in this case. Though, it should be considered that each of the polymers will have different interactions with water and will therefore likely have different degrees of hydration. Without estimates for mass densities that exclude water, we cannot account for these differences here.

4.4. Conclusions. Polyelectrolyte charge density is thought to be critically important for the function of many engineered and naturally occurring systems, including spherical nucleic acids, antimicrobial surfaces, nonviral vectors, and in the formation of films and gels. However, concrete – as opposed to hypothetical – interfacial charge density data have been difficult to obtain, largely because of a lack of label-free, surface specific measurement techniques that can provide electrostatic information at buried aqueous/solid interfaces. As an important first step towards understanding how charge density correlates to the formation of these complex assemblies, we have presented here an experimental tool that pairs QCM-D with nonlinear optical spectroscopy, specifically, SHG that is used to estimate the charge densities of the adsorbed layers formed on supported lipid bilayers. These studies are important not only for the

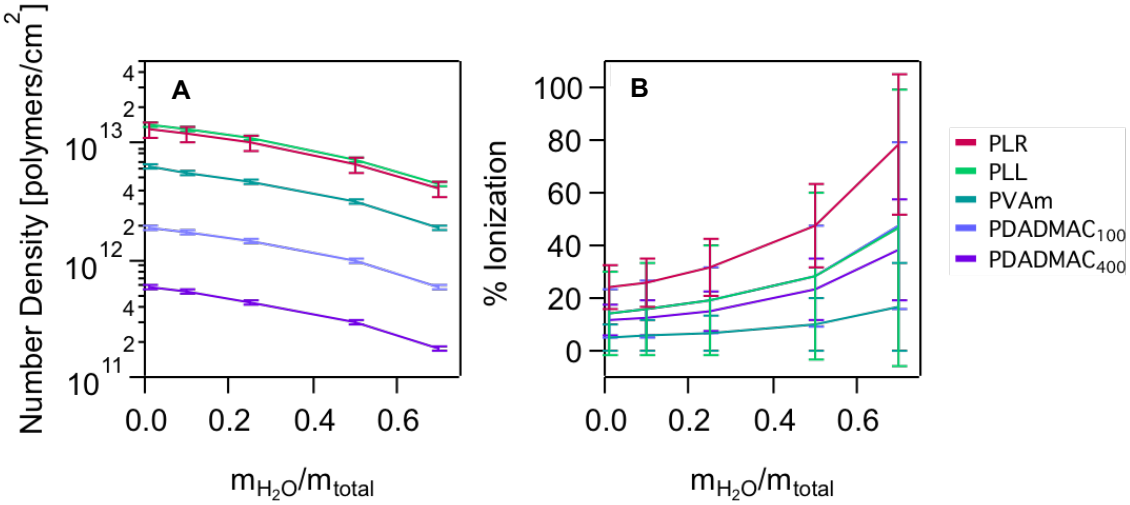

Figure 4.7. (A) Number density expressed as polymers/cm^2 and (B) percent of ionization (the number of ionizable groups carrying charge under these conditions) as a function of the fraction of total acoustic mass that is attributable to the mass of water.

study of the interactions of polyelectrolytes and model membranes but also in the study of similarly formed thin films and polymer-cushioned SLBs.[53-57]

Using surface charge densities determined using the SHG Eisenthal $\chi^{(3)}$ method and the attached mass from the QCM-D experiments, we estimate the number of charges associated with a polyelectrolyte attached to a lipid bilayer. These polyelectrolytes include poly(vinylamine hydrochloride), poly(diallyldimethylammonium chloride), poly-L-lysine hydrobromide, and poly-L-arginine hydrochloride. Through these studies, we have begun to explore a structure-charge density relationship that compares the various polycations and their subsequent interactions with idealized model bilayers. We find that upon accounting for the number of positive charges associated with each polyelectrolyte, the free energies of adsorption are comparable despite differences in molecular masses and functionalities. Further, these results provide information regarding the role of electrostatics in these interactions, but also indicates that other interactions are important to polyelectrolyte/membrane interactions. Future work will focus on polyelectrolytes with tunable polyelectrolytes that can be systematically altered to yield better control over the number of associated positive charges. In Chapter 5, we will further build on this approach and discuss the connections that can be made to atomistic molecular dynamics simulations when employing polyelectrolytes on shorter length scales.

CHAPTER 5

Counting Charges on Membrane-bound Peptides

Portions of this chapter are reproduced with permission from the Royal Society of Chemistry:

A. C. McGeachy,[†] E. R. Caudill,[†] D. Liang,[†] Q. Cui, J. A. Pedersen and F. Geiger, Counting Charges on Membrane-bound Peptides, *Chem. Sci.*, 2018, **9**, 4285-4298.

[†]ACM, ERC, and DL contributed equally to this work.

5.1. Introduction. As discussed in Chapter 4, polymers and peptides and their interactions with biological and engineered membranes are of relevance in a number of applications. Cell penetrating peptides containing cationic amino acids such as arginine and lysine can be used to cross cell membranes[1] and deliver compounds to the cell interior by exploiting the surface charge of biological membranes.[2] Small peptides also provide an opportunity to probe how short segments of polycations may interact with surfaces, with direct relevance to understanding how engineered nanomaterials, often manufactured with polycationic wrappings, interact with their environment.[3,4] Despite the importance of charge density in these cases, a need remains to quantify polypeptide/membrane interactions from a perspective of the number of charge present at interfaces and the extent to which these charges are subject to contact ion pairing or pK_a shifts.[5-7] Indeed, the ability to "count" the number of charges on peptides attached to solid or soft matter surfaces, especially in a label-free fashion, would represent a significant step towards understanding, controlling, and predicting peptide-surface interactions. However, doing so requires reliable estimates of (i) surface coverage and (ii) surface charge, both of which are notoriously difficult parameters to obtain at solid/water interfaces, especially if one wishes to avoid complications commonly associated with the use of external labels.

Recent mechanistic studies pairing molecular dynamic simulations and fluorescence assays have shown that arginine nonamers bind to lipid bilayers with a higher degree of cooperativity than do lysine nonamers,[6] possibly explaining the cell-penetrating effectiveness of peptides containing arginine groups.[1] Other studies of peptide interactions with lipid bilayers and cellular surfaces have reported on concomitant structural[8-11] and electrostatic potential changes.[6,12,13] The recent work by Cremer and co-workers employed a pH-sensitive fluorescence assay to provide qualitative and semi-quantitative information about the binding of lysine and

arginine nonamers to supported lipid bilayers formed from zwitterionic (phosphatidylcholine, PC) and negatively charged (phosphatidylglycerol, PG) lipids on the basis of changes in local proton concentration upon nonamer adsorption.[6] However, the surface charge density of the bilayer and those of the attached oligomers was not provided. To this end, the mass of the attached peptides and the interfacial charge density are necessary, albeit elusive, parameters which we focus on here.

Our present work combines estimates of interfacial mass with nonlinear spectroscopic studies of interfacial electrostatics and atomistic simulations of octamers of lysine (Lys_8) and arginine (Arg_8) interacting with supported lipid bilayers used as idealized model systems mimicking some aspects of biological membranes (see Figure 4.1 for peptide structures). These peptides are amenable to investigations by atomistic computer simulations, which we employ to obtain further mechanistic information on the peptide-bilayer interactions.

We quantify attached mass using acoustic and optical sensing techniques which are commonly used to monitor the adsorption of biomacromolecules to surfaces,[14-19] including cell surface models.[20-23] Quartz crystal microbalance with dissipation (QCM-D) monitoring is used to obtain the acoustic mass of the attached oligomers (including the mass of dynamically coupled water).[15] Simultaneous optical sensing by localized surface plasmon resonance spectroscopy (LSPR) yields estimates of the optical (solvent-free) mass of adsorbed species. Using this combined acoustic and optical sensing approach, we report on the water contents of oligomer films adsorbed to the supported lipid bilayer surface. The interfacial charge density and potentials and free adsorption energies are estimated by second harmonic generation spectroscopy (SHG), specifically using the Eisenthal $\chi^{(3)}$ method, as described in Chapters 2 and 4 and discussed elsewhere.[24,25] Analysis of electrostatic potential and charge distribution from

atomistic simulations helps evaluate mean-field models (e.g., Gouy-Chapman)[26] which are commonly used to map surface potential through the Eisenthal $\chi^{(3)}$ method to an apparent surface charge density, when the interface is rough at the molecular scale.

5.2. Experimental Methods.

5.2.1. Oligopeptide and Lipid Vesicle Preparation. Lys_8 and Arg_8 were synthesized by and purchased from GenScript (Piscataway, NJ, purity ≥ 98%). Powders of Lys_8 and Arg_8 were stored in sealed plastic vials at –20 °C prior to use and were used without further purification. Powders (~50 mg) were dissolved in 50-100 μL of ultrapure water (>18 MΩ·cm; GenPure Pro or Millipore, Thermo Scientific) containing 0.001 M NaCl and vortexed, producing solutions with concentrations on the order of hundreds of mM. Lower concentrations were achieved through serial dilution. These stock solutions were then covered with Parafilm and stored in glass vials or microcentrifuge tubes at 4 °C. Immediately before use, the appropriate volume of oligomer solution was diluted to the desired concentration in 0.1 M NaCl buffered to pH 7.4 with 0.01 M Tris.

Small unilamellar vesicles were prepared at 9:1 molar ratios from 1,2-dimyristoyl-*sn*-glycero-3-phosphocholine (DMPC, Avanti Polar Lipids) and 1,2-dimyristoyl-*sn*-glycero-3-phospho-(1'-rac-glycerol) (sodium salt) (DMPG, Avanti Polar Lipids) as described in Chapters 3 and 4. Here, we use Method 2 described in Chapter 4 for reconstituting lipid films, preparing lipid vesicles, and forming SLBs for study by SHG spectroscopy. For reference, all experiments described in the remainder of this chapter employed solutions buffered to pH 7.4 with 0.01 M Tris in the presence of 0.1 M NaCl.

5.2.2. Determination of Lys_8 and Arg_8 Surface Mass Densities. Acoustic sensing techniques, like QCM-D, are commonly used as quantitative tools for monitoring the adsorption of

polymers,[22,23,27] to supported lipid bilayers and cellular membranes.[28,29] While QCM-D reports on acoustic masses, which includes the mass of the adsorbed oligomer along with dynamically coupled water associated with the oligomer, and provides insight on viscoelasticity, other techniques based on nanoplasmonic sensing (NPS)[30] can be used to report on the dry mass of adsorbed species.[15] NPS relies on, and is sensitive to, changes in local refractive index of the localized surface plasmon resonance produced by illumination of noble metal nanoparticles.[31] Through this combination of experimental tools, we provide lower estimates for the amount of dynamically coupled water molecules captured in QCM-D measurements. Specific details about QCM-D and LSPR experimental methods and details about data analysis are described elsewhere.[32]

QCM-D measures changes in the resonance frequency (Δf_v) and energy dissipation (ΔD_v) of the fundamental frequency and odd harmonics (v = 3–11) of a (coated) AT-cut piezoelectric quartz crystal caused by interaction with an analyte.[33] The acoustic mass sensed by QCM-D includes the mass of the analyte and that of any dynamically coupled solvent. For rigidly coupled adlayers (taken as those with $\Delta D_v/(\Delta f_v/v) << 0.4 \times 10^{-6}$ Hz^{-1}),[34] the acoustic surface mass density ($\Delta\Gamma_{\text{QCM-D}}$) can be estimated here for the supported lipid bilayers from the Sauerbrey relation:[34, 35]

$$\Delta\Gamma_{QCM-D} = -C\frac{\Delta f_v}{v} \qquad 5.1$$

where C is the mass sensitivity constant (18 ng·cm^{-2}·Hz^{-1} at the fundamental frequency, f_1 = 4.95 MHz used here) and depends on the properties of the quartz crystal. In the present study, the Sauerbrey relation was used to estimate acoustic surface mass densities of the supported lipid bilayers and the octapeptide adlayers on the Si_3N_4-coated sensors. For more dissipative (i.e., $\Delta D_v/(\Delta f_v/v) > 0.4 \times 10^{-6}$ Hz^{-1}), laterally homogeneous adlayers (in this study, the octapeptides on

the supported lipid bilayers), acoustic mass can be estimated from the frequency and dissipation response for multiple harmonics using a Kelvin-Voigt model.[34,36]

5.3. Results and Discussion

5.3.1. Peptide Mass Adsorbed to Bilayers Formed from 9:1 DMPC/DMPG. As discussed above, we use a combined QCM-D and NPS setup to examine the initial rates of Lys_8 and Arg_8 attachment to supported lipid bilayers formed from 9:1 DMPC/DPMG, the surface mass densities of octapeptides adsorbed onto the supported lipid bilayers, and the extent of reversibility (Figure 5.1). QCM-D and LSPR experiments were carried out by Emily Caudill, who is advised by Joel Pedersen, at the University of Wisconsin-Madison. We find that the initial rate of octapeptide attachment to bilayers formed from 9:1 DMPC/DMPG, as well as, the maximum acoustic and optical surface mass densities attained by Arg_8 are larger than those of Lys_8. The maximum optical surface mass densities of Lys_8 and Arg_8 correspond to $3 \pm 0.3 \times 10^{16}$ and $5.7 \pm 0.63 \times 10^{16}$ molecules per m^2.

LSPR measurements indicate that dynamically coupled water contributes considerably to the overall acoustic mass estimated by QCM-D for both peptides. In fact, a comparison of the acoustic and optical surface mass densities for Lys_8 and Arg_8 reveals that 83 ± 11 % and 93 ± 3 % of the acoustic masses reported in our QCM-D measurements is attributable to dynamically coupled water. Studies that employ both acoustic and optical sensing techniques find similarly high water contents for amino acids or amino acid-rich polymers adsorbed to surfaces.[37,38] The large number of coupled water molecules associated with the highly charged Arg_8 is likely a consequence of solvation effects which help to stabilize Arg-Arg pairs at the interface.[39]

5.3.2. Interfacial Free Binding Energy and Cooperativity. SHG adsorption isotherms for Lys_8 and Arg_8 were recorded by exposing supported lipid bilayers formed from 9:1 DMPC/DMPG to

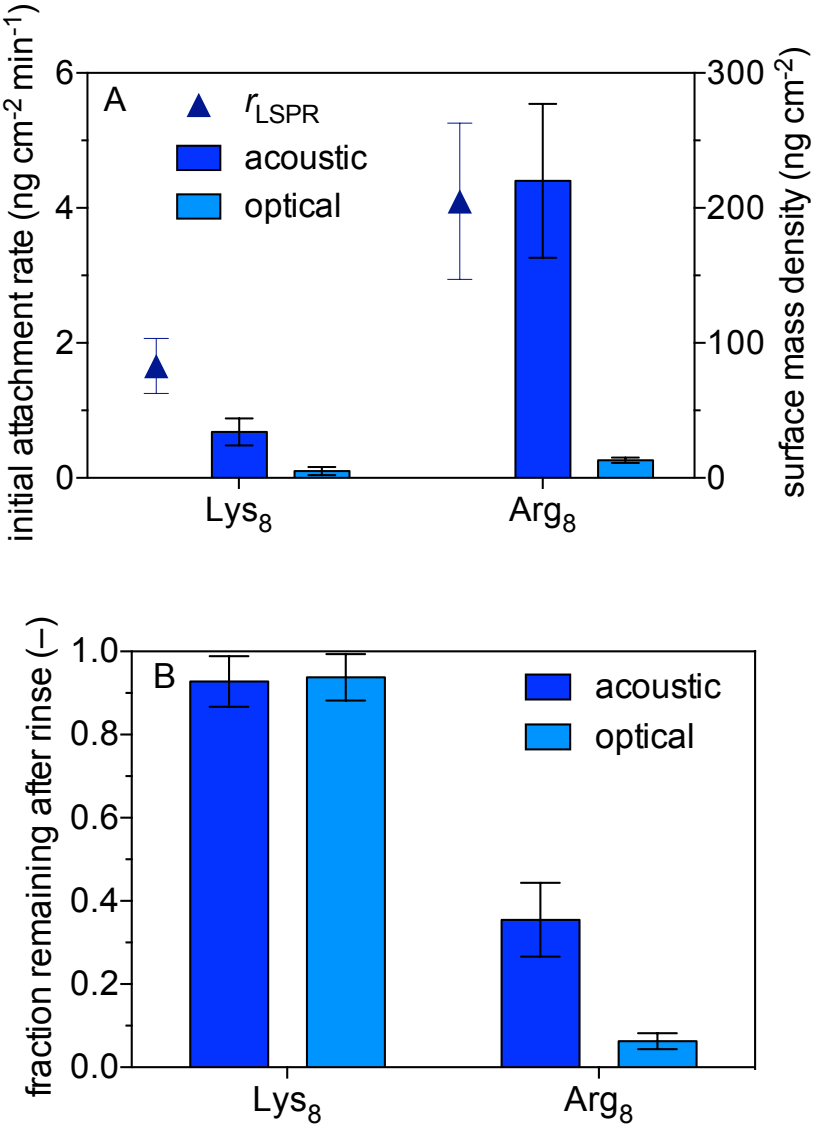

Figure 5.1. Attachment of octamers of lysine (Lys_8) and arginine (Arg_8) to supported lipid bilayers formed from 9:1 DMPC/DMPG. (A) Initial attachment rates and maximum acoustic and optical surface mass densities. The initial attachment rates were based on optical masses calculated from localized surface plasmon resonance data. (B) Acoustic and optical surface mass densities after 10 min rinse with oligomer-free solution (0.1 M NaCl Tris buffer). Error bars represent one standard deviation of triplicate measurements.

increasingly higher concentrations of the respective octamers. An expected outcome of these surface potential-sensitive SHG experiments is that the observed SHG signal intensity decreases as the concentration, and thus the surface coverage, of the cationic Lys_8 and Arg_8 increases. Figure 5.2.A and 5.2.B shows that this response is indeed observed. Moreover, we observe a nearly 10% larger decrease in the SHG *E*-field in the case of Arg_8 than Lys_8, suggesting that the adsorption of Lys_8 results in a smaller change in interfacial potential than Arg_8. These observations are in line with previous experimental[6] and theoretical[40] studies of these systems, which indicate that the interfacial potential (i.e., surface charge) does indeed decrease (becoming more positive) upon exposure to lysine and arginine oligomers.

Over the timescales of our experiments, Lys_8 and Arg_8 interaction with the bilayer is partially reversible, as determined by SHG reversibility studies (Figure 5.2.C) and confirmed by QCM-D/LSPR mass estimates during and after exposure to peptides. Yet, we cannot rule out that at $t = \infty$, the binding events are fully reversible. We therefore analyzed our adsorption isotherms, described next, with the caveat that full reversibility is not observed over the timescales of our experiments.

We fit our SHG adsorption isotherms using the combined Gouy-Chapman and Hill models which we have also apply in Chapter 4 to obtain estimates of apparent equilibrium constants, charge densities, and Hill coefficients. The latter parameter describes the degree of cooperativity (or the lack thereof) as discussed in detail in Chapter 2. While our isotherms approach surface saturation, due to the limited amounts of peptide available to us, complete saturation is not reached. Fitting these datasets results in large errors in the apparent equilibrium constants and charge densities likely because of difficulty achieving sufficiently high concentrations (>0.01 M) in our SHG experiments. However, prior literature indicates that

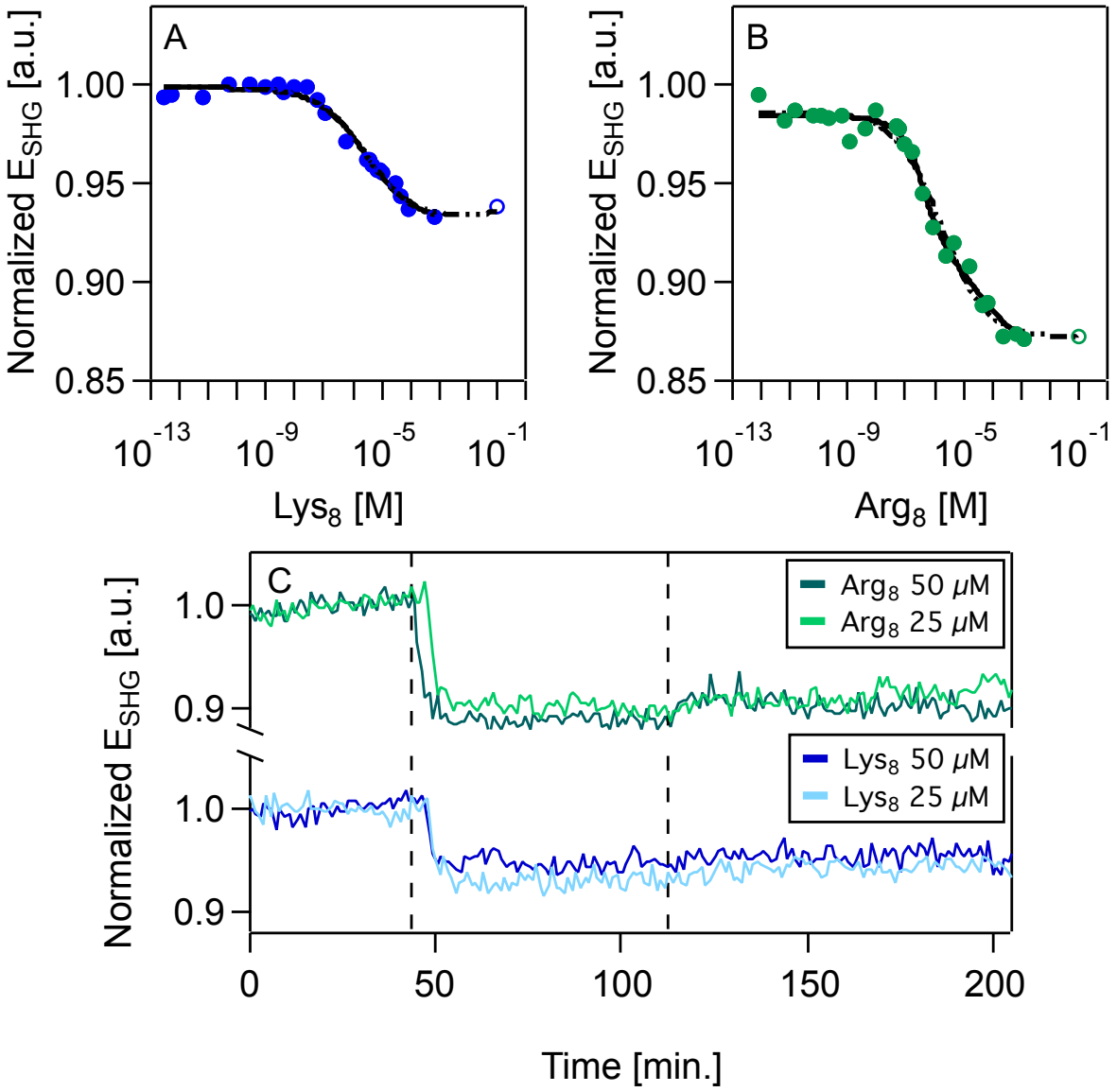

Figure 5.2. Normalized SHG E-field as a function of polymer concentration, in molarity, at 0.1 M NaCl, 0.01 M Tris, pH 7.4 for (A) Lys_8 and (B) Arg_8. Data sets include an extrapolated data point (shown as an open circle) that is the average of the last three measured data points. SHG E-field is normalized to that associated with the supported lipid bilayer formed from 9:1 DMPC/DMPG prior to exposure to oligomers. Each individual adsorption isotherm is shown with the corresponding fit with the combined Hill/Gouy-Chapman equation applied to the acquired data (black solid line) and complete data set with extrapolated data point (dashed black line). (C) Normalized SHG E-field as a function of time in the presence of supported lipid bilayers formed from 9:1 DMPC/DMPG for 25 μM and 50 μM octapeptide concentrations at 0.1 M NaCl, 0.01 M Tris, pH 7.4. At $t = 0$, the supported lipid bilayer is unperturbed and the SHG signal is monitored at 0.1 M NaCl. At $t = 43$ min, oligomer solution is introduced into the flow cell and at $t = 112$ min the flow cell is rinsed with oligomer-free solution composed of otherwise identical composition.

saturation coverage is reached in the mM peptide concentration regime.[6,41] We therefore analyzed the SHG adsorption isotherms by including one extrapolated SHG signal point at 0.1 M peptide concentration which was determined by averaging the three data points at the highest peptide concentrations achieved experimentally. This approach yielded similar point estimates relative to the ones obtained from fitting the isotherms while excluding the SHG signal intensity estimated for 0.1 M peptide concentration as discussed below.

In contrast to the study by Cremer and co-workers,[6] who reported significant differences in the cooperativity of adsorption of Lys_9 (n = 0.22) and Arg_9 (n = 0.73) to lipid bilayers formed from 9:1 molar ratios of 1-palmitoyl-2-oleoyl-*sn*-glycero-3-phosphocholine (POPC) and 1-palmitoyl-2-oleoyl-*sn*-glycero-3-phospho-(1′-*rac*-glycerol) (sodium salt) (POPG) (and 0.5 mol% *ortho*-rhodamine B which impacted at least Arg_9 to POPC bilayers), we find comparable Hill coefficients of ~0.5 (Table 5.1) for Lys_8 and Arg_8. This result suggests that the adsorption process is not cooperative for either octapeptide. The large Hill coefficient reported by Cremer and co-workers for Arg_9 may be attributable to differences in bilayer fluidity between POPC/POPG and the addition of *ortho*-rhodamine B studied in their work in contrast to the label-free DMPC/DMPG system used here. The authors speculated that the inability of the lysine peptide to penetrate the lipid headgroup region could contribute to the apparent anti-cooperativity of lysine.[6] However, we note that lower n values may also be explained by molecular heterogeneity where the experimentally derived binding curve is actually composed of an ensemble of individual binding curves.[42] Indeed, such heterogeneity could arise from a number of factors including those introduced by differences in bilayer phase (liquid *versus* gel crystalline phases) and propensity and favorability of the octamers to bind to PC and/or PG lipid headgroups.

Table 5.1. Summary of Experimental Data for Arg_8/Lys_8

	binding constant K_{ads} [$\times 10^6$ M^{-1}]	adsorption free energy ΔG_{ads} [kJ/mol]	surface charge density σ [C/m^2]	Hill coefficient n	acoustic[a] and optical mass density [ng/cm^2]	% ionization
Arg_8	1.6 ± 0.4	− 45 ± 1	0.10 ± 0.02	0.54 ± 0.09	210 ± 56, 13 ± 2	~100
Lys_8	1.0 ± 0.3	− 44 ± 1	0.12 ± 0.03	0.52 ± 0.09	34 ± 10, 5 ± 3	~100

[a]Maximum adsorbed acoustic mass at from viscoelastic modeling of 7th, 9th, 11th harmonics prior to rinsing with peptide-free buffer.

Previous studies by McLaughlin and co-workers have reported that the incremental increase in the free energy of adsorption upon elongating Lys oligomers by one Lys residue is approximately –5.9 kJ/mol per residue (similar results were noted for arginine).[41,43] We therefore expect free binding energies of –5.9 kJ/mol × 8 = –47.2 kJ/mol for our octamers. Our experiments show the binding energy estimate from the isotherms is –44 ± 1 kJ/mol and – 45 ± 1 kJ/mol for Lys_8 and Arg_8, respectively. Moreover, recently published molecular dynamics (MD) simulations exploring the binding of Arg monomers to PC-lipid monolayers report similar binding free energies (–43.8 kJ/mol). As the comparison to McLaughin's data shows, the octamers attached without much noticeable cooperativity or anti-cooperativity (2 kJ/mol[1] destabilization for the octamers vs. the purely additive expectation value) in terms of the free energy of adsorption. We therefore interpret the Hill coefficients from our fits (0.5) to indicate not anti-cooperativity but instead structural heterogeneity at the interface (as observed in atomistic molecular dynamics simulations, see below), a common alternate reason for Hill coefficients smaller than unity.[42,44]

5.3.3. Interfacial Charge Densities and Number of Charges per Attached Peptide. Fitting SHG adsorption isotherms yields charge density estimates for Lys_8 and Arg_8 of 0.12 ± 0.03 C/m^2 and 0.10 ± 0.02 C/m^2, respectively. A sensitivity analysis shows that the approach is robust, as varying the value of the SHG intensity estimated for the 0.1 M peptide concentrations by 10% results in comparable charge densities, ranging from 0.02 – 0.16 C/m^2 and 0.02 – 0.2 C/m^2 for Lys_8 and Arg_8, respectively (Figure 5.3). Based on our previous estimates for the charge density of supported lipid bilayers formed from 9:1 DMPC/DMPG on fused silica (–0.1 C/m^2),[45,46] Lys_8 and Arg_8 attachment to the bilayers appears to result in charge neutralization.

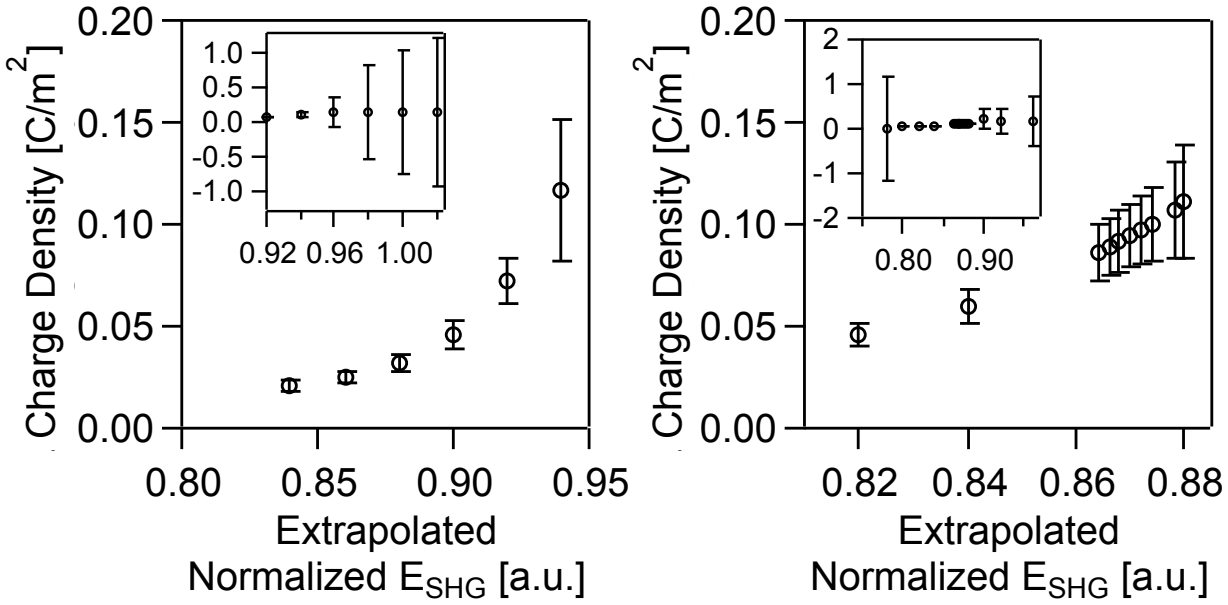

Figure 5.3. Charge density of Lys_8 (left) and Arg_8 (right) adsorbed to an SLB formed from 9:1 DMPC/DMPG as a function of the normalized SHG E-field used for the extrapolated data point at 0.1 M NaCl. Insets are a zoomed-out view of the same data to highlight the large errors associated with charge density values at higher and lower extremes for the extrapolated signal intensity at 0.1 M octamer concentrations.

Using the calculated charge densities from our SHG adsorption isotherms and the mass estimates derived from QCM-D and LPSR measurements, we provide the lower and upper limits for the fraction of ionizable groups that remain charged upon adsorption to the membrane. Optical mass estimates correspond to surface coverages of about 10^{16} peptides (both Lys_8 and Arg_8) per m^2, or 0.04 ± 0.02 C/m^2 and 0.08 ± 0.01 C/m^2 for Lys_8 and Arg_8, respectively, assuming they are fully (eight-fold) charged. Our estimates of charge densities from the LSPR data (0.04 ± 0.02 C/m^2), assuming the attached peptides are fully ionized, and the SHG experiments (0.12 ± 0.03 C/m^2) vary by a factor of about 3 for Lys_8. In the absence of more reliable point estimates for the interfacial charge densities obtained from fitting Equation 2.13 to the SHG adsorption isotherms, we cannot comment further on this difference. Taken together though, the charge density estimates from LSPR and SHG suggest that attached Lys_8 and Arg_8 are fully ionized under our experimental condition, consistent with their high bulk solution pK_a value.[47]

5.3.4. Bound Conformations of Peptides and Interfacial Electrostatics from Atomistic Simulations. The following work was completed by Dongyue Liang who is advised by Qiang Cui (Boston University). To complement and provide additional insights for the experimental results, we performed MD simulations to explore Lys_8 and Arg_8 adsorption to lipid bilayers formed from DMPC and 9:1 DMPC/DMPG. While each Lys_8 peptide is most likely to bind with the bilayer through one or two sidechains with the bilayer, which is qualitatively similar to observations from previous atomistic MD simulations,[40] Arg_8 is most likely to attach to the bilayer *via* 3-5 binding sidechains (Figure 5.4). Mass density and binding site distributions suggest that Arg_8 tends to interact more strongly with lipid bilayers than Lys_8, especially in the presence of anionic lipids which is in agreement with the conclusions drawn from other studies.[43]

Examination of these snapshots also reveals stacking of Arg sidechains[48] from either the same peptide or neighboring peptides, and association of Arg_8 mediated by the C-terminal carboxylate group, as discussed in recent studies.[49-51] These observations indicate that while Lys_8 is inclined to "stand-up" on the surface, Arg_8 is likely to assume a "buried" conformation, as also evident from the mass density distribution.

An explicit binding free energy simulation of Arg_8/Lys_8 to the lipid bilayers was not pursued here. Considering the diverse binding modes of the peptides observed in the unbiased atomistic simulations, it is not straightforward to identify a simple collective variable (e.g., the center-of-mass separation of the peptide and bilayer) that defines the bound state of the peptide while ensuring an extensive sampling of distinct peptide conformations. Nevertheless, mass density and binding site distributions suggest that Arg_8 tends to interact more strongly with lipid bilayers than Lys_8, especially in the presence of anionic lipids[32] which is in agreement with the conclusions drawn from other studies.[43] The similar apparent binding free energies for Arg_8 and Lys_8 obtained in our SHG studies likely reflects the notion that the probe depth in our SHG studies is on the order of several nanometers under the specific salt concentration, thus the amount of "bound" peptides may have included those in the interfacial region that are only weakly associated with the bilayer. Yet, we caution that the distance dependence in the SHG signal generation process from charged interfaces, which is subject to phase matching, is only now beginning to be understood.[25,52-54,69]

Despite a considerable number of peptides adsorbed on the lipid bilayer, the net charge distribution at the interface is rather small (the integrated charge density is less than 0.01 C/m^2), due to the strong charge compensation by the salt ions and also oriented water molecules. This observation is qualitatively consistent with the SHG estimated charge density, although a direct

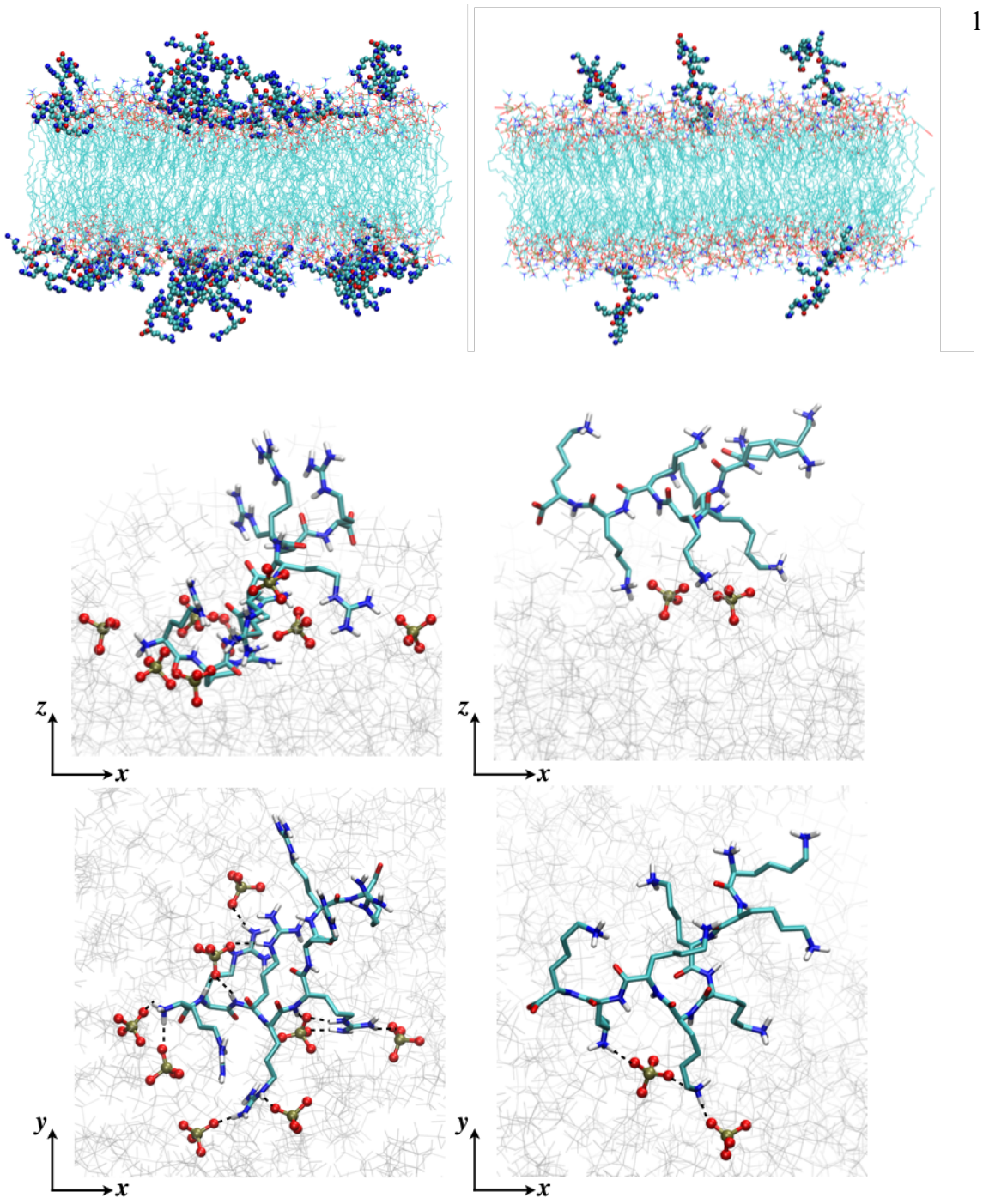

Figure 5.4. Snapshots from MD simulations (Arg_8/Lys_8 interacting with a 9:1 DMPC/DMPG bilayer) illustrate the different binding modes of the peptides. The left column is for Arg_8, and right column for Lys_8. The top two rows are sideviews (showing multiple peptides and a single peptide, respectively), which illustrate that due to the different numbers of sidechains interacting with the lipids, Lys_8 peptides tend to point into the solution, while Arg_8 peptides lay closer to the membrane. The bottom row contains the top view of close-ups of the binding interactions; while Arg_8 are engaged with multiple phosphate groups (those within 3 Å from Arg_8 are shown in CPK), only a few lipid phosphate groups interact with the Lys sidechains.

comparison is difficult since the adsorption densities in the simulation and experiment likely differ.

The microscopic simulations also provide an opportunity to evaluate the relationship between electrostatics (e.g., surface potential) and charge distribution in the interfacial region. In particular, we are interested in the quantitative accuracy of the Gouy-Chapman model,[26] which is widely used to map the measured interfacial electrostatic potential to an apparent surface charge density. In the Gouy-Chapman model, the solvent is treated as a dielectric continuum with the bulk dielectric constant and considers the electrostatic interaction between only the surface charge and salt ions. Such approximations are unlikely to be valid for the lipid-water interface, where water molecules are known be strongly oriented and thus contribute significantly to interfacial electrostatics.[55,56]

Since systems with adsorbed peptides exhibit significant heterogeneity in the mass and charge distributions in the *x,y* dimensions (e.g., see Figure 5.4 top row), it is not straightforward to define an interface and conduct electrostatic analysis. Thus, we focus our electrostatic potential analysis on the 9:1 DMPC/DMPG system without any peptides. Due to preferential orientation of water at the interface, the integrated charge density from the lipid center to a given distance along the membrane normal (z) has considerable contributions from water (Figure 5.5 top panel). As a result, the average electrostatic potential at the interface, $\phi(z)$, exhibits a strong compensation between interfacial water molecules and membrane/ions (Fig. 5.5 middle panel). Fitting the electrostatic potential (ϕ) and integrated surface charge density (σ) for a series of z values to the Grahame equation leads to an apparent dielectric constant of 27 for the solvent at the bulk water/lipid bilayer interface. This value is considerably less than the bulk dielectric constant for water (~78 at 300 K), which is expected due to the preferential orientation for

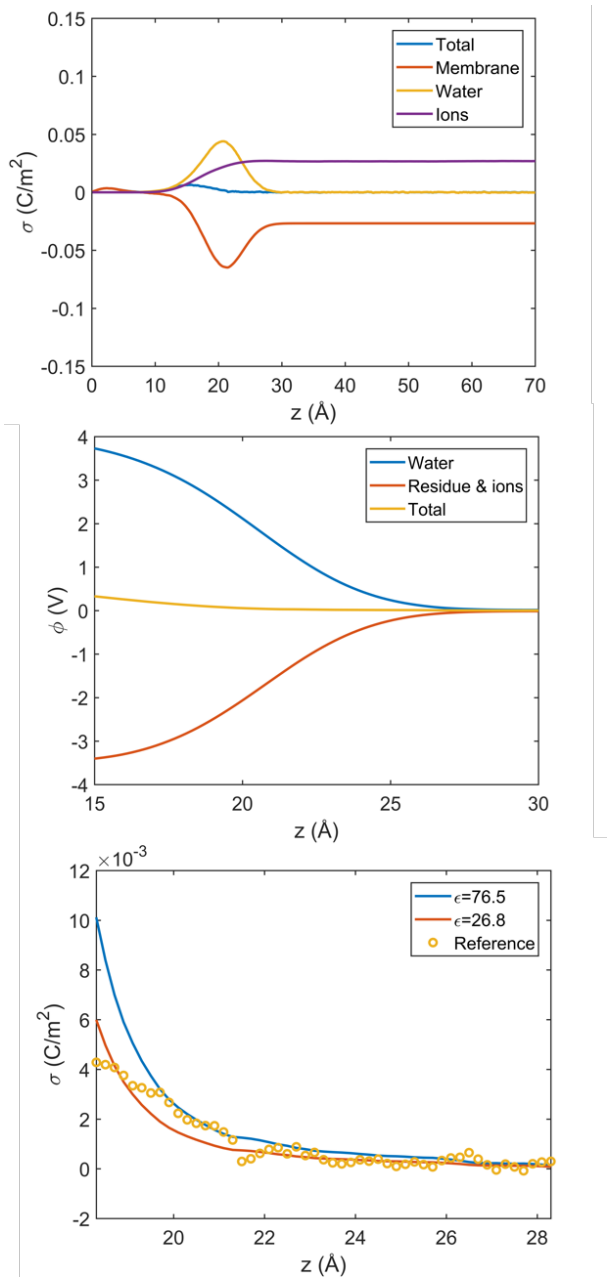

Figure 5.5. Top: Integrated charge density from the center of the 9:1 DMPC/DMPG bilayer (z=0), $\sigma(z) = \int_0^z \rho(z')dz'$, where $\rho(z')$ is the charge density binned along z (the direction of the membrane normal) averaged over snapshots from MD simulations. Middle: electrostatic potential computed based on the charge density from MD simulations. Bottom: Surface charge density computed with Grahame's Equation and the electrostatic potential from MD simulations using different values of dielectric constant for the interfacial solvent. The open circles indicate integrated charge density from MD simulations (i.e., the top panel). Since the precise location of the interface is not straightforward to determine, calculations based on the Grahame's equation are done for a series of z values near the location of the phosphate groups (z~20 Å).

interfacial water molecules at the bilayer surface. Nevertheless, the apparent dielectric constant we find here is also substantially larger than the value (~6) used to compute differential charge capacitance for charged solid surfaces.[56] This can be explained by the considerable thermal fluctuation of the lipid/water interface, which leads to a rather broad distribution of water orientation compared to the solid/water interface.[57,58] Therefore, considering the uncertainty in the surface potential measured from SHG due to the assumption of a sharp interface, the current analysis suggests that the use of Gouy-Chapman model to map the surface potential to an apparent surface charge density is justified at a semi-quantitative level.

5.3.5. Comparing SHG Results for PLL/PLR to Lys_8/Arg_8. In Chapter 4, we explore the adsorption of higher molecular weight polymers of L -lysine and L -arginine. In those studies, we find that the free energy of adsorption for both PLL and PLR was approximately – 50 kJ/mol. Comparatively, we estimate free energies of adsorption for Lys_8 and Arg_8 of about – 40 kJ/mol. If, however, we compare PLL/PLR to Lys_8/Arg_8 on the basis of charge concentration instead of polymer concentration, we find that the difference in free energy between PLL/PLR and Lys_8/ Arg_8 is actually much smaller (Table 5.2). To determine the number of charged groups per polymer, we divide the average polymer concentration by the molar mass of the molar mass of either a lysine or arginine sub-unit (including mass contributions from the associated anion in the case of PLL and PLR). In the case of PLL and PLR, we used the combined Langmuir/Gouy-Chapman model instead of the Hill/Gouy-Chapman for reasons explained in Chapter 4. Fitting the SHG E-fields versus polymer concentration or charge concentration does not change the overall charge density, demonstrating the robustness of the fitting models.

5.4. Conclusions. Building on the framework developed in Chapter 4, here we present experiments and MD simulations aimed at providing molecular insights into the thermodynamics

Table 5.2. Comparison of fitting parameters and free energies for Lys_8/Arg_8 and PLL/PLR

	Arg_8		PLR		Lys_8		PLL	
	Arg_8 conc. [mol. polymer/L]	Gdm conc. [mol. charge/L]	PLR conc. [mol. polymer/L]	Gdm conc. [mol. charge/L]	Lys_8 conc. [mol. polymer/L]	NH_3^+ conc. [mol. charge/L]	PLL conc. [mol. polymer/L]	NH_3^+ conc. [mol. charge/L]
A	0.87 ± 0.01	0.87 ± 0.01	0.88 ± 0.01	0.88 ± 0.01	0.94 ± 0.02	0.94 ± 0.01	0.93 ± 0.02	0.93 ± 0.02
B	-1.4 ± 0.4	-1.3 ± 0.13	-1.1 ± 0.08	-1.1 ± 0.08	-0.65 ± 0.2	-0.68 ± 0.07	-0.68 ± 0.2	-0.69 ± 0.2
K **[$\times 10^6$ M^{-1}]**	1.6 ± 0.5	0.20 ± 0 .06	44 ± 4.9	0.94 ± 0.1	1.2± 0.4	0.14 ± .04	15 ± 13	0.34 ± 0.3
n	0.54 ± 0 .09	0.54 ± 0 .09	–	–	0.52 ± 0.1	0.51 ± 0.09	–	–
σ **[C/m^2]**	0.10 ± 0.02	0.10 ± 0.01	0.17 ± 0.02	0.17 ± 0.02	0.11 ± 0.02	0.11 ± 0.01	0.28 ± 0.22	0.27 ± 0.22
ΔG [kJ/mol]	-45.3 ± 0.7	-40.2 ± 0.7	-54 ± 0.3	-44 ± 0.3	-44.6± 0.5	-39.3 ± 0.7	-51 ± 2	-41 ± 2
ΔG [kcal/mol]	-10.8	-9.6	-12.96	-10.56	-10.8	-9.36	-12.24	-9.84

Gdm is the guanidinium functional group. Charge concentrations are based on the average molecular weight of the polymer. Each repeat unit is assigned a charge of + 1.PLL and PLR data is based on fit with Gouy-Chapman Langmuir fit. For Lys and Arg, the Hill/Gouy-Chapman fit was used. A and B are fitting parameters related to the second- and third- order nonlinear susceptibilities, K is the apparent equilibrium constant, n is the Hill coefficient which describes cooperativity, and σ is the charge density.

and electrostatics that govern the interactions of octamers of L-lysine and L-arginine (Lys_8 and Arg_8) with supported lipid bilayers formed from 9:1 DMPC/DMPG. Comparison of acoustic and optical surface mass density estimates for Arg_8 and for Lys_8 indicate the presence of considerable amounts of dynamically coupled water. These interfacial water molecules, and how they respond to varying conditions of charge density due to peptide adsorption, can be probed using surface-specific vibrational spectroscopies, such as vibrational sum frequency generation (SFG),[59,60] which is underway in one of our laboratories but with a specific emphasis on properly accounting for the interfacial potential-dependent $\chi^{(3)}$ contribution and the resulting absorptive-dispersive mixing with the $\chi^{(2)}$ contributions.[61] SHG adsorption measurements sensitive to surface potential indicate that Lys_8 and Arg_8 attach without exhibiting noticeable cooperativity, as indicated by Hill coefficients of 0.5 ± 0.1 for both peptides. Yet, the binding free energies (-44 ± 1 kJ/mol and -45 ± 1 kJ/mol for Lys_8 and Arg_8, respectively) are purely additive when compared to those reported for arginine and lysine monomers. As such, the Hill coefficients found here are likely to report on interfacial heterogeneity, and not anti-cooperativity. Further, mass estimates from QCM-D and LSPR, and MD simulations suggest that Arg_8 binds to a larger extent than Lys_8. We find comparable equilibrium constants for both octapeptides by SHG (*n. b.* we did not determine K_{ads} by QCM-D or LSPR, due to the approximately 2 ng/cm^2 sensitivity limit of QCM-D, which would prevent detection of sub-monolayer surface coverages needed to determine Kads in this case). Yet, we caution that the K_{ads} point estimates were derived from the Langmuir-based adsorption model (Hill), whose assumptions (single site, monolayer limit, full reversibility) may not necessarily be applicable for our experimental conditions. In the molecular simulations, we found that Lys_8 is more likely to "stand-up" on the bilayer surface, where it

interacts through one to two sites, while Arg_8 is more likely to assume a "buried" conformation, interacting with the bilayer through up to five sites. However, these simulations do not lead to a straightforward inference of the apparent "binding free energy" of Arg_8 *vs*. Lys_8, which is a balance between interaction energy, number of dominant binding modes, and configurational entropy of the bound oligomer. These are the subjects of ongoing investigations by our groups.

The binding free energies for the peptides are about 10 kJ/mol smaller than those shown in Chapter 4 for the polymeric counterparts poly-L-lysine (PLL) and poly-L-arginine (PLR).[37] However, when we compute the free energy binding estimates for the octamers and polymers using charge, as opposed to molecular concentration, we find that this difference in binding free energy is considerably smaller (Table 5.2).

Upon accounting for the charge density of the bare bilayer, the attached peptides show an interfacial charge density that is approximately two times smaller (0.12 ± 0.03 C/m^2 for Lys_8 and 0.10 ± 0.02 C/m^2 for Arg_8) when compared to PLL and PLR. These results, and atomistic simulations, indicate that the surface charge density of the supported lipid bilayer is neutralized by the attached cationic peptides. Further, analysis of interfacial electrostatics and charge density based on atomistic simulations supports that the Gouy-Chapman model used in the analysis of SHG data is appropriate at a semi-quantitative level, especially considering the subtleties associated with the $\chi^{(3)}$ approach. From our surface mass density estimates, we find that the number of charges associated with each attached peptide is commensurate with those found in buffer solution, i.e. Lys_8 and Arg_8 are fully ionized when attached to the bilayer, in contrast to the large range of ionization of the attached polycationic counterparts we report in Chapter 4. Overall, the electrostatic, thermodynamic, and structural information reported here provides the

opportunity to further understand, control, and predict the charge-charge interactions that govern peptide/membrane interactions at biological and engineered interfaces.

CHAPTER 6

Improving Biomimetic Models for Probing Nano/Bio Interactions

6.1. Introduction and Motivation. As we discuss in Chapter 1 and demonstrate in Chapters 3-5, supported lipid bilayers (SLB) serve as a useful model for exploring and understanding the fundamental drivers of nano/bio interactions. Moreover, these systems, coupled with tools for probing these interactions, yield valuable insight into the mechanism of toxicity in biological systems. The majority of experiments that we discuss in Chapters 3-5 explore the interactions of oxidized multiwalled carbon nanotubes (Chapter 3), polyelectrolytes (Chapter 4), and oligomers (Chapter 5) with SLBs formed from phosphatidylcholine (PC) or mixtures of PC and phosphatidylglycerol (PG). While this combination of phospholipids allows us to explore the role of electrostatics in nano/bio and polymer/bio interactions, PG lipids are only a minor component in mammalian cells (1-2% in most mammalian cells, but up to 11% in lung surfactant).[1] Therefore, the generalizability of our findings may be rather limited. As we move forward it is important to understand and appreciate the role of individual lipids in biological systems and not to underestimate the role of specific lipid chemistry that can ultimately drive many cellular processes and interactions.[1] For example, while often used interchangeably in model SLBs as zwitterionic lipids, PC and phosphatidylethanolamine (PE) have different chemical structures (PE bears an ionizable amine while PC has a quaternary amine), different footprints (PE has a smaller headgroup than PC), and demonstrate different propensities to undergo bilayer-to-nonbilayer physical transitions.[1] PC lipids are chosen here because 1) PC lipids are more abundant in most biological systems relative to PE lipids and 2) PC lipids are essential for preserving the fluidity and structural integrity of membranes and are thus biologically relevant.[2]

Recognizing the important role that individual lipids can play in modulating lipid interactions with external species (ions, polymers, or nanoparticles), we now seek to explore beyond our simple single- or bi-component SLBs into a broader class of lipids and essential

membrane components. As a comparison to bilayer systems containing negatively charged PG-lipids, we explore other anionic lipid types including phosphatidylserine (PS), cardiolipin (CL), and phosphatidylinositol (PI) in PC-rich SLBs (For relevant chemical structures, see Scheme 1.1). In addition to incorporating various lipids into the SLB matrix, we discuss first steps towards developing SLBs coupled with important peripheral membrane proteins (cytochrome *c*, Cyt*c*). Finally, we conclude this Chapter with a discussion of the next steps that can be taken to build on the insights that we develop here.

6.2. Experimental Details.

6.2.1. Lipid Vesicle Preparation. 1,2-dimyristoyl-*sn*-glycero-3-phosphocholine (DMPC), 1,2-dioleoyl-*sn*-glycero-3-phosphocholine (DOPC), L-α-phosphatidylinositol (Liver, Bovine) (LPI), 1,2-dimyristoyl-*sn*-glycero-3-phospho-L-serine (sodium salt) (DMPS), 1',3'-bis[1,2-dioleoyl-*sn*-glycero-3-phospho]-*sn*-glycerol (sodium salt) (18:1, Cardiolipin) are purchased from Avanti Polar Lipids. Lipids dissolved in chloroform are mixed to achieve a lipid mass of 2 mg at the desired molar ratios. The lipid mixtures are then dried under a gentle stream of N_2 and placed in a vacuum desiccator for at least 3 hours. SLBs used for this study are prepared in a similar fashion to those discussed in Chapter 5. Specifically, lipid films are rehydrated with 0.001 M NaCl buffer with either 0.01 M Tris or HEPES buffers adjusted to pH 7.4. The concentration of buffer and pH conditions are conserved throughout this chapter and will therefore be omitted. Henceforth these conditions of buffer concentration and pH will simply be referred to as buffer.

6.2.2. DMPC/DMPS. For DMPC/DMPS we follow Method 2 described in Chapter 5. Specifically, the hydrated lipid films are then subjected to three freeze-thaw cycles and mechanically extruded at a concentration of 2 mg/mL. Immediately before use, the vesicle solution is diluted to achieve a final concentration of 0.5 mg/mL at 0.15 M NaCl, 0.005 M $CaCl_2$ Tris

buffer. The Teflon flow cell is equilibrated with 0.15 M NaCl, 0.005 M $CaCl_2$ Tris buffer. Lipid vesicle containing solutions (0.5 mg/mL, 4 mL) are introduced into the flow cell at a flow rate of ~2 mL/min and SLBs are allowed to form via the vesicle fusion method for at least 10 minutes or until a steady SHG signal is achieved. After allowing the SLB to form, the bilayer is rinsed with 1) 10 mL of 0.15 M NaCl, 0.005 M $CaCl_2$ Tris buffer, 2) 10 mL of 0.15 M NaCl Tris buffer, and 3) 20 mL of 0.1 M NaCl Tris buffer. In an effort to quantify the charge density of SLBs formed from 9:1 DMPC/DMPS, we perform charge screening experiments in which we reduce the NaCl concentration to 0 M NaCl (0.01 M Tris buffer) and then introduce 20 mL of sequentially higher concentrations of NaCl while maintaining the Tris concentration and pH conditions. To estimate the charge density of the SLB, we employ the Gouy-Chapman model as discussed in detail in Chapter 2.

6.2.3. DOPC/CL and DOPC/LPI. For the majority of experiments, vesicles formed from DOPC and CL or LPI, are pre-treated with the freeze-thaw method. All other details that we outline above for DMPC/DMPS related to bilayer formation are the same except for the buffer identity. In these studies, HEPES buffer is used in place of Tris buffer. One important amendment to the rinsing procedure outline: following the rinse with 0.15 M NaCl HEPES buffer, the flow cell is flushed with 20 mL of 0.01 M NaCl HEPES buffer. These conditions are then maintained throughout the experiment.

6.2.4. Charge Screening of Bare Silica Substrate Exposed to HEPES buffer. In SHG charge screening experiments, the flow cell is first equilibrated with 0.01 M NaCl, 0.01 M HEPES buffer. The flow cell is then flushed with 20 mL of 0.01 M HEPES buffer (no added NaCl) at a flow rate of 2 mL/min. Sequentially higher concentrations of NaCl are introduced into the cell under the same volume and flow rate, while maintaining HEPES concentration (0.01 M HEPES adjusted to

pH 7.4). SHG signal is collected for at least 15 minutes or until signal is stable. To correct for fluctuations in power, the SHG signal intensity is divided by the square of the input power which is constantly monitored as discussed in Chapter 2. We then use the Gouy-Chapman model (Equation 6.1) to estimate the charge density of the fused silica substrate (Figure 6.1).

$$E_{SHG} \propto A + 0.0505\ [\mathrm{V}] \times B \left\{ \sinh^{-1} \left((\sigma_{total}) \left(\frac{8.5\ [\mathrm{M}^{\frac{1}{2}}\mathrm{m}^{2}\mathrm{C}^{-1}]}{\sqrt{C_{elec}}} \right) \right) \right\} \qquad 6.1$$

The interfacial charge density can be expressed as the sum of the various "interfacial layers" ($\sigma_{total} = \sigma_{SiO_2} + \sigma_{HEPES} + \sigma_{SLB}$) where σ_{SiO_2} is the charge density of the fused silica substrate, σ_{HEPES} is the charge density of the interfacial HEPES layer, and σ_{SLB} accounts for the charge density of the SLB. We find that the fused silica substrate, in the presence of HEPES buffer at pH 7.4, carries a charge density of – 0.08 ± 0.04 C/m^2 which corresponds to $\sigma_{SiO_2} + \sigma_{HEPES}$. In a previous report on the charge density of the same silica substrates in the presence of 0.01 M Tris buffer adjusted to pH 7.4, we found a charge density of + 0.02 ± 0.01 C/m^2.[3] We know from previous work that Tris buffer does adsorb to the silica substrate and that in the absence of buffer, fused silica carries a charge density of ~ – 0.01 C/m^2 at pH 7.[4] Having determined the charge density of the fused silica substrate in the presence of HEPES buffer, we can now determine the charge density of any SLBs on silica supports under these conditions of HEPES concentration and pH.

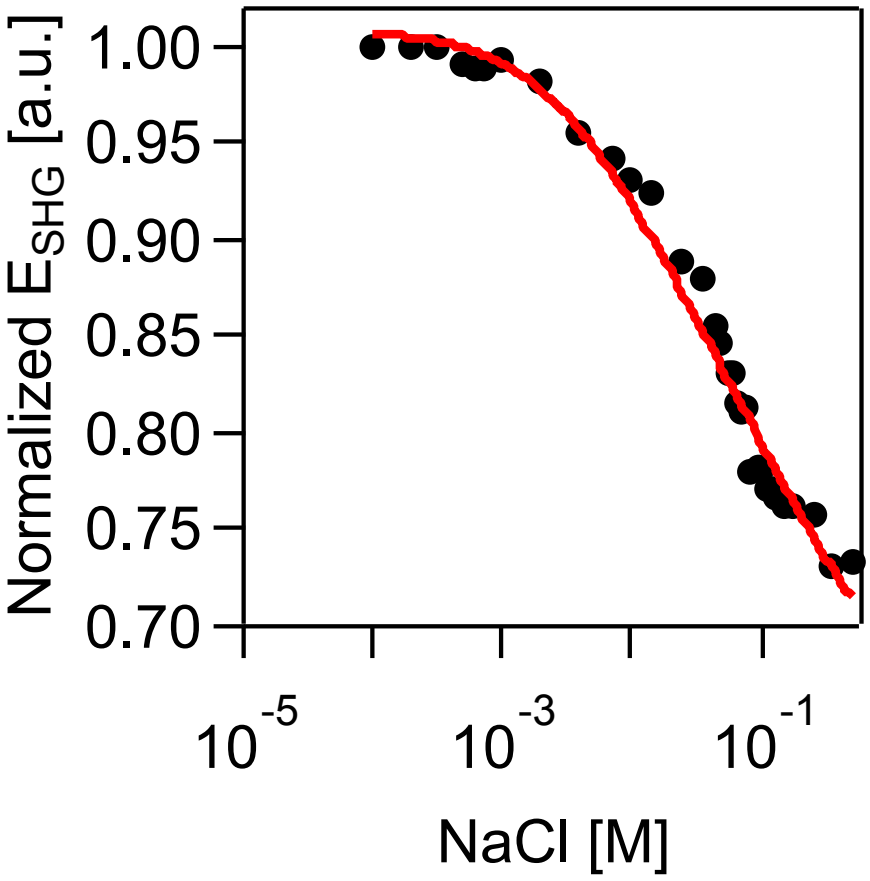

Figure 6.1. Normalized SHG E-field as a function of NaCl concentration in the presence of fused silica substrate with 0.01 M HEPES buffer adjusted to pH 7.4 fit with Gouy-Chapman model (red, solid line, Equation 6.1).

6.2.5. Cytochrome *c* (Cyt*c*) Adsorption to SLBs. Cyt*c* (12 kDa) is purchased from Sigma-Aldrich (C7752, Equine heart). Solutions of Cyt*c* are prepared in 0.01 M NaCl, 0.01 M HEPES buffered to pH 7.4 and special care is taken not to vigorously stir or vortex protein solution so as to avoid denaturation. The Cyt*c* solutions are gently mixed by pipetting solution in and out of the microcentrifuge tube in which the solutions are prepared. The solutions are then divided into small aliquots and frozen at –20ºC. Immediately before use, aliquots are thawed by sitting the aliquot on the benchtop. Once thawed, solutions are used within one week. [Note: Stored aqueous solutions should not be used after 6 months even when stored at –20ºC as per vendor specifications.]

6.2.6. Characterization of Vesicles with/without Cyt*c*. Lipid vesicles of varying compositions of DOPC and LPI or CL, are analyzed with dynamic light scattering (DLS) and laser Doppler micro-electrophoresis using a Zetasizer Nano ZS (Malvern Instruments, 632.8 nM laser, 173º scattering angle, 50 V, T = 25ºC). Vesicle solutions are diluted to 0.0625 mg/mL lipid concentrations in 0.01 M NaCl HEPES buffer. UV-Vis spectra are collected using a Flame Integrated Sampling System (FLAME-CHEM-UV-VIS Spectrometer, FLAME-DA-CUV-UV-VIS system, Ocean Optics). We use the same solution conditions in UV-Vis studies as outlined above for DLS.

6.3. Integrating PS Lipids into the SLB Matrix. Our first steps towards building more complex systems involves determining the surface charge density of SLBs composed from 9:1 DMPC and DMPS. PS headgroups are comprised of a phosphate group and a serine group, which can form intramolecular hydrogen bonds between the PS ammonium and carboxylate groups. This is in contrast to the PG lipids which have been extensively used in the preceding Chapters. PG lipid headgroups are composed of glycerol and phosphate groups. From an electrostatics perspective, both PG and PS lipids carry a net charge of –1. While experimentally we have not observed

differences in the binding affinity or mechanism of interactions with SLBs incorporating PG or PS lipids,[5] there is some indication in biological systems that these two lipids do behave differently.[1] We find that with increasing NaCl concentration in the presence of 9:1 DMPC/DMPS, there is a decrease in SHG signal intensity as shown in Figure 6.2. Unfortunately, applying a Gouy-Chapman fit to our experimental data results in unreasonably large errors associated with the charge density of the SLB (+0.003 ± 0.05 C/m^2). Additional data points would be useful in estimating the surface charge density of SLBs formed from 9:1 DMPC/DMPS. We expect the charge density of this SLB is comparable to, but perhaps not identical to, that of 9:1 DMPC/DMPG which is ~ –0.1 C/m^2.[3,6]

6.4. Cytochrome *c* as a Model Peripheral Membrane Protein. Fundamentally, Cyt*c* was chosen as a first step towards increasing the complexity of our model biological systems because it is widely studied,[7-12] relatively small, and has relevance to bacterial and mammalian systems, alike.[13] Cyt*c* is a small (~12 kDa) globular heme protein that plays a key role in mitochondrial electron transport processes and in the mediation of apoptosis. As a protein that is critically important to the function of mitochondria, and for the reasons specified above, we currently explore Cyt*c* interactions with SLBs composed of lipids that are represented in mitochondrial membranes.

Whether through intentional design for targeting mitochondria[14,15] or through passive or active transport of nanoparticles through the cellular membrane,[16] it is possible that nanoparticles will make direct contact with the surface of mitochondria. In fact, some studies suggest that nanoparticles can liberate Cyt*c* from mitochondria[17] and acquire soft protein coronas that contain Cyt*c*.[18] For these reasons, there are a number of experimental and computational studies that explore the interactions of nanoparticles with Cyt*c*.[16,19,20] Upon interaction with graphene oxide[20] or manganese[21] nanoparticles, for instance, Cyt*c* undergoes a conformational change from hexa-

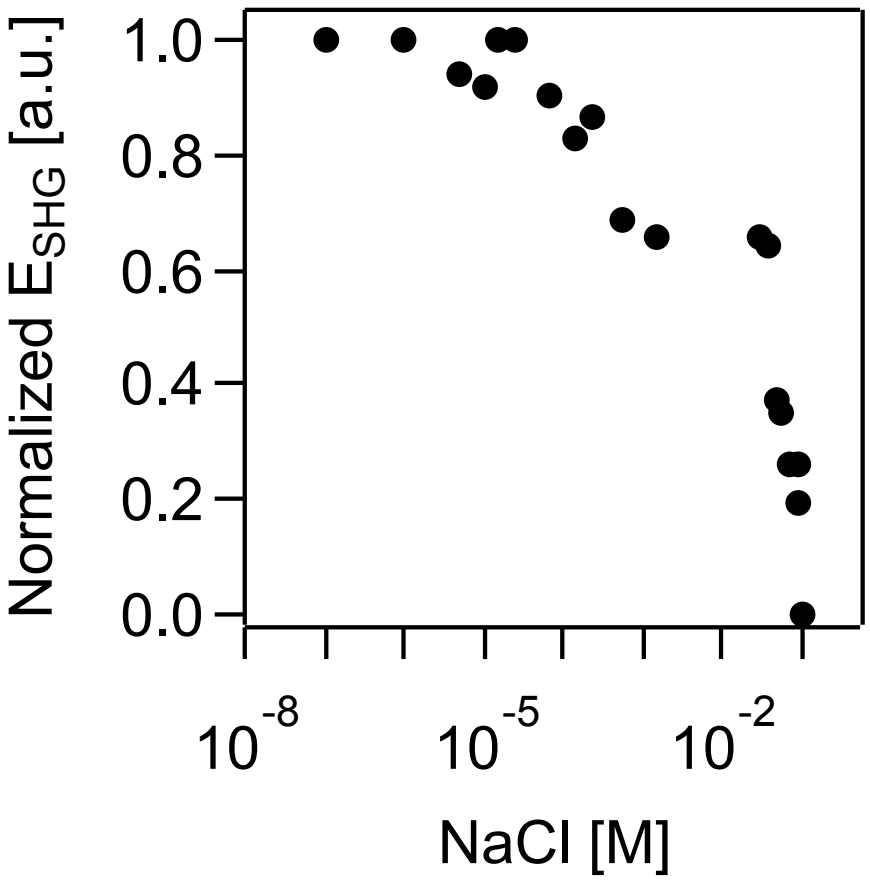

Figure 6.2. Normalized SHG E-field as a function of NaCl concentration in the presence of supported lipid bilayers formed from 9:1 DMPC/DMPS with 0.01 M Tris buffer adjusted to pH 7.4.

coordinated to a penta-coordinated electron configuration which activates a peroxidase-like activity. Similar conformational changes, and subsequent induction of peroxidase activity, is also noted with Cyt*c* adsorbing to CL (and to a smaller extent with PS and PI)[9] in the early stages of apoptosis.[11] Both CL[22] and PI[2] are present in the outer mitochondrial membrane and are integral in a number of cellular processes, including the regulation of protein binding and transport. In fact, peripheral proteins, like Cyt*c*, interact strongly with both CL and PI,[1,9,10] thus motivating their study herein. CL is an essential diphosphatidylglycerol and as such, CL may or may not be doubly ionized under physiological conditions.[22] Given the particular interactions that Cyt*c* can have with CL and PI lipids, we pay special attention to those lipids here. Specifically, we explore the adsorption of Cyt*c* to PC-rich SLBs with varying amounts of CL and PI lipids. These experiments serve as the foundation for exploring nano/bio interactions with these SLB-Cyt*c* systems.

6.4.1. Adsorption of Cyt*c* to Lipid Vesicles. The hydrodynamic diameters that we report in Table 6.1 are the average of three measurements for one sample. To convert electrophoretic mobilities to ζ-potentials, the Smoluchowski equation was used and the average of three measurements for one sample is shown in Figure 6.3. In addition to characterizing the extruded vesicles, we also report the calculated ζ-potentials of vesicles mixed with 0.16 mg/mL Cyt*c* in Figure 6.3. After exposing lipid vesicles to Cyt*c*, the ζ-potentials generally become less negative. In the presence of vesicles composed from 8.24:1.76 DOPC/CL, the ζ-potential becomes slightly positive (Figure 6.3.A). These results indicate that Cyt*c* is indeed adsorbing to the surface of the small unilamellar vesicles which are used to form SLBs in our SHG experiments. UV-Vis measurements of Cyt*c* in solution and in the presence of vesicles show a maximum absorbance intensity centered around ~410 nm which corresponds to the Soret band (electronic transitions in heme group).[23] A second feature at ~520 nm is associated with the Q-band. (Figure 6.3.B). With these data in mind, we

Table 6.1. Properties of Cardiolipin and LPI-Containing Lipid Vesicles[a]

Vesicle Composition	Hydrodynamic Diameter (nm)	ζ-potential (mV)
9.56:0.44 DOPC/CL	86 ± 2	– 23 ± 4
9.12:0.88 DOPC/CL	87 ± 0.3	– 33 ± 7
8.24:1.76 DOPC/CL	84 ± 1	– 32 ± 3
9.12:0.88 DOPC/LPI[b]	76 ± 0.6	–

[a] Solution conditions: 0.0625 mg/mL lipid, 0.01 M NaCl, 0.01 M HEPES buffer (pH 7.4). Reported errors are the standard deviation of three averaged measurements. [b]Lipid concentration of 0.5 mg/mL.

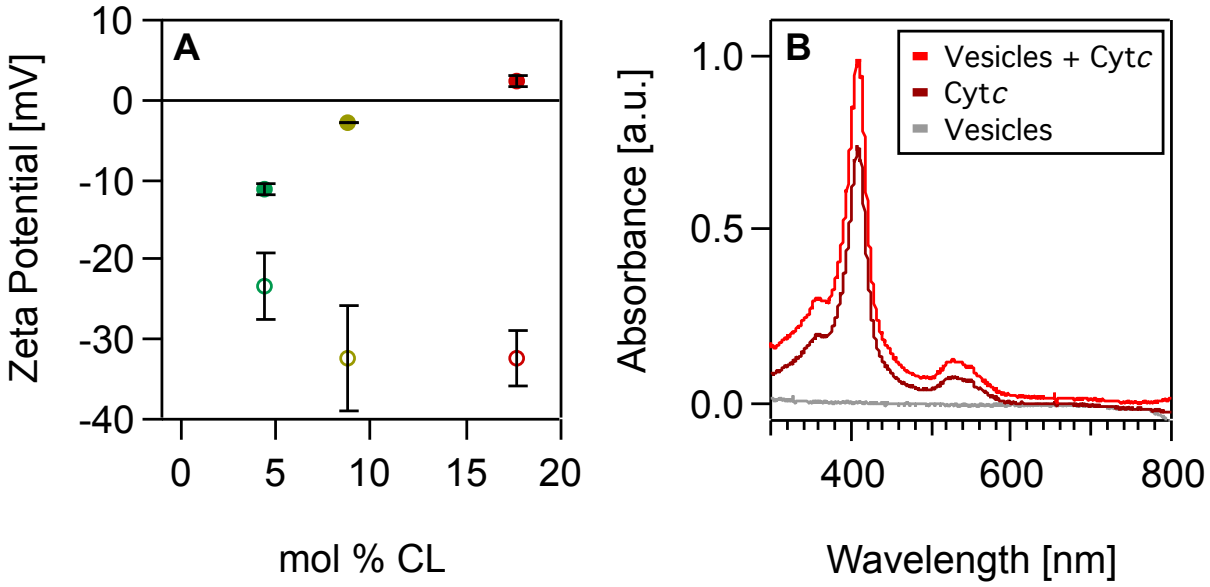

Figure 6.3. (A) Zeta-potential as a function of CL concentration in a DOPC vesicle formed in 0.01 M NaCl, 0.01 M HEPES buffer. Empty circles indicate no Cyt*c* present and filled circles indicate that Cyt*c* is present at a concentration of 0.16 mg/mL (~10 μM). Under these conditions and in the absence of vesicles, Cyt*c* carries an apparent slight negative charge of – 4 ± 2 mV. **(B)** UV-Vis spectrum of 1) 0.0625 mg/mL of 8.24:1.76 DOPC/CL (gray), 2) 0.16 mg/mL (~10 μM) Cyt*c* (dark red), or 3) 0.0625 mg/mL of 8.24:1.76 CL + 0.16 mg/mL (~10 μM) Cyt*c* (red).

moved on to generating SHG adsorption isotherms from which the charge densities and equilibrium constants of the adsorbed Cyt*c* adlayer can be determined.

6.4.2. Nonlinear Optical Studies of SLBs Containing PS, CL, and LPI. Previous studies have already demonstrated the applicability of SHG towards studying Cyt*c* adsorption to model biological interfaces.[23, 24] Adsorption of Cyt*c* to SLBs formed from 8:2 mixtures of 1,2-dioleoyl-*sn*-glycero-3-phosphocholine (DOPC) and 1,2-dioleoyl-*sn*-glycero-3-phospho-(1'-rac-glycerol) (DOPG) is associated with a maximum charge density of ~0.2 C/m^2 (1.3 × 10^{14} charges/cm^2).[24] In our exploration of Cyt*c* adsorption to SLBs formed from DOPC and CL or LPI, we find that the signal decreases after initially increasing in intensity as was also shown in the work of Salafsky and Eisenthal[24] (Figure 6.4). Preliminarily, we find that there is a larger decrease in SHG signal intensity for bilayers with higher CL contents (Figure 6.5). We also note negligible net changes in signal at the lowest CL concentration and in the presence of LPI lipids, which suggests that Cyt*c* does not significantly adsorb to these membranes. At the highest CL concentrations, we find that the SHG signal intensity decreases by ~15% and that the signal remains suppressed even after rinsing with protein-free buffers, which could indicate that some portion of Cyt*c* binds irreversibly to the SLB. Yet, to determine the charge density of the bilayers studied herein, along with adsorbed protein layer charge densities, requires additional data points.

6.4.3. Future Studies Employing Cyt*c*-containing SLBs. One possibility for future directions involving Cyt*c*-containing SLBs, and building on the work discussed in Chapter 5, is to explore the interactions of SLB-Cyt*c* systems with gold nanoparticles (or any core material) functionalized with arginine and lysine. Gold nanoparticles functionalized with amino-acids and peptides are used as mimics for proteins and serve as useful platforms for the study of protein-protein interactions.[25, 26] Given the reduction in surface charge that is expected to occur upon adsorption of Cyt*c* to SLB

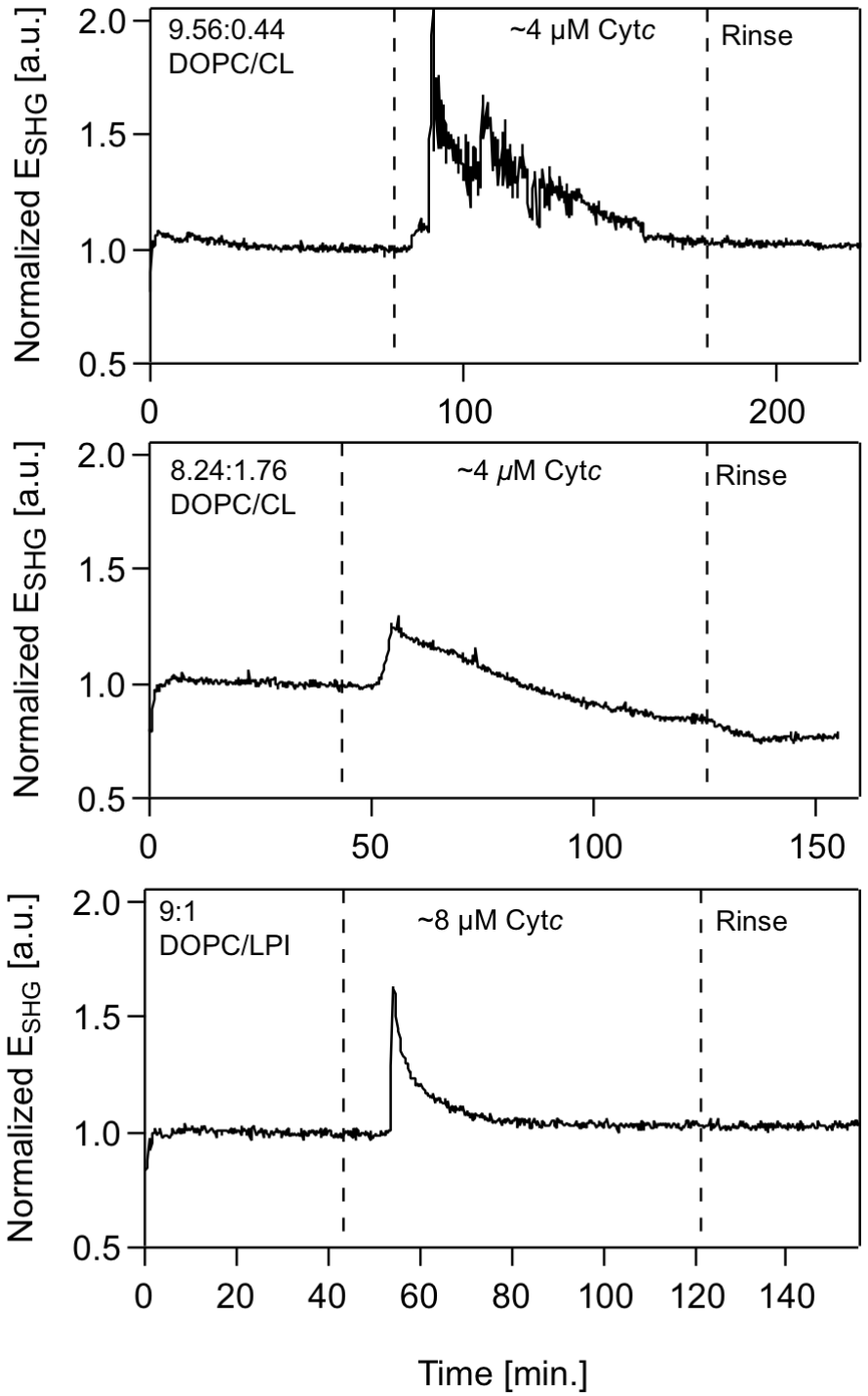

Figure 6.4. Normalized SHG E-field as a function of time in the presence of supported lipid bilayers formed from DOPC, Cardiolipin (CL) and Liver PI (LPI) in background conditions of 0.01 M NaCl, 0.01 M HEPES buffer pH adjusted to 7.4. At $t = 0$ min., the SLB is unperturbed and signal is monitored under the background solution conditions. At first dashed line., the SLB is exposed to Cyt*c* while maintaining the background solution conditions. At second dashed line, the flow cell is flushed with Cyt*c* buffer. All traces are shown with 10 second sliding average.

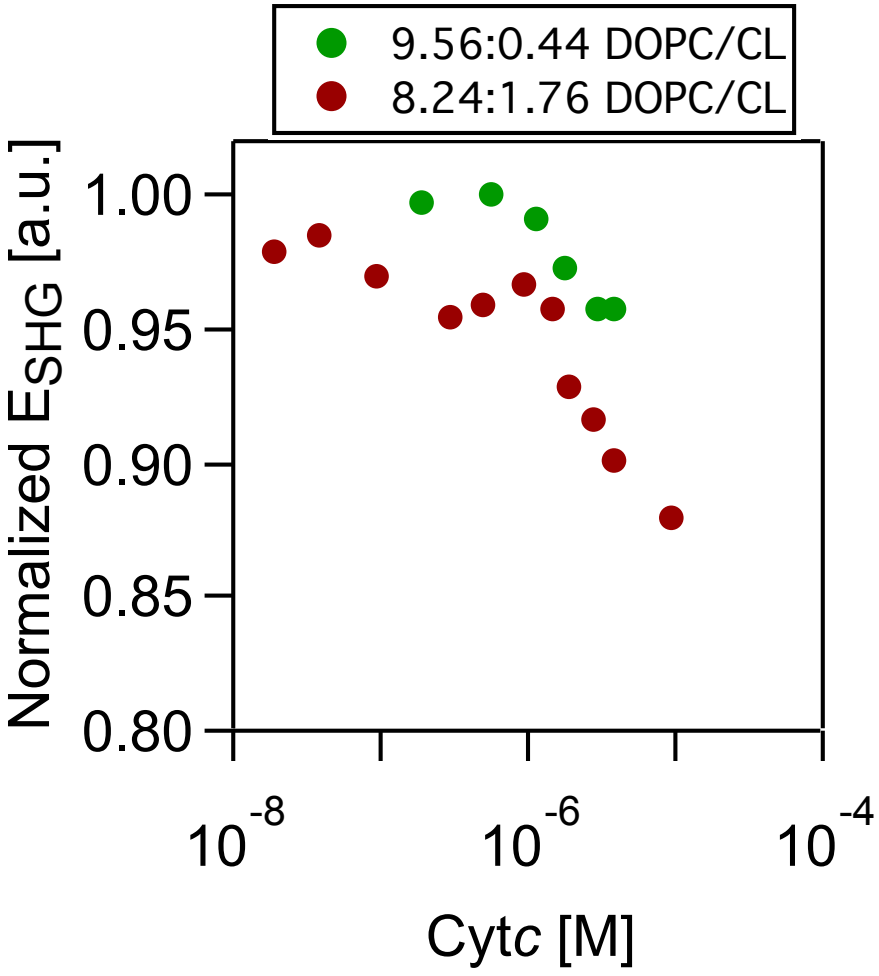

Figure 6.5. Normalized SHG E-field as a function of Cyt*c* concentration in molarity, M, in presence of SLBs containing varying CL content at 0.01 M NaCl, 0.01 M HEPES buffer adjusted to pH 7.4. SHG signal is normalized to the signal from the unperturbed SLB.

surfaces, we might expect to see less adsorption of cationic gold nanoparticles as a consequence of increased electrostatic repulsion. Providing estimates for charge densities and free energies of adsorption from these experiments would require confirmation that Cyt*c* remains irreversibly adsorbed to the SLB surface.

Additionally, Cyt*c* has been shown to destabilize neutral, fluid-phase lipid bilayers.[27] It is conceivable that the addition of Cyt*c* to bilayers above their transition temperature (i.e. in fluid-phase) could make it easier for nanoparticles to remove lipids from the SLB to acquire lipid corona. Particularly in the case of anionic-nanoparticles, it might be possible to extract Cyt*c* from the surface of membranes. It should be easiest to extract Cyt*c* from SLBs containing PC and PG lipids,[28] because Cyt*c* is expected to interact relatively weakly with these lipids. As there is limited research in the influence of membrane-associated Cyt*c* on nano/bio interactions, these studies would be among the first reported.

6.5. Future Directions for Modifying Biomimetic Systems. In addition to developing our understanding of the role of peripheral proteins in modulating nano/bio interactions, we can explore the role of cholesterol in dictating nano/bio interactions and extend on the currently employed systems to include other proteins.

6.5.1. Addition of Cholesterol to SLBs. Cholesterol plays a critical role in maintaining the fluidity of cellular membranes as well as in the formation of lipid rafts,[29] which are important in cellular transport processes. In addition to inducing ordering of the alkyl chains associated with phospholipids, cholesterol has been shown to decrease the surface charge of the cellular membrane by reducing the extent of Na^+ binding.[29] Thus, it is expected that the addition of cholesterol to the SLB matrix will decrease the extent of adsorption for like-charged adsorbates because of increased electrostatic repulsion.

In addition to the role of electrostatics, considered above, in the adsorption of species to the SLB surface, cholesterol can alter the bilayer fluidity in a manner that is both temperature and concentration dependent[30] which can influence the outcome of nano/bio interactions. For instance, oxidized carbon nanospheres are found to associate more with cholesterol-containing membranes in the fluid-phase as opposed to gel-phase membranes.[31] Other reports on carbon-based nanomaterials interacting with cholesterol-containing model lipid membranes indicate that these particles can extract cholesterol from lipid bilayers[32] and modulate the C_{60} permeability into lipid membranes.[33] The influence of cholesterol on nano/bio interactions is not restricted to carbon-based nanoparticles though. In unpublished work examining the adsorption of gold nanoparticles functionalized with PAH (PAH-AuNPs) adsorb less to bilayers containing cholesterol as assessed by quartz-crystal microbalance with dissipation monitoring.[34] To date, there are few studies that systematically explore the relationship between cholesterol content and nanoparticle attachment. Such a systematic study would no doubt be useful to advancing our understanding of nano/bio interactions.

6.5.2. Biologically Relevant Proteins for Fundamental Studies. Upon introducing nanomaterials into biological media, various proteins adsorb to the nanoparticle surface, forming a dynamic protein corona around the nanoparticle thus changing: the identity of the nanomaterial, its associated toxicity, cellular uptake, and transport. In addition to Cyt*c*, albumin, a protein prevalent in plasma could serve as a useful model proein.[35,36] As an alternative to integrating albumin into the cellular matrix, where it would only minimally adsorb to the cellular membrane,[37] we could consider allowing the nanoparticle and albumin proteins to pre-equilibrate and then expose the SLB to the nanoparticle-protein complex. Albumin is expected to carry a negative charge under physiological conditions, yet, it has been shown to readily adsorb to the surface of

carbon nanotubes (CNTs)[35,38,39] and other carbon-based nanomaterials despite expected electrostatic repulsion,[39] and even reduce their ζ-potentials. These unintuitive findings regarding the binding of albumin to negatively-charged carbon-based nanoparticles can be rationalized by pockets of positive charges in the albumin structure, conformational flexibility of albumin, and the relatively small size of albumin which allows the protein to adsorb to unfunctionalized gaps on the nanoparticle surface.[35] It can be hypothesized that there will be greater adsorption of the albumin-nanoparticle complexes to SLBs than in the absence of albumin if the SLB carries a negative surface charge.

6.5.3. Naturally-Derived Membranes for Spectroscopic Studies. Understanding that there is ultimately a limit to the extent to which we can develop a model that accurately reflects the nature of the cellular membrane, we can complement, and, to some degree, validate the appropriateness of these models by working with native cellular membranes and conducting interaction studies with biological systems of greater complexity (i.e. live cells). One question that can be answered by the latter is how our SHG results translate to toxicity in real systems. With the new capabilities afforded to us by our updated SHG microscope, these studies are almost in reach. Indeed, SHG microscopy has been performed on live cells[40,41] and whole organisms,[42] which indicates that such systems are ones that we can realistically explore. While we do not currently have the expertise to work with these systems, yet, we can take advantage of the expertise and resources available from the Center for Sustainable Nanotechnology.

Chapter 1 References.

1. R. H. Baughman, A. A. Zakhidov and W. A. de Heer, Carbon nanotubes - The Route Toward Applications, *Science*, 2002, **297**, 787-792.

2. S. Eustis and M. A. El-Sayed, Why Gold Nanoparticles Are More Precious than Pretty Gold: Noble Metal Surface Plasmon Resonance and Its Enhancement of the Radiative and Nonradiative Properties of Nanocrystals of Different Shapes, *Chem. Soc. Rev.*, 2006, **35**, 209-217.

3. W. Lu and C. M. Lieber, Nanoelectronics from the Bottom Up, *Nat. Mater.*, 2007, **6**, 841-850.

4. N. Toshima and T. Yonezawa, Bimetallic nanoparticles - novel materials for chemical and physical applications, *New Journal of Chemistry*, 1998, **22**, 1179-1201.

5. B. Song, J. Liu, X. L. Feng, M. Wei and L. Q. Shao, A review on potential neurotoxicity of titanium dioxide nanoparticles, *Nanoscale Res. Lett.*, 2015, **10**, 17.

6. C. Contado, Nanomaterials in Consumer Products: A Challenging Analytical Problem, *Front. Chem.*, 2015, **3**, 20.

7. F. Rosei, Nanostructured Surfaces: Challenges and Frontiers in Nanotechnology, *J. Phys. Condens. Matter.*, 2004, **16**, S1373-S1436.

8. S. Griffin, M. I. Masood, M. J. Nasim, M. Sarfraz, A. P. Ebokaiwe, K. H. Schafer, C. M. Keck and C. Jacob, Natural Nanoparticles: A Particular Matter Inspired by Nature, *Antioxidants*, 2018, **7**, 21.

9. X. Chen and S. S. Mao, Titanium Dioxide Nanomaterials: Synthesis, Properties, Modifications, and Applications, *Chem. Rev.*, 2007, **107**, 2891-2959.

10. E. Rascol, J. M. Devoisselle and J. Chopineau, The Relevance of Membrane Models to Understand Nanoparticles-cell Membrane Interactions, *Nanoscale*, 2016, **8**, 4780-4798.

11. C. N. R. Rao, G. U. Kulkarni, P. J. Thomas and P. P. Edwards, Metal Nanoparticles and Their Assemblies, *Chem. Soc. Rev.*, 2000, **29**, 27-35.

12. J. Z. Zhang and C. Noguez, Plasmonic Optical Properties and Applications of Metal Nanostructures, *Plasmonics*, 2008, **3**, 127-150.

13. J. B. Kim, J. W. Grate and P. Wang, Nanobiocatalysis and its potential applications, *Trends Biotechnol.*, 2008, **26**, 639-646.

14. Q. Cui, R. Hernandez, S. E. Mason, T. Frauenheim, J. A. Pedersen and F. Geiger, Sustainable Nanotechnology: Opportunities and Challenges for Theoretical/Computational Studies, *J. Phys. Chem. B*, 2016, **120**, 7297-7306.

15. M. F. L. De Volder, S. H. Tawfick, R. H. Baughman and A. J. Hart, Carbon Nanotubes: Present and Future Commercial Applications, *Science*, 2013, **339**, 535-539.

16. W. X. Zhang, Nanoscale Iron Particles for Environmental Remediation: An Overview, *J. Nanopart. Res.*, 2003, **5**, 323-332.

17. Z. Q. Cai, A. D. Dwivedi, W. N. Lee, X. Zhao, W. Liu, M. Sillanpaa, D. Y. Zhao, C. H. Huang and J. Fu, Application of Nanotechnologies for Removing Pharmaceutically Active Compounds from Water: Development and Future Trends, *Environ. Sci. Nano.*, 2018, **5**, 27-47.

18. B. Levy, Photochemistry of nanostructured materials for energy applications, *J. Electroceramics*, 1997, **1**, 239-272.

19. M. De, P. S. Ghosh and V. M. Rotello, Applications of Nanoparticles in Biology, *Adv. Mater.*, 2008, **20**, 4225-4241.

20. R. A. Sperling, P. Rivera gil, F. Zhang, M. Zanella and W. J. Parak, Biological applications of gold nanoparticles, *Chem. Soc. Rev.*, 2008, **37**, 1896-1908.

21. Y. Cheng, H. Yang, Y. Yang, J. Y. Huang, K. Wu, Z. Chen, X. Q. Wang, C. J. Lin and Y. K. Lai, Progress in TiO2 Nanotube Coatings for Biomedical Applications: A Review, *J. Mater. Chem. B*, 2018, **6**, 1862-1886.

22. P. J. Rivero, A. Urrutia, J. Goicoechea and F. J. Arregui, Nanomaterials for Functional Textiles and Fibers, *Nanoscale Res. Lett.*, 2015, **10**. DOI: 10.1186/s11671-015-1195-6.

23. A. K. Yetisen, H. Qu, A. Manbachi, H. Butt, M. R. Dokmeci, J. P. Hinestroza, M. Skorobogatiy, A. Khademhosseini and S. H. Yun, Nanotechnology in Textiles, *ACS Nano*, 2016, **10**, 3042-3068.

24. D. Jariwala, V. K. Sangwan, L. J. Lauhon, T. J. Marks and M. C. Hersam, Carbon Nanomaterials for Electronics, Optoelectronics, Photovoltaics, and Sensing, *Chem. Soc. Rev.*, 2013, **42**, 2824-2860.

25. Q. Zhang, J. Q. Huang, W. Z. Qian, Y. Y. Zhang and F. Wei, The Road for Nanomaterials Industry: A Review of Carbon Nanotube Production, Post-Treatment, and Bulk Applications for Composites and Energy Storage, *Small*, 2013, **9**, 1237-1265.

26. G. Pulido-Reyes, F. Leganes, F. Fernandez-Pinas and R. Rosal, Bio-nano Interface and Environment: A Critical Review, *Environ. Toxicol. Chem.*, 2017, **36**, 3181-3193.

27. F. Gottschalk, T. Sonderer, R. W. Scholz and B. Nowack, Modeled Environmental Concentrations of Engineered Nanomaterials (TiO2, ZnO, Ag, CNT, Fullerenes) for Different Regions, *Environ. Sci. Technol.*, 2009, **43**, 9216-9222.

28. G. Oberdorster, E. Oberdorster and J. Oberdorster, Nanotoxicology: An Emerging Discipline Evolving from Studies of Ultrafine Particles, *Environ. Health Perspect.*, 2005, **113**, 823-839.

29. V. L. Colvin, The Potential Environmental Impact of Engineered Nanomaterials, *Nat. Biotechnol.*, 2003, **21**, 1166-1170.

30. R. Chelladurai, K. Debnath, N. R. Jana and J. K. Basu, Nanoscale Heterogeneities Drive Enhanced Binding and Anomalous Diffusion of Nanoparticles in Model Biomembranes, *Langmuir*, 2018, **34**, 1691-1699.

31. M. Dogangun, M. N. Hang, J. Machesky, A. C. McGeachy, N. Dalchand, R. J. Hamers and F. M. Geiger, Evidence for Considerable Metal Cation Concentrations from Lithium Intercalation Compounds in the Nano-Bio Interface Gap, *J. Phys. Chem. C*, 2017.

32. A. C. McGeachy, L. L. Olenick, J. M. Troiano, R. S. Lankone, E. S. Melby, T. R. Kuech, E. Ehimiaghe, D. H. Fairbrother, J. A. Pedersen and F. M. Geiger, Resonantly Enhanced Nonlinear Optical Probes of Oxidized Multiwalled Carbon Nanotubes at Supported Lipid Bilayers, *J. Phys. Chem. B*, 2017, **121**, 1321-1329.

33. J. M. Troiano, T. R. Kuech, A. M. Vartanian, M. D. Torelli, A. Sen, L. M. Jacob, R. J. Hamers, C. J. Murphy, J. A. Pedersen and F. M. Geiger, On Electronic and Charge Interference in Second Harmonic Generation Responses from Gold Metal Nanoparticles at Supported Lipid Bilayers, *J. Phys. Chem. C*, 2016, **120**, 20659-20667.

34. M. Dogangun, M. N. Hang, J. M. Troiano, A. C. McGeachy, E. S. Melby, J. A. Pedersen, R. J. Hamers and F. M. Geiger, Alteration of Membrane Compositional Asymmetry by LiCoO2 Nanosheets, *ACS Nano*, 2015, **9**, 8755-8765.

35. J. M. Troiano, L. L. Olenick, T. R. Kuech, E. S. Melby, D. Hu, S. E. Lohse, A. C. Mensch, M. Dogangun, A. M. Vartanian, M. D. Torelli, E. Ehimiaghe, S. R. Walter, L. Fu, C. R. Anderton, Z. Zhu, H. Wang, G. Orr, C. J. Murphy, R. J. Hamers, J. A. Pedersen and F. M. Geiger, Direct Probes of 4 nm Diameter Gold Nanoparticles Interacting with Supported Lipid Bilayers, *J. Phys. Chem. C*, 2015, ***119*** 534-546.

36. S. Pogodin and V. A. Baulin, Can a Carbon Nanotube Pierce through a Phospholipid Bilayer?, *ACS Nano*, 2010, **4**, 5293-5300.

37. P. Yi and K. L. Chen, Interaction of Multiwalled Carbon Nanotubes with Supported Lipid Bilayers and Vesicles as Model Biological Membranes, *Environ. Sci. Technol.*, 2013, **47**, 5711-5719.

38. C. Corredor, W.-C. Hou, S. A. Klein, B. Y. Moghadam, M. Goryll, K. Doudrick, P. Westerhoff and J. D. Posner, Disruption of Model Cell Membranes by Carbon Nanotubes, *Carbon*, 2013, **60**, 67-75.

39. B. Y. Moghadam, W. C. Hou, C. Corredor, P. Westerhoff and J. D. Posner, Role of Nanoparticle Surface Functionality in the Disruption of Model Cell Membranes, *Langmuir*, 2012, **28**, 16318-16326.

40. A. C. Mensch, R. T. Hernandez, J. E. Kuether, M. D. Torelli, Z. V. Feng, R. J. Hamers and J. A. Pedersen, Natural Organic Matter Concentration Impacts the Interaction of Functionalized Diamond Nanoparticles with Model and Actual Bacterial Membranes, *Environ. Sci. Technol.*, 2017, **51**, 11075-11084.

41. J. V. M. Giron, R. V. Vico, B. Maggio, E. Zelaya, A. Rubert, G. Benitez, P. Carro, R. C. Salvarezza and M. E. Vela, Role of the Capping Agent in the Interaction of Hydrophilic Ag Nanoparticles with DMPC as a Model Biomembrane, *Environ. Sci. Nano.*, 2016, **3**, 462-472.

42. E. Kovacec, M. Regvar, J. T. van Elteren, I. Arcon, T. Papp, D. Makovec and K. Vogel-Mikus, Biotransformation of Copper Oxide Nanoparticles by the Pathogenic Fungus Botrytis cinerea, *Chemosphere*, 2017, **180**, 178-185.

43. S. Ma and D. H. Lin, The Biophysicochemical Interactions at the Interfaces between Nanoparticles and Aquatic Organisms: Adsorption and Internalization, *Environ. Sci. Process. Impact*, 2013, **15**, 145-160.

44. L. K. Adams, D. Y. Lyon and P. J. J. Alvarez, Comparative Eco-toxicity of Nanoscale TiO2, SiO2, and ZnO Water Suspensions, *Water Res.*, 2006, **40**, 3527-3532.

45. Z. V. Feng, I. L. Gunsolus, T. A. Qiu, K. R. Hurley, L. H. Nyberg, H. Frew, K. P. Johnson, A. M. Vartanian, L. M. Jacob, S. E. Lohse, M. D. Torelli, R. J. Hamers, C. J. Murphy and C. L. Haynes, Impacts of Gold Nanoparticle Charge and Ligand Type on Surface Binding and Toxicity to Gram-negative and Gram-positive bacteria, *Chem. Sci.*, 2015, **6**, 5186-5196.

46. I. Velzeboer, E. Peeters and A. A. Koelmans, Multiwalled Carbon Nanotubes at Environmentally Relevant Concentrations Affect the Composition of Benthic Communities, *Environ. Sci. Technol.*, 2013, **47**, 7475-7482.

47. P. C. Ke and R. Qiao, Carbon Nanomaterials in Biological Systems, *J. Phys. Condens. Matter.*, 2007, **19**, 25.

48. E. Oberdorster, S. Q. Zhu, T. M. Blickley, P. McClellan-Green and M. L. Haasch, Ecotoxicology of Carbon-based Engineered Nanoparticles: Effects of Fullerene (C-60) on Aquatic Organisms, *Carbon*, 2006, **44**, 1112-1120.

49. A. E. Nel, L. Madler, D. Velegol, T. Xia, E. M. V. Hoek, P. Somasundaran, F. Klaessig, V. Castranova and M. Thompson, Understanding Biophysicochemical Interactions at the Nano-bio Interface, *Nat. Mater.*, 2009, **8**, 543-557.

50. A. Bhaumik, A. M. Shearin, R. Delong, A. Wanekaya and K. Ghosh, Probing the Interaction at the Nano-Bio Interface Using Raman Spectroscopy: ZnO Nanoparticles and Adenosine Triphosphate Biomolecules, *J. Phys. Chem. C*, 2014, **118**, 18631-18639.

51. J. E. Gagner, S. Shrivastava, X. Qian, J. S. Dordick and R. W. Siegel, Engineering Nanomaterials for Biomedical Applications Requires Understanding the Nano-Bio Interface: A Perspective, *J. Phys. Chem. Lett.*, 2012, **3**, 3149-3158.

52. K. L. Garner and A. A. Keller, Emerging Patterns for Engineered Nanomaterials in the Environment: A Review of Fate and Toxicity Studies, *J. Nanopart. Res.*, 2014, **16**, 28.

53. B. Pelaz, G. Charron, C. Pfeiffer, Y. Zhao, J. M. de la Fuente, X.-J. Liang, W. J. Parak and P. del Pino, Interfacing Engineered Nanoparticles with Biological Systems: Anticipating Adverse Nano-Bio Interactions, *Small*, 2013, **9**, 1573-1584.

54. R. Podila, J. M. Brown, A. Kahru and A. M. Rao, Illuminating Nano-bio Interactions: A Spectroscopic Perspective, *MRS Bulletin*, 2014, **39**, 990-995.

55. W. Y. Wang, A. Sedykh, H. N. Sun, L. L. Zhao, D. P. Russo, H. Y. Zhou, B. Yan and H. Zhu, Predicting Nano-Bio Interactions by Integrating Nanoparticle Libraries and Quantitative Nanostructure Activity Relationship Modeling, *ACS Nano*, 2017, **11**, 12641-12649.

56. X. Zhang, X. Han, F. Wu, J. Jasensky and Z. Chen, Nano-bio Interfaces Probed by Advanced Optical Spectroscopy: From Model System Studies to Optical Biosensors, *Chin. Sci. Bull.*, 2013, **58**, 2537-2556.

57. M. Edidin, Timeline - Lipids on the Frontier: A Century of Cell-membrane Bilayers, *Nat. Rev. Mol. Cell Biol.*, 2003, **4**, 414-418.

58. J. van Weerd, M. Karperien and P. Jonkheijm, Supported Lipid Bilayers for the Generation of Dynamic Cell-Material Interfaces, *Adv. Healthc. Mater.*, 2015, **4**, 2743-2779.

59. M. Mahmoudi, J. Meng, X. Xue, X. J. Liang, M. Rahman, C. Pfeiffer, R. Hartmann, P. R. Gil, B. Pelaz, W. J. Parak, P. del Pino, S. Carregal-Romero, A. G. Kanaras and S. T. Selvan, Interaction of Stable Colloidal Nanoparticles with Cellular Membranes, *Biotechnol. Adv.*, 2014, **32**, 679-692.

60. S. G. Boxer, Molecular Transport and Organization in Supported Lipid Membranes, *Curr. Opin. Chem. Biol.*, 2000, **4**, 704-709.

61. N. Y. Lu, K. Yang, J. L. Li, B. Yuan and Y. Q. Ma, Vesicle Deposition and Subsequent Membrane-melittin Interactions on Different Substrates: A QCM-D Experiment, *Biochim. Biophys. Acta*, 2013, **1828**, 1918-1925.

62. J. Groves, in *BioMEMS and Biomedical Nanotechnology*, eds. M. Ferrari, T. Desai and S. Bhatia, Springer US, 2007, ch. 17, pp. 305-323.

63. C. Dietrich, L. A. Bagatolli, Z. N. Volovyk, N. L. Thompson, M. Levi, K. Jacobson and E. Gratton, Lipid Rafts Reconstituted in Model Membranes, *Biophys. J.*, 2001, **80**, 1417-1428.

64. T. G. Pomorski, T. Nylander and M. Cardenas, Model Cell Membranes: Discerning Lipid and Protein Contributions in Shaping the Cell, *Adv. Colloid Interface Sci.*, 2014, **205**, 207-220.

65. S. Nandi, R. Malishev, S. K. Bhunia, S. Kolusheva, J. Jopp and R. Jelinek, Lipid-Bilayer Dynamics Probed by a Carbon Dot-Phospholipid Conjugate, *Biophys. J.*, 2016, **110**, 2016-2025.

66. C. Steinem, A. Janshoff and H. J. Galla, Evidence for Multilayer Formation of Melittin on Solid-supported Phospholipid Membranes by Shear-wave Resonator Measurements, *Chem. Phys. Lipids*, 1998, **95**, 95-104.

67. J. T. Groves and M. L. Dustin, Supported Planar Bilayers in Studies on Immune Cell Adhesion and Communication, *J. Immunol. Methods*, 2003, **278**, 19-32.

68. K. L. Chen and G. D. Bothun, Nanoparticles Meet Cell Membranes: Probing Nonspecific Interactions. using Model Membranes, *Environ. Sci. Technol.*, 2014, **48**, 873-880.

69. J. M. Troiano, A. C. McGeachy, L. L. Olenick, D. Fang, D. Liang, J. Hong, T. R. Kuech, E. R. Caudill, J. A. Pedersen, Q. Cui and F. M. Geiger, Quantifying the Electrostatics of Polycation–Lipid Bilayer Interactions, *J. Am. Chem. Soc.*, 2017, **139**, 5808-5816.

70. J. Andersson and I. Koper, Tethered and Polymer Supported Bilayer Lipid Membranes: Structure and Function, *Membranes*, 2016, **6**, 14.

71. T. K. Lind, M. Cardenas and H. P. Wacklin, Formation of Supported Lipid Bilayers by Vesicle Fusion: Effect of Deposition Temperature, *Langmuir*, 2014, **30**, 7259-7263.

72. J. Milhaud, M. A. Hartmann and J. Bolard, Interaction of the Polyene Antibiotic Amphotericin-B with Model Membranes - Differences Between Small and Large Unilamellar Vesicles, *Biochimie*, 1989, **71**, 49-56.

73. M. Laurencin, T. Georgelin, B. Malezieux, J. M. Siaugue and C. Menager, Interactions Between Giant Unilamellar Vesicles and Charged Core-Shell Magnetic Nanoparticles, *Langmuir*, 2010, **26**, 16025-16030.

74. G. Rusciano, A. C. De Luca, G. Pesce and A. Sasso, On the Interaction of Nano-sized Organic Carbon Particles with Model Lipid Membranes, *Carbon*, 2009, **47**, 2950-2957.

75. A. Rice and J. Wereszczynski, Probing the Disparate Effects of Arginine and Lysine Residues on Antimicrobial Peptide/Bilayer Association, *Biochim. Biophys. Acta*, 2017, **1859**, 1941-1950.

76. P. Mueller, W. C. Wescott, D. O. Rudin and H. T. Tien, Methods for Formation of Single Bimolecular Lipid Membranes in Aqueous Solution, *J. Phys. Chem.*, 1963, **67**, 534-535.

77. P. Mueller, D. O. Rudin, H. T. Tien and W. C. Wescott, Reconstitution of Cell Membrane Structure in Vitro and Its Transformation into an Excitable System, *Nature*, 1962, **194**, 979-980.

78. I. C. Shieh and J. A. Zasadzinski, Visualizing Monolayers with a Water-soluble Fluorophore to Quantify Adsorption, Desorption, and the Double Layer, *Proc. Natl. Acad. Sci. U.S.A*, 2015, **112**, E826-E835.

79. R. Cseh and R. Benz, The Adsorption of Phloretin to Lipid Monolayers and Bilayers cannot be Explained by Langmuir Adsorption Isotherms Alone, *Biophys. J.*, 1998, **74**, 1399-1408.

80. A. K. Berkovich, E. P. Lukashev and N. S. Melik-Nubarov, Dipole Potential as a Driving Force for the Membrane Insertion of Polyacrylic Acid in Slightly Acidic Milieu, *Biochim. Biophys. Acta*, 2012, **1818**, 375-383.

81. P. C. Chiang, K. Tanady, L. T. Huang and L. Chao, Rupturing Giant Plasma Membrane Vesicles to Form Micron-sized Supported Cell Plasma Membranes with Native Transmembrane Proteins, *Sci. Rep.*, 2017, **7**, 8.

82. I. Moller and S. Seeger, Solid Supported Lipid Bilayers from Artificial and Natural Lipid Mixtures - Long-term Stable, Homogeneous and Reproducible, *J. Mater. Chem. B*, 2015, **3**, 6046-6056.

83. T. H. Anderson, Y. Min, K. L. Weirich, H. Zeng, D. Fygenson and J. N. Israelachvili, Formation of Supported Bilayers on Silica Substrates, *Langmuir*, 2009, **25**, 6997-7005.

84. B. Seantier, C. Breffa, O. Felix and G. Decher, Dissipation-enhanced Quartz Crystal Microbalance Studies on the Experimental Parameters Controlling the Formation of Supported Lipid Bilayers, *J. Phys. Chem. B*, 2005, **109**, 21755-21765.

85. A. C. McGeachy, N. Dalchand, E. R. Caudill, T. Li, M. Dogangun, L. L. Olenick, H. Chang, J. A. Pedersen and F. M. Geiger, Interfacial Electrostatics of Poly(vinylamine hydrochloride), Poly(diallyldimethylammonium chloride), Poly-L-lysine, and Poly-L-Arginine Interacting with Lipid Bilayers, *Phys. Chem. Chem. Phys.*, 2018. DOI: 10.1039/C7CP07353D

86. L. L. Olenick, H. M. Chase, L. Fu, Y. Zhang, A. C. McGeachy, M. Dogangun, S. R. Walter, H.-f. Wang and F. M. Geiger, Single-component Supported Lipid Bilayers Probed Using Broadband Nonlinear Optics, *Phys. Chem. Chem. Phys.*, 2018, **20**, 3063-3072.

87. J. Xu, M. J. Stevens, T. A. Oleson, J. A. Last and N. Sahai, Role of Oxide Surface Chemistry and Phospholipid Phase on Adsorption and Self-Assembly: Isotherms and Atomic Force Microscopy, *J. Phys. Chem. C*, 2009, **113**, 2187-2196.

88. E. Kalb, S. Frey and L. K. Tamm, Formation of Supported Planar Bilayers by Fusion of Vesicles to Supported Phospholipid Monolayers, *Biochim. Biophys. Acta*, 1992, **1103**, 307-316.

89. F. W. S. Stetter, S. H. Hyun, S. Brander, J. M. Urban, D. H. Thompson and T. Hugel, Nanomechanical Characterization of Lipid Bilayers with AFM-based Methods, *Polymer*, 2016, **102**, 326-332.

90. J. A. Jackman, S. R. Tabaei, Z. L. Zhao, S. Yorulmaz and N. J. Cho, Self-Assembly Formation of Lipid Bilayer Coatings on Bare Aluminum Oxide: Overcoming the Force of Interfacial Water, *ACS Appl. Mater. Interfaces*, 2015, **7**, 959-968.

91. N. J. Cho and C. W. Frank, Fabrication of a Planar Zwitterionic Lipid Bilayer on Titanium Oxide, *Langmuir*, 2010, **26**, 15706-15710.

92. M. D. Mager, B. Almquist and N. A. Melosh, Formation and Characterization of Fluid Lipid Bilayers on Alumina, *Langmuir*, 2008, **24**, 12734-12737.

93. J. T. Marques, R. F. M. de Almeida and A. S. Viana, Biomimetic Membrane Rafts Stably Supported on Unmodified Gold, *Soft Matter*, 2012, **8**, 2007-2016.

94. A. Kilic, M. F. Jadidi, H. O. Ozer and F. N. Kok, The Effect of Thiolated Phospholipids on Formation of Supported Lipid Bilayers on Gold Substrates Investigated by Surface-Sensitive Methods, *Colloids Surf. B*, 2017, **160**, 117-125.

95. Z. Salamon, Y. Wang, G. Tollin and H. A. Macleod, Assembly and Molecular-Organization of Self-Assembled Lipid Bilayers on Solid Substrates Monitored by Surface-Plasmon Resonance Spectroscopy, *Biochim. Biophys. Acta*, 1994, **1195**, 267-275.

96. E. Diamanti, P. Andreozzi, R. Anguiano, L. Yate, D. Gregurec, N. Politakos, R. F. Ziolo, E. Donath and S. E. Moya, The Effect of Top-layer Chemistry on the Formation of Supported Lipid Bilayers on Polyelectrolyte Multilayers: Primary versus Quaternary Amines, *Phys. Chem. Chem. Phys.*, 2016, **18**, 32396-32405.

97. H. Y. Liu, W. L. Chen, C. K. Ober and S. Daniel, Biologically Complex Planar Cell Plasma Membranes Supported on Polyelectrolyte Cushions Enhance Transmembrane Protein Mobility and Retain Native Orientation, *Langmuir*, 2018, **34**, 1061-1072.

98. E. Diamanti, D. Gregurec, M. J. Rodriguez-Presa, C. A. Gervasi, O. Azzaroni and S. E. Moya, High Resistivity Lipid Bilayers Assembled on Polyelectrolyte Multilayer Cushions: An Impedance Study, *Langmuir*, 2016, **32**, 6263-6271.

99. H. Pace, L. S. Nystrom, A. Gunnarsson, E. Eck, C. Monson, S. Geschwindner, A. Snijder and F. Hook, Preserved Transmembrane Protein Mobility in Polymer-Supported Lipid Bilayers Derived from Cell Membranes, *Anal. Chem.*, 2015, **87**, 9194-9203.

100. J. Majewski, J. Y. Wong, C. K. Park, M. Seitz, J. N. Israelachvili and G. S. Smith, Structural studies of polymer-cushioned lipid bilayers, *Biophys. J.*, 1998, **75**, 2363-2367.

101. M. L. Wagner and L. K. Tamm, Tethered Polymer-supported Planar Lipid Bilayers for Reconstitution of Integral Membrane Proteins: Silane-polyethyleneglycol-lipid As A Cushion and Covalent Linker, *Biophys. J.*, 2000, **79**, 1400-1414.

102. J. C. Munro and C. W. Frank, Adsorption of Disulfide-modified Polyacrylamides to Gold and Silver Surfaces as Cushions for Polymer-supported Lipid Bilayers, *Polymer*, 2003, **44**, 6335-6344.

103. G. van Meer, D. R. Voelker and G. W. Feigenson, Membrane Lipids: Where They are and How They Behave, *Nat. Rev. Mol. Cell Biol.*, 2008, **9**, 112-124.

104. M. Ikeda, A. Kihara and Y. Igarashi, Lipid Asymmetry of the Eukaryotic Plasma Membrane: Functions and Related Enzymes, *Biol. Pharm. Bull.*, 2006, **29**, 1542-1546.

105. W. Dowhan, Molecular Basis for Membrane Phospholipid Diversity: Why are There So Many Lipids?, *Annu. Rev. Biochem.*, 1997, **66**, 199-232.

106. M. J. Whittle, A. I. Macgillivray, K. P. Hanretty, H. G. Dobbie and C. A. Howie, Phosphatidylglycerol and Neonatal-Mortality and Morbidity, *J. Obstet. Gynaecol.*, 1986, **7**, 23-26.

107. E. M. Mejia and G. M. Hatch, Mitochondrial phospholipids: role in mitochondrial function, *J. Bioenerg. Biomembr.*, 2016, **48**, 99-112.

108. J. Yue, T. J. Feliciano, W. L. Li, A. Lee and T. W. Odom, Gold Nanoparticle Size and Shape Effects on Cellular Uptake and Intracellular Distribution of siRNA Nanoconstructs, *Bioconjugate Chem*., 2017, **28**, 1791-1800.

109. H. Lee and T. W. Odom, Controlling Ligand Density on Nanoparticles As A Means to Enhance Biological Activity, *Nanomedicine*, 2015, **10**, 177-180.

110. Q. S. Mu, C. A. David, J. Galceran, C. Rey-Castro, L. Krzeminski, R. Wallace, F. Bamiduro, S. J. Milne, N. S. Hondow, R. Brydson, G. Vizcay-Barrena, M. N. Routledge, L. J. C. Jeuken and A. P. Brown, Systematic Investigation of the Physicochemical Factors That Contribute to the Toxicity of ZnO Nanoparticles, *Chem. Res. Toxicol*., 2014, **27**, 558-567.

111. D. McShan, P. C. Ray and H. T. Yu, Molecular Toxicity Mechanism of Nanosilver, *J. Food Drug Anal*., 2014, **22**, 116-127.

112. A. C. Balazs, T. Emrick and T. P. Russell, Nanoparticle Polymer Composites: Where Two Small Worlds Meet, *Science*, 2006, **314**, 1107-1110.

113. R. P. Bagwe, L. R. Hilliard and W. H. Tan, Surface Modification of Silica Nanoparticles to Reduce Aggregation and Nonspecific Binding, *Langmuir*, 2006, **22**, 4357-4362.

114. A. K. Singh, *Engineered Nanoparticles: Structure, Properties and Mechanisms of Toxicity*, Elsevier Science, 2015.

115. A. Sasidharan, L. S. Panchakarla, P. Chandran, D. Menon, S. Nair, C. N. R. Rao and M. Koyakutty, Differential Nano-bio Interactions and Toxicity Effects of Pristine versus Functionalized Graphene, *Nanoscale*, 2011, **3**, 2461-2464.

116. Y. M. Cao, A. Stavrinadis, T. Lasanta, D. So and G. Konstantatos, The Role of Surface Passivation for Efficient and Photostable PbS Quantum Dot Solar Cells, *Nat. Energy*, 2016, **1**, 16035.

117. Y. Zhang, C. G. Fry, J. A. Pedersen and R. J. Hamers, Dynamics and Morphology of Nanoparticle-Linked Polymers Elucidated by Nuclear Magnetic Resonance, *Anal. Chem*., 2017, **89**, 12399-12407.

118. V. T. Huynh, D. Nguyen, C. H. Such and B. S. Hawkett, Polymer Coating of Graphene Oxide via Reversible Addition-Fragmentation Chain Transfer Mediated Emulsion Polymerization, *J. Polym. Sci. A*, 2015, **53**, 1413-1421.

119. M. Amirilargani, A. Ghadimi, M. A. Tofighy and T. Mohammadi, Effects of Poly (allylamine hydrochloride) As A New Functionalization Agent for Preparation of Poly vinyl alcohol/Multiwalled Carbon Nanotubes Membranes, *J. Memb. Sci*., 2013, **447**, 315-324.

120. J. M. Dennison, J. M. Zupancic, W. Lin, J. H. Dwyer and C. J. Murphy, Protein Adsorption to Charged Gold Nanospheres as a Function of Protein Deformability, *Langmuir*, 2017, **33**, 7751-7761.

121. T. Hajnalka-Mária, B. Bea, N. Katalin, P. Áron, H. Rudi and K. Katalin, Infrared and Raman Investigation of Carbon Nanotube-polyallylamine Hybrid Systems, *Physica Status Solidi B*, 2010, **247**, 2884-2886.

122. J. B. Kim, T. Premkumar, K. Lee and E. Geckeler Kurt, A Facile Approach to Single-Wall Carbon Nanotube/Poly(allylamine) Nanocomposites, *Macromol. Rapid Commun.*, 2007, **28**, 276-280.

123. R. F. Fakhrullin, L. V. Shlykova, A. I. Zamaleeva, D. K. Nurgaliev, Y. N. Osin, J. Garcia-Alonso and V. N. Paunov, Interfacing Living Unicellular Algae Cells with Biocompatible Polyelectrolyte-Stabilised Magnetic Nanoparticles, *Macromol. Biosci.*, 2010, **10**, 1257-1264.

124. M. F. Haase, D. Grigoriev, H. Moehwald, B. Tiersch and D. G. Shchukin, Nanoparticle Modification by Weak Polyelectrolytes for pH-Sensitive Pickering Emulsions, *Langmuir*, 2011, **27**, 74-82.

125. R. C. Luo, B. Neu and S. S. Venkatraman, Surface Functionalization of Nanoparticles to Control Cell Interactions and Drug Release, *Small*, 2012, **8**, 2585-2594.

126. Y. A. Zhang, D. Xu, W. Q. Li, J. Yu and Y. Chen, Effect of Size, Shape, and Surface Modification on Cytotoxicity of Gold Nanoparticles to Human HEp-2 and Canine MDCK Cells, *J. Nanomater.*, 2012, 7.

127. J. S. Martinez, T. C. S. Keller and J. B. Schlenoff, Cytotoxicity of Free versus Multilayered Polyelectrolytes, *Biomacromolecules*, 2011, **12**, 4063-4070.

128. M. Wytrwal, P. Koczurkiewicz, K. Wojcik, M. Michalik, B. Kozik, M. Zylewski, M. Nowakowska and M. Kepczynski, Synthesis of Strong Polycations with Improved Biological Properties, *J. Biomed. Mater. Res. A*, 2014, **102**, 721-731.

129. T. A. Qiu, M. D. Torelli, A. M. Vartanian, N. B. Rackstraw, J. T. Buchman, L. M. Jacob, C. J. Murphy, R. J. Hamers and C. L. Haynes, Quantification of Free Polyelectrolytes Present in Colloidal Suspension, Revealing a Source of Toxic Responses for Polyelectrolyte-Wrapped Gold Nanoparticles, *Anal. Chem.*, 2017, **89**, 1823-1830.

130. F. Zaera, Probing Liquid/Solid Interfaces at the Molecular Level, *Chem. Rev.*, 2012, **112**, 2920-2986.

131. Z. F. Zhang, D. Yomo and C. Gradinaru, Choosing the Right Fluorophore for Single-molecule Fluorescence Studies in a Lipid Environment, *Biochim. Biophys. Acta*, 2017, **1859**, 1242-1253.

132. A. D. Robison, S. Sun, M. F. Poyton, G. A. Johnson, J. P. Pellois, P. Jungwirth, M. Vazdar and P. S. Cremer, Polyarginine Interacts More Strongly and Cooperatively than Polylysine with Phospholipid Bilayers, *J. Phys. Chem. B*, 2016, **120**, 9287-9296.

133. J. K. Vaishnav and T. K. Mukherjee, Tuning of Resonance Energy Transfer from 4 ',6-diamidino-2-phenylindole to An Ultrasmall Silver Nanocluster Across the Lipid Bilayer, *Phys. Chem. Chem. Phys.*, 2017, **19**, 27305-27312.

134. L. Zuccarello, E. Rampazzo, L. Petrizza, L. Prodi and C. Satriano, The Influence of Fluorescent Silica Nanoparticle Surface Chemistry on the Energy Transfer Processes with Lipid Bilayers, *RSC Adv.*, 2016, **6**, 52674-52682.

135. F. A. Heberle, J. Wu, S. L. Goh, R. S. Petruzielo and G. W. Feigenson, Comparison of Three Ternary Lipid Bilayer Mixtures: FRET and ESR Reveal Nanodomains, *Biophys. J.*, 2010, **99**, 3309-3318.

136. M. L. Frazier, J. R. Wright, A. Pokorny and P. F. F. Almeida, Investigation of Domain Formation in Sphingomyelin/cholesterol/POPC Mixtures by Fluorescence Resonance Energy Transfer and Monte Carlo Simulations, *Biophys. J.*, 2007, **92**, 2422-2433.

137. J. Barauskas, C. Cervin, M. Jankunec, M. Spandyreva, K. Ribokaite, F. Tiberg and M. Johnsson, Interactions of Lipid-based Liquid Crystalline Nanoparticles with Model and Cell Membranes, *Int. J. Pharm.*, 2010, **391**, 284-291.

138. X. X. Wu, S. Sun, Y. H. Wang, J. L. Zhu, K. Jiang, Y. M. Leng, Q. H. Shu and H. W. Lin, A Fluorescent Carbon-dots-based Mitochondria-targetable Nanoprobe for Peroxynitrite Sensing in Living Cells, *Biosens. Bioelectron.*, 2017, **90**, 501-507.

139. A. J. Haes and R. P. Van Duyne, A nanoscale optical blosensor: Sensitivity and Selectivity of An Approach Based on the Localized Surface Plasmon Resonance Spectroscopy of Triangular Silver Nanoparticles, *J. Am. Chem. Soc.*, 2002, **124**, 10596-10604.

140. T. H. Lee, D. J. Hirst and M. I. Aguilar, New Insights into the Molecular Mechanisms of Biomembrane Structural Changes and Interactions by Optical Biosensor Technology, *Biochim. Biophys. Acta*, 2015, **1848**, 1868-1885.

141. W. M. Henderson, D. Bouchard, X. J. Chang, S. R. Al-Abed and Q. Teng, Biomarker Analysis of Liver Cells Exposed to Surfactant-wrapped and Oxidized Multi-walled Carbon Nanotubes (MWCNTs), *Sci. Total Environ.*, 2016, **565**, 777-786.

142. R. Dojcilovic, J. D. Pajovic, D. K. Bozanic, V. V. Vodnik, S. Dimitrijevic-Brankovic, A. R. Milosavljevic, S. Kascakova, M. Refregiers and V. Djokovic, A Fluorescent Nanoprobe for Single Bacterium Tracking: Functionalization of Silver Nanoparticles with Tryptophan to Probe the Nanoparticle Accumulation with Single Cell Resolution, *Analyst*, 2016, **141**, 1988-1996.

143. Y. S. Hwang, X. Qu and Q. Li, The Role of Photochemical Transformations in the Aggregation and Deposition of Carboxylated Multiwall Carbon Nanotubes Suspended in Water, *Carbon*, 2013, **55**, 81-89.

144. T. Zhang, M. Tang, L. Kong, H. Li, Y. Y. Xue and Y. P. Pu, Surface Modification of Multiwall Carbon Nanotubes Determines the Pro-inflammatory Outcome in Macrophage, *J. Hazard. Mater.*, 2015, **284**, 73-82.

145. I. D. Rosca, F. Watari, M. Uo and T. Akaska, Oxidation of multiwalled carbon nanotubes by nitric acid, *Carbon*, 2005, **43**, 3124-3131.

146. Y. Yang, K. M. Mayer and J. H. Hafner, Quantitative Membrane Electrostatics with the Atomic Force Microscope, *Biophys. J.*, 2007, **92**, 1966-1974.

147. A. S. Johnson, C. L. Nehl, M. G. Mason and J. H. Hafner, Fluid Electric Force Microscopy for Charge Density Mapping in Biological Systems, *Langmuir*, 2003, **19**, 10007-10010.

148. C. Rotsch and M. Radmacher, Mapping Local Electrostatic Forces with the Atomic Force Microscope, *Langmuir*, 1997, **13**, 2825-2832.

149. K. B. Eisenthal, Second Harmonic Spectroscopy of Aqueous Nano- and Microparticle Interfaces, *Chem. Rev.*, 2006, **106**, 1462-1477.

150. M. B. Raschke and Y. R. Shen, Nonlinear Optical Spectroscopy of Solid Interfaces, *Curr. Opin. Solid State Mater. Sci.*, 2004, **8**, 343-352.

Chapter 2 References.

1. H. Wang, E. C. Y. Yan, E. Borguet and K. B. Eisenthal, Second Harmonic Generation from the Surface of Centrosymmetric Particles in Bulk Solution, *Chem. Phys. Lett.*, 1996, **259**, 15-20.

2. K. B. Eisenthal, Equilibrium and Dynamic Processes at Interfaces by 2nd Harmonic and Sum Frequency Generation, *Annu. Rev. Phys. Chem.*, 1992, **43**, 627-661.

3. R. M. Corn and D. A. Higgins, Optical 2nd-Harmonic Generation as a Probe of Surface-Chemistry, *Chem. Rev.*, 1994, **94**, 107-125.

4. P. L. Hayes, J. N. Malin, D. S. Jordan and F. M. Geiger, Get Charged Up: Nonlinear Optical Voltammetry for Quantifying the Thermodynamics and Electrostatics of Metal Cations at Aqueous/Oxide Interfaces, *Chem. Phys. Lett.*, 2010, **499**, 183-192.

5. F. M. Geiger, Second Harmonic Generation, Sum Frequency Generation, and chi((3)): Dissecting Environmental Interfaces with a Nonlinear Optical Swiss Army Knife, *Annu. Rev. Phys. Chem.*, 2009, **60**, 61-83.

6. J. N. Malin and F. M. Geiger, Uranyl Adsorption and Speciation at the Fused Silica/Water Interface Studied by Resonantly Enhanced Second Harmonic Generation and the chi((3)) Method, *J. Phys. Chem. A*, 2010, **114**, 1797-1805.

7. J. N. Malin, P. L. Hayes and F. M. Geiger, Interactions of Ca, Zn, and Cd Ions at Buried Solid/Water Interfaces Studied by Second Harmonic Generation, *J. Phys. Chem. C*, 2009, **113**, 2041-2052.

8. M. S. Azam and J. M. Gibbs-Davis, Monitoring DNA Hybridization and Thermal Dissociation at the Silica/Water Interface Using Resonantly Enhanced Second Harmonic Generation Spectroscopy, *Anal. Chem.*, 2013, **85**, 8031-8038.

9. J. L. Achtyl, I. V. Vlassiouk, S. P. Surwade, P. F. Fulvio, S. Dai and F. M. Geiger, Interaction of Magnesium Ions with Pristine Single-Layer and Defected Graphene/Water Interfaces Studied by Second Harmonic Generation, *J. Phys. Chem. B*, 2014, **118**, 7739-7749.

10. Y. Rao, S. J. J. Kwok, J. Lombardi, N. J. Turro and K. B. Eisenthal, Label-free Probe of HIV-1 TAT Peptide Binding to Mimetic Membranes, *Proc. Natl. Acad. Sci. U. S.A.*, 2014, **111**, 12684-12688.

11. M. Dogangun, M. N. Hang, J. Machesky, A. C. McGeachy, N. Dalchand, R. J. Hamers and F. M. Geiger, Evidence for Considerable Metal Cation Concentrations from Lithium Intercalation Compounds in the Nano-Bio Interface Gap, *J. Phys. Chem. C*, 2017, **121**, 27473-27482.

12. A. C. McGeachy, L. L. Olenick, J. M. Troiano, R. S. Lankone, E. S. Melby, T. R. Kuech, E. Ehimiaghe, D. H. Fairbrother, J. A. Pedersen and F. M. Geiger, Resonantly Enhanced Nonlinear Optical Probes of Oxidized Multiwalled Carbon Nanotubes at Supported Lipid Bilayers, *J. Phys. Chem. B*, 2017, **121**, 1321-1329.

13. A. C. McGeachy, N. Dalchand, E. R. Caudill, T. Li, M. Dogangun, L. L. Olenick, H. Chang, J. A. Pedersen and F. M. Geiger, Interfacial Electrostatics of Poly(vinylamine hydrochloride), Poly(diallyldimethylammonium chloride), Poly-L-lysine, and Poly-L-Arginine Interacting with Lipid Bilayers, *Phys. Chem. Chem. Phys.*, 2018. DOI: 10.1039/C7CP07353D.

14. L. L. Olenick, H. M. Chase, L. Fu, Y. Zhang, A. C. McGeachy, M. Dogangun, S. R. Walter, H.-f. Wang and F. M. Geiger, Single-component Supported Lipid Bilayers Probed Using Broadband Nonlinear Optics, *Phys. Chem. Chem. Phys.*, 2018, **20**, 3063-3072.

15. J. M. Troiano, A. C. McGeachy, L. L. Olenick, D. Fang, D. Liang, J. Hong, T. R. Kuech, E. R. Caudill, J. A. Pedersen, Q. Cui and F. M. Geiger, Quantifying the Electrostatics of Polycation–Lipid Bilayer Interactions, *J. Am. Chem. Soc.*, 2017, **139**, 5808-5816.

16. Y. Liu, C. Y. Yan, X. L. Zhao and K. B. Eisenthal, Surface Potential of Charged Liposomes Determined by Second Harmonic Generation, *Langmuir*, 2001, **17**, 2063-2066.

17. S. W. Ong, X. L. Zhao and K. B. Eisenthal, Polarization of Water Molecules at a Charged Interface: Second Harmonic Studies of the Silica/Water Interface, *Chem. Phys. Lett.*, 1992, **191**, 327-335.

18. J. S. Salafsky and K. B. Eisenthal, Protein Adsorption at Interfaces Detected by Second Harmonic Generation, *J. Phys. Chem. B*, 2000, **104**, 7752-7755.

19. S. A. Saslow Gomez, D. S. Jordan, J. M. Troiano and F. M. Geiger, Uranyl Adsorption at the Muscovite (Mica)/Water Interface Studied by Second Harmonic Generation, *Environ. Sci. Technol.*, 2012, **46**, 11154-11161.

20. D. S. Jordan, J. N. Malin and F. M. Geiger, Interactions of Al(III), La(III), Gd(III), and Lu(III) with the Fused Silica/Water Interface Studied by Second Harmonic Generation, *Environ. Sci. Technol.*, 2010, **44**, 5862-5867.

21. D. S. Jordan, C. J. Hull, J. M. Troiano, S. C. Riha, A. B. F. Martinson, K. M. Rosso and F. M. Geiger, Second Harmonic Generation Studies of Fe(II) Interactions with Hematite (alpha-Fe2O3), *J. Phys. Chem. C*, 2013, **117**, 4040-4047.

22. J. M. Troiano, D. S. Jordan, C. J. Hull and F. M. Geiger, Interaction of Cr(III) and Cr(VI) with Hematite Studied by Second Harmonic Generation, *J. Phys. Chem. C*, 2013, **117**, 5164-5171.

23. J. S. Salafsky, Second-harmonic Generation for Studying Structural Motion of Biological Molecules in Real Time and Space, *Phys. Chem. Chem. Phys.*, 2007, **9**, 5704-5711.

24. J. Duboisset, D. Ait-Belkacem, M. Roche, H. Rigneault and S. Brasselet, Generic Model of the Molecular Orientational Distribution Probed by Polarization-resolved Second-harmonic Generation, *Phys. Rev. A*, 2012, **85**, 9.

25. J. M. Troiano, L. L. Olenick, T. R. Kuech, E. S. Melby, D. Hu, S. E. Lohse, A. C. Mensch, M. Dogangun, A. M. Vartanian, M. D. Torelli, E. Ehimiaghe, S. R. Walter, L. Fu, C. R. Anderton, Z. Zhu, H. Wang, G. Orr, C. J. Murphy, R. J. Hamers, J. A. Pedersen and F. M. Geiger, Direct Probes of 4 nm Diameter Gold Nanoparticles Interacting with Supported Lipid Bilayers, *J. Phys. Chem. C*, 2015, ***119*** 534-546.

26. J. M. Troiano, T. R. Kuech, A. M. Vartanian, M. D. Torelli, A. Sen, L. M. Jacob, R. J. Hamers, C. J. Murphy, J. A. Pedersen and F. M. Geiger, On Electronic and Charge Interference in Second Harmonic Generation Responses from Gold Metal Nanoparticles at Supported Lipid Bilayers, *J. Phys. Chem. C*, 2016, **120**, 20659-20667.

27. K. B. Eisenthal, Second Harmonic Spectroscopy of Aqueous Nano- and Microparticle Interfaces, *Chem. Rev.*, 2006, **106**, 1462-1477.

28. P. E. Ohno, H.-f. Wang and F. M. Geiger, Second-order Spectral Lineshapes from Charged Interfaces, *Nat. Commun.*, 2017, **8**, 1032.

29. G. Gonella, C. Lutgebaucks, A. G. F. de Beer and S. Roke, Second Harmonic and Sum-Frequency Generation from Aqueous Interfaces Is Modulated by Interference, *J. Phys. Chem. C*, 2016, **120**, 9165-9173.

30. M. D. Boamah, P. E. Ohno, F. M. Geiger and K. B. Eisenthal, Relative Permittivity in the Electrical Double Layer from Nonlinear Optics, *arXiv 1702.02496*, 2017.

31. Y.-C. Wen, S. Zha, X. S. Liu, S. Yang, P. Guo, G. Shi, H. Fang, Y. R. Shen and C. Tian, Unveiling Microscopic Structures of Charged Water Interfaces by Surface-Specific Vibrational Spectroscopy, *Phys. Rev. Lett.*, 2016, **116**, 016101.

32. H.-f. Wang, Sum Frequency Generation Vibrational Spectroscopy (SFG-VS) for Complex Molecular Surfaces and Interfaces: Spectral Lineshape Measurement and Analysis Plus Some Controversial Issues, *Prog. Surf. Sci.*, 2016, **91**, 155-182.

33. P. E. Ohno, S. A. Saslow, H.-f. Wang, F. M. Geiger and K. B. Eisenthal, Phase-referenced Nonlinear Spectroscopy of the alpha-Quartz/Water Interface, *Nat. Commun.*, 2016, **7**, 13587.

34. X. Zhao, S. Ong, H. Wang and K. B. Eisenthal, New Method for Determination of Surface pKa Using Second Harmonic Generation, *Chem. Phys. Lett.*, 1993, **214**, 203-207.

35. J. P. Fitts, X. Shang, G. W. Flynn, T. F. Heinz and K. B. Eisenthal, Electrostatic Surface Charge at Aqueous/a-Al2O3 Single-Crystal Interfaces as Probed by Optical Second-Harmonic Generation, *J. Phys. Chem. B*, 2005, **109**, 7981-7986.

36. R. Araya, J. Jiang, K. B. Eisenthal and R. Yuste, The Spine Neck Filters Membrane Potentials, *Proc. Natl. Acad. Sci. U.S.A.*, 2006, **103**, 17961-17966.

37. E. H. Chen, S. A. Saslow, S. T. Nguyen and F. M. Geiger, Zinc Ion-Hydroxyl Interactions at Undecanol-Funcationalized Fused Silica/Water Interfaces Quantified Using the Eisenthal chi(3) Technique, *J. Phys. Chem. C*, 2012, **116**, 19886-19892.

38. P. L. Hayes, E. H. Chen, J. L. Achtyl and F. M. Geiger, An Optical Voltmeter for Studying Cetyltrimethylammonium Interacting with Fused Silica/Aqueous Interfaces at High Ionic Strength, *J. Phys. Chem. A*, 2009, **113**, 4269-4280.

39. J. L. Achtyl, R. R. Unocic, L. Xu, Y. Cai, M. Raju, W. Zhang, R. L. Sacci, I. V. Vlassiouk, P. F. Fulvio, P. Ganesh, D. J. Wesolowski, S. Dai, A. C. T. van Duin, M. Neurock and F. M. Geiger, Aqueous Proton Transfer Across Single-layer Graphene, *Nat. Commun.*, 2015, **6**.

40. C. Macias-Romero, I. Nahalka, H. I. Okur and S. Roke, Optical Imaging of Surface Chemistry and Dynamics in Confinement, *Science*, 2017, **25**, 784-788.

41. F. Träger, *Springer Handbook of Lasers and Optics*, Springer, New York, 2007.

42. C. T. Williams and D. A. Beattie, Probing Buried Interfaces with Non-linear Optical Spectroscopy, *Surf. Sci.*, 2002, **500**, 545-576.

43. H. S. T. Driver, H. A. Elliott and P. W. Linder, Application of the Gouy—Chapman Equation in Metal Speciation Modelling, *Chem. Speciation Bioavailability*, 1991, **3**, 61-62.

44. W. Stumm and J. J. Morgan, *Aquatic Chemistry: Chemical Equilibria and Rates in Natural Waters*, Wiley, New York, 1996.

45. L. H. Klausen, T. Fuhs and M. D. Dong, Mapping Surface Charge Density of Lipid Bilayers by Quantitative Surface Conductivity Microscopy, *Nat. Commun.*, 2016, **7**, 10.

46. R. M. Peitzsch, M. Eisenberg, K. A. Sharp and S. McLaughlin, Calculations of the Electrostatic Potential Adjacent to Model Phospholipid-Bilayers, *Biophys. J.*, 1995, **68**, 729-738.

47. R. Burt, G. Birkett and X. S. Zhao, A Review of Molecular Modelling of Electric Double Layer Capacitors, *Phys. Chem. Chem. Phys.*, 2014, **16**, 6519-6538.

48. E. J. W. Verwey, The Electrical Double Layer and the Stability of Lyophobic Colloids, *Chem. Rev.*, 1935, **16**, 363-415.

49. P. Maity, B. Saha, G. S. Kumar and S. Karmakar, Binding of Monovalent Alkali Metal Ions with Negatively Charged Phospholipid Membranes, *Biochim. Biophys. Acta*, 2016, **1858**, 706-714.

50. T. M. Domingues, B. Mattei, J. Seelig, K. R. Perez, A. Miranda and K. A. Riske, Interaction of the Antimicrobial Peptide Gomesin with Model Membranes: A Calorimetric Study, *Langmuir*, 2013, **29**, 8609-8618.

51. R. Lehrmann and J. Seelig, Adsorption of Ca2+ and La3+ to Bilayer Membranes: Measurement of the Adsorption Enthalpy and Binding Constant with Titration Calorimetry, *Biochim. Biophys. Acta*, 1994, **1189**, 89-95.

52. D. Langmuir, *Aqueous Environmental Geochemistry*, Prentice Hall, Upper Saddle River, N.J., 1997.

53. P. Leroy and A. Revil, A Triple-layer Model of the Surface Electrochemical Properties of Clay Minerals, *J. Colloid Interface Sci.*, 2004, **270**, 371-380.

54. J. A. Davis, R. O. James and J. O. Leckie, Surface Ionization and Complexation at Oxide-Water Interface .1. Computation of Electrical Double-Layer Properties in Simple Electrolytes, *J. Colloid Interface Sci.*, 1978, **63**, 480-499.

55. Y. Nakayama and D. Andelman, Differential Capacitance of the Electric Double Layer: The Interplay Between Ion Finite Size and Dielectric Decrement, *J. Chem. Phys.*, 2015, **142**. DOI: 10.1063/1.4906319.

56. B. E. Conway, J. O. Bockris and I. A. Ammar, The Dielectric Constant of the Solution in the Diffuse and Helmholtz Double Layers at a Charged Interface in Aqueous Solution, *J. Chem. Soc. Faraday Trans.*, 1951, **47**, 756-766.

57. J. R. Macdonald and C. A. Barlow, Theory of Double-Layer Differential Capacitance in Electrolytes, *J. Chem. Phys.*, 1962, **36**, 3062-3063.

58. E. Gongadze, A. Velikonja, S. Perutkova, P. Kramar, A. Macek-Lebar, V. Kralj-Iglic and A. Iglic, Ions and Water Molecules in an Electrolyte Solution in Contact with Charged and Dipolar Surfaces, *Electrochim. Acta*, 2014, **126**, 42-60.

59. I. Langmuir, The Constitution and Fundamental Properties of Solids and Liquids Part I Solids, *J. Am. Chem. Soc.*, 1916, **38**, 2221-2295.

60. R. I. Masel, *Principles of Adsorption and Reaction on Solid Surfaces*, Wiley, New York [u.a.], 1996.

61. J. Barcroft and A. V. Hill, The Nature of oxyh ae moglobin, With A Note on its Molecular Weight, *J. Physiol.*, 1910, **39**, 411-428.

62. M. Mosior and S. McLaughlin, Electrostatics and Reduction Of Dimensionality Produce Apparent Cooperativity When Basic Peptides Bind To Acidic Lipids In Membranes, *Biochim. Biophys. Acta*, 1992, **1105**, 185-187.

63. F. Torrens, G. Castellano, A. Campos and C. Abad, Negatively Cooperative Binding of Melittin to Neutral Phospholipid Vesicles, *J. Mol. Struct.*, 2007, **834**, 216-228.

64. S. V. Solomatin, M. Greenfeld and D. Herschlag, Implications of Molecular Heterogeneity for the Cooperativity of Biological Macromolecules, *Nat. Struct. Mol. Biol.*, 2011, **18**, 732-734.

Chapter 3 References.

1. S. K. Shriyan and A. K. Fontecchio, Analysis of Effects of Oxidized Multiwalled Carbon Nanotubes on Electro-optic Polymer/liquid Crystal Thin Film Gratings, *Opt. Express*, 2010, **18**, 24842-24852.

2. N. A. M. Taib, N. Bidin, H. Haris, N. N. Adnan, M. F. S. Ahmad and S. W. Harun, Multi-walled Carbon Nanotubes Saturable Absorber in Q-switching Flashlamp Pumped Nd:YAG Laser, *Opt. Laser Technol.*, 2016, **79**, 193-197.

3. Z. L. Huang, M. Gao, Z. C. Yan, T. S. Pan, F. Y. Liao and Y. Lin, Flexible Infrared Detectors Based on p-n Junctions of Multi-walled Carbon Nanotubes, *Nanoscale*, 2016, **8**, 9592-9599.

4. D. Wang, H. Y. Li, M. F. Li, H. Q. Jiang, M. Xia and Z. Zhou, Stretchable Conductive Polyurethane Elastomer In Situ Polymerized with Multi-walled Carbon Nanotubes, *J. Mater. Chem. C*, 2013, **1**, 2744-2749.

5. A. Servant, I. Jacobs, C. Bussy, C. Fabbro, T. da Ros, E. Pach, B. Ballesteros, M. Prato, K. Nicolay and K. Kostarelos, Gadolinium-functionalised Multi-walled Carbon Nanotubes as A T-1 Contrast Agent for MRI Cell Labelling and Tracking, *Carbon*, 2016, **97**, 126-133.

6. S. Fedeli, A. Brandi, L. Venturini, P. Chiarugi, E. Giannoni, P. Paoli, D. Corti, G. Giambastiani, G. Tuci and S. Cicchi, The "Click-on-Tube" Approach for the Production of Efficient Drug Carriers Based on Oxidized Multi-walled Carbon Nanotubes, *J. Mater. Chem. B*, 2016, **4**, 3823-3831.

7. B. Mandal, D. Das, A. P. Rameshbabu, S. Dhara and S. Pal, A Biodegradable, Biocompatible Transdermal Device Derived from Carboxymethyl Cellulose and Multi-walled Carbon Nanotubes for Sustained Release of Diclofenac Sodium, *RSC Adv.*, 2016, **6**, 19605-19611.

8. R. Afshari, S. Mazinani and M. Abdouss, Nanohybrid Nanoparticles Based on Chitosan/Functionalized Carbon Nanotubes as Anti-HIV Nanocarrier, *Nano*, 2015, **10**, 12.

9. H. Moradian, H. Fasehee, H. Keshvari and S. Faghihi, Poly(Ethyleneimine) Functionalized Carbon Nanotubes as Efficient Nano-Vector for Transfecting Mesenchymal Stem Cells, *Colloids Surf. B*, 2014, **122**, 115-125.

10. N. M. Mubarak, J. N. Sahu, E. C. Abdullah and N. S. Jayakumar, Removal of Heavy Metals from Wastewater Using Carbon Nanotubes, *Sep. Purif. Rev.*, 2014, **43**, 311-338.

11. R. Das, M. E. Ali, S. B. Abd Hamid, S. Ramakrishna and Z. Z. Chowdhury, Carbon Nanotube Membranes for Water Purification: A Bright Future in Water Desalination, *Desalination*, 2014, **336**, 97-109.

12. S. H. Kim, A. Umar, R. Kumar, H. Algarni and M. S. Al-Assiri, Poly(Acrylic Acid)/Multi-Walled Carbon Nanotube Composites: Efficient Scaffold for Highly Sensitive 2-Nitrophenol Chemical Sensor, *Nanosci. Nanotechnol. Lett.*, 2016, **8**, 200-206.

13. H. Q. Sun, C. Kwan, A. Suvorova, H. M. Ang, M. O. Tade and S. B. Wang, Catalytic Oxidation of Organic Pollutants on Pristine and Surface Nitrogen-Modified Carbon Nanotubes with Sulfate Radicals, *Appl. Catal. B.*, 2014, **154**, 134-141.

14. H. B. Gu, S. B. Rapole, Y. D. Huang, D. M. Cao, Z. P. Luo, S. Y. Wei and Z. H. Guo, Synergistic Interactions Between Multi-walled Carbon Nanotubes and Toxic Hexavalent Chromium, *J. Mater. Chem. A*, 2013, **1**, 2011-2021.

15. R. R. Salunkhe, H. Ahn, J. H. Kim and Y. Yamauchi, Rational Design of Coaxial Structured Carbon Nanotube-manganese Oxide (CNT-MnO2) for Energy Storage Application, *Nanotechnology*, 2015, **26**, 7.

16. F. De Nicola, M. Salvato, C. Cirillo, M. Crivellari, M. Boscardin, M. Scarselli, F. Nanni, I. Cacciotti, M. De Crescenzi and P. Castrucci, Record Efficiency of Air-stable Multi-walled Carbon Nanotube/silicon Solar Cells, *Carbon*, 2016, **101**, 226-234.

17. M. F. L. De Volder, S. H. Tawfick, R. H. Baughman and A. J. Hart, Carbon Nanotubes: Present and Future Commercial Applications, *Science*, 2013, **339**, 535-539.

18. W. J. G. M. Peijnenburg, M. Baalousha, J. W. Chen, Q. Chaudry, F. Von der kammer, T. A. J. Kuhlbusch, J. Lead, C. Nickel, J. T. K. Quik, M. Renker, Z. Wang and A. A. Koelmans, A Review of the Properties and Processes Determining the Fate of Engineered Nanomaterials in the Aquatic Environment, *Crit. Rev. Environ. Sci. Technol.*, 2015, **45**, 2084-2134.

19. A. E. Nel, L. Madler, D. Velegol, T. Xia, E. M. V. Hoek, P. Somasundaran, F. Klaessig, V. Castranova and M. Thompson, Understanding Biophysicochemical Interactions at the Nano-bio Interface, *Nat. Mater.*, 2009, **8**, 543-557.

20. C. Chen, Y.-F. Li, Y. Qu, Z. Chai and Y. Zhao, Advanced Nuclear Analytical and Related Techniques for the Growing Challenges in Nanotoxicology, *Chem. Soc. Rev.*, 2013, **42**, 8266-8303.

21. Y. Xiao and M. R. Wiesner, Characterization of Surface Hydrophobicity of Engineered Nanoparticles, *J. Hazard. Mater.*, 2012, **215**, 146-151.

22. B. Pelaz, G. Charron, C. Pfeiffer, Y. Zhao, J. M. de la Fuente, X.-J. Liang, W. J. Parak and P. del Pino, Interfacing Engineered Nanoparticles with Biological Systems: Anticipating Adverse Nano-Bio Interactions, *Small*, 2013, **9**, 1573-1584.

23. K. L. Chen and G. D. Bothun, Nanoparticles Meet Cell Membranes: Probing Nonspecific Interactions. using Model Membranes, *Environ. Sci. Technol.* 2014, **48**, 873-880.

24. M. Hassellöv, J. Readman, J. Ranville and K. Tiede, Nanoparticle Analysis and Characterization Methodologies in Environmental Risk Assessment of Engineered Nanoparticles, *Ecotoxicology*, 2008, **17**, 344-361.

25. P. Yi and K. L. Chen, Influence of Solution Chemistry on the Release of Multiwalled Carbon Nanotubes from Silica Surfaces, *Environ. Sci. Technol.* 2013, **47**, 12211-12218.

26. S. J. Sarma, I. Bhattacharya, S. K. Brar, R. D. Tyagi and R. Y. Surampalli, Carbon Nanotube-Bioaccumulation and Recent Advances in Environmental Monitoring, *Crit. Rev. Environ. Sci. Technol.*, 2015, **45**, 905-938.

27. C. J. Murphy, A. M. Vartania, F. M. Geiger, R. J. Hamers, J. A. Pedersen, Q. Cui, C. L. Haynes, E. E. Carlson, R. Hernandez, R. D. Klaper, G. Orr and Z. Rosenzweig, Biological Responses to Engineered Nanomaterials: Needs for the Next Decade, *ACS Cent. Sci.*, 2015, **1**, 117-123.

28. C. Bussy, M. Pinault, J. Cambedouzou, M. J. Landry, P. Jegou, M. Mayne-L'hermite, P. Launois, J. Boczkowski and S. Lanone, Critical Role of Surface Chemical Modifications Induced by Length Shortening on Multi-walled Carbon Nanotubes-induced Toxicity, *Part. Fibre Toxicol.*, 2012, **9**, 15.

29. B. Q. Luan, T. Huynh and R. H. Zhou, Complete Wetting of Graphene by Biological Lipids, *Nanoscale*, 2016, **8**, 5750-5754.

30. C. Corredor, W.-C. Hou, S. A. Klein, B. Y. Moghadam, M. Goryll, K. Doudrick, P. Westerhoff and J. D. Posner, Disruption of Model Cell Membranes by Carbon Nanotubes, *Carbon*, 2013, **60**, 67-75.

31. V. C. Sanchez, A. Jachak, R. H. Hurt and A. B. Kane, Biological Interactions of Graphene-Family Nanomaterials: An Interdisciplinary Review, *Chem. Res. Toxicol.*, 2012, **25**, 15-34.

32. R. P. Carney, Y. Astier, T. M. Carney, K. Voitchovsky, P. H. J. Silva and F. Stellacci, Electrical Method to Quantify Nanoparticle Interaction with Lipid Bilayers, *ACS Nano*, 2013, **7**, 932-942.

33. P. Yi and K. L. Chen, Interaction of Multiwalled Carbon Nanotubes with Supported Lipid Bilayers and Vesicles as Model Biological Membranes, *Environ. Sci. Technol.* 2013, **47**, 5711-5719.

34. V. K. Gangupomu and F. M. Capaldi, Interactions of Carbon Nanotube with Lipid Bilayer Membranes, *J. Nanomater.*, 2011, 6.

35. C. A. Jimenez-Cruz, S. G. Kang and R. H. Zhou, Large Scale Molecular Simulations of Nanotoxicity, *Wiley Interdisciplinary Reviews-Systems Biology and Medicine*, 2014, **6**, 265-279.

36. R. Saria, F. Mouchet, A. Perrault, E. Flahaut, C. Laplanche, J. C. Boutonnet, E. Pinelli and L. Gauthier, Short Term Exposure to Multi-walled Carbon Nanotubes Induce Oxidative Stress and DNA Damage in Xenopus laevis Tadpoles, *Ecotoxicol. Environ. Saf.*, 2014, **107**, 22-29.

37. Q. X. Mu, D. L. Broughton and B. Yan, Endosomal Leakage and Nuclear Translocation of Multiwalled Carbon Nanotubes: Developing a Model for Cell Uptake, *Nano Letters*, 2009, **9**, 4370-4375.

38. M. Bottini, S. Bruckner, K. Nika, N. Bottini, S. Bellucci, A. Magrini, A. Bergamaschi and T. Mustelin, Multi-walled Carbon Nanotubes Induce T Lymphocyte Apoptosis, *Toxicol. Lett.*, 2006, **160**, 121-126.

39. D. X. Cui, F. R. Tian, C. S. Ozkan, M. Wang and H. J. Gao, Effect of Single Wall Carbon Nanotubes on Human HEK293 cells, *Toxicol. Lett.*, 2005, **155**, 73-85.

40. N. A. Monteiro-Riviere, R. J. Nemanich, A. O. Inman, Y. Y. Y. Wang and J. E. Riviere, Multi-walled Carbon Nanotube Interactions with Human Epidermal Keratinocytes, *Toxicol. Lett.*, 2005, **155**, 377-384.

41. L. E. Murr, K. M. Garza, K. F. Soto, A. Carrasco, T. G. Powell, D. A. Ramirez, P. A. Guerrero, D. A. Lopez and J. Venzor, 3rd, Cytotoxicity Assessment of Some Carbon Nanotubes and Related Carbon Nanoparticle Aggregates and the Implications for Anthropogenic Carbon Nanotube Aggregates in The Environment, *Int. J. Environ. Res. Public Health*, 2005, **2**, 31-42.

42. X. H. Shi, Y. Kong and H. J. Gao, Coarse Grained Molecular Dynamics and Theoretical Studies of Carbon Nanotubes Entering Cell Membrane, *Acta Mech. Sinica*, 2008, **24**, 161-169.

43. S. Pogodin and V. A. Baulin, Can a Carbon Nanotube Pierce through a Phospholipid Bilayer?, *ACS Nano*, 2010, **4**, 5293-5300.

44. Y. C. Bai, F. C. Wu, D. H. Lin and B. S. Xing, Aqueous Stabilization of Carbon Nanotubes: Effects of Surface Oxidization and Solution Chemistry, *Environ. Sci. Pollut. Res.*, 2014, **21**, 4358-4365.

45. D. X. Fores-Cervantes, H. M. Maes, A. Schaffer, J. Hollender and H. P. E. Kohler, Slow Biotransformation of Carbon Nanotubes by Horseradish Peroxidase, *Environ. Sci. Technol.* 2014, **48**, 4826-4834.

46. J. L. Bitter, J. Yang, S. B. Milani, C. T. Jafvert and D. H. Fairbrother, Transformations of Oxidized Multiwalled Crbon Nanotubes Exposed to UVC (254 nm) Irradiation, *Environmental Science: Nano*, 2014, 324-337.

47. J. Yang, J. L. Bitter, B. A. Smith, D. H. Fairbrother and W. P. Ball, Transport of Oxidized Multi-Walled Carbon Nanotubes through Silica Based Porous Media: Influences of Aquatic Chemistry, Surface Chemistry, and Natural Organic Matter, *Environ. Sci. Technol.*, 2013, **47**, 14034-14043.

48. T. Savage, S. Bhattacharya, B. Sadanadan, J. Gaillard, T. M. Tritt, Y.-P. Sun, Y. Wu, Y. W. Nayak, R. Car, N. Marzari, P. M. Ajayan and A. M. Rao, Photoinduced oxidation of carbon nanotubes, *J. Phys. Condens. Matter*, 2003, **15**, 5915-5921.

49. I. D. Rosca, F. Watari, M. Uo and T. Akasaka, Oxidation of multiwalled carbon nanotubes by nitric acid, *Carbon*, 2005, **43**, 3124-3131.

50. Y. Wang, Z. Iqbal and S. Mitra, Rapidly Functionalized, Water-Dispersed Carbon Nanotubes at High Concentration, *J. Am. Chem. Soc.*, 2006, **128**, 95-99.

51. P. Yi and K. L. Chen, Influence of Surface Oxidation on the Aggregation and Deposition Kinetics of Multiwalled Carbon Nanotubes in Monovalent and Divalent Electrolytes, *Langmuir*, 2011, **27**, 3588-3599.

52. K. A. Wepasnick, B. A. Smith, K. E. Schrote, H. K. Wilson, S. R. Diegelmann and D. H. Fairbrother, Surface and Structural Characterization of Multi-Walled Carbon Nanotubes Following Different Oxidative Treatments, *Carbon*, 2011, **49**, 24-36.

53. Q. Zhang, J.-Q. Huang, W.-Z. Qian, Y.-Y. Zhang and F. Wei, The Road for Nanomaterials Industry: A Review of Carbon Nanotube Production, Post-Treatment, and Bulk Applications for Composites and Energy Storage, *Small*, 2013, **9**, 1237-1265.

54. B. Smith, K. Wepasnick, K. E. Schrote, H.-H. Cho, W. P. Ball and D. H. Fairbrother, Influence of Surface Oxides on the Colloidal Stability of Multi-Walled Carbon Nanotubes: A Structure-Property Relationship, *Langmuir*, 2009, **25**, 9767-9776.

55. B. Smith, K. Wepasnick, K. E. Schrote, A. H. Bertele, W. P. Ball, C. O'Melia and D. H. Fairbrother, Colloidal Properties of Aqueous Suspensions of Acid-Treated, Multi-Walled Carbon Nanotubes, *Environ. Sci. Technol.* 2009, **43**, 819-825.

56. T. Y. Sun, N. A. Bornhoft, K. Hungerbuhler and B. Nowack, Dynamic Probabilistic Modeling of Environmental Emissions of Engineered Nanomaterials, *Environ. Sci. Technol.* 2016, **50**, 4701-4711.

57. I. Velzeboer, E. Peeters and A. A. Koelmans, Multiwalled Carbon Nanotubes at Environmentally Relevant Concentrations Affect the Composition of Benthic Communities, *Environ. Sci. Technol.* 2013, **47**, 7475-7482.

58. M. Lelimousin and M. S. P. Sansom, Membrane Perturbation by Carbon Nanotube Insertion: Pathways to Internalization, *Small*, 2013, **9**, 3639-3646.

59. S. Prylutska, R. Bilyy, T. Shkandina, D. Rotko, A. Bychko, V. Cherepanov, R. Stoika, V. Rybalchenko, Y. Prylutskyy, N. Tsierkezos and U. Ritter, Comparative Study of Membranotropic Action of Single- and Multi-walled Carbon Nanotubes, *J. Biosci. Bioeng.*, 2013, **115**, 674-679.

60. S. A. Saslow Gomez, D. S. Jordan, J. M. Troiano and F. M. Geiger, Uranyl Adsorption at the Muscovite (Mica)/Water Interface Studied by Second Harmonic Generation, *Environ. Sci. Technol.* 2012, **46**, 11154-11161.

61. P. L. Hayes, J. N. Malin, C. T. Konek and F. M. Geiger, Interaction of Nitrate, Barium, Strontium and Cadmium Ions with Fused Quartz/water Interfaces Studied by Second Harmonic Generation, *J. Phys. Chem. A*, 2008, **112**, 660-668.

62. J. L. Achtyl, I. V. Vlassiouk, S. P. Surwade, P. F. Fulvio, S. Dai and F. M. Geiger, Interaction of Magnesium Ions with Pristine Single-Layer and Defected Graphene/Water Interfaces Studied by Second Harmonic Generation, *J. Phys. Chem. B*, 2014, **118**, 7739-7749.

63. J. M. Troiano, L. L. Olenick, T. R. Kuech, E. S. Melby, D. Hu, S. E. Lohse, A. C. Mensch, M. Dogangun, A. M. Vartanian, M. D. Torelli, E. Ehimiaghe, S. R. Walter, L. Fu, C. R. Anderton, Z. Zhu, H. Wang, G. Orr, C. J. Murphy, R. J. Hamers, J. A. Pedersen and F. M. Geiger, Direct Probes of 4 nm Diameter Gold Nanoparticles Interacting with Supported Lipid Bilayers, *J. Phys. Chem. C*, 2015, ***119*** 534-546.

64. A. C. McGeachy, L. L. Olenick, J. M. Troiano, R. S. Lankone, E. S. Melby, T. R. Kuech, E. Ehimiaghe, D. H. Fairbrother, J. A. Pedersen and F. M. Geiger, Resonantly Enhanced Nonlinear Optical Probes of Oxidized Multiwalled Carbon Nanotubes at Supported Lipid Bilayers, *J. Phys. Chem. B*, 2017, **121**, 1321-1329.

65. J. Marra and J. Israelachvili, Direct Measurements of Forces Between Phosphatidylcholine and Phosphatidylethanolamine Bilayers In Aqueous-Electrolyte Solutions, *Biochemistry*, 1985, **24**, 4608-4618.

66. T. H. Anderson, Y. Min, K. L. Weirich, H. Zeng, D. Fygenson and J. N. Israelachvili, Formation of Supported Bilayers on Silica Substrates, *Langmuir*, 2009, **25**, 6997-7005.

67. M. Dogangun, M. N. Hang, J. M. Troiano, A. C. McGeachy, E. S. Melby, J. A. Pedersen, R. J. Hamers and F. M. Geiger, Alteration of Membrane Compositional Asymmetry by LiCoO2 Nanosheets, *ACS Nano*, 2015, **9**, 8755-8765.

68. P. A. Covert and D. K. Hore, Assessing the Gold Standard: The Complex Vibrational Nonlinear Susceptibility of Metals, *J. Phys. Chem. C*, 2015, **119**, 271-276.

69. I. Reviakine, D. Johannsmann and R. P. Richter, Hearing What You Cannot See and Visualizing What You Hear: Interpreting Quartz Crystal Microbalance Data from Solvated Interfaces, *Anal. Chem.*, 2011, **83**, 8838-8848.

70. R. M. Corn and D. A. Higgins, Optical Second Harmonic Generation as a Probe of Surface Chemistry, *Chem. Rev.*, 1994, **94**, 107.

71. F. M. Geiger, Second Harmonic Generation, Sum Frequency Generation, and chi(3): Dissecting Environmental Interfaces with a Nonlinear Optical Swiss Army Knife, *Annu. Rev. Phys. Chem.*, 2009, **60**, 61-83.

72. K. B. Eisenthal, Liquid Interfaces Probed by Second-harmonic and Sum-frequency Spectroscopy, *Chem. Rev.*, 1996, **96**, 1343-1360.

73. D. Langmuir, *Aqueous Environmental Chemistry*, Prentice Hall, Upper Saddle River, NJ 1997.

74. R. I. Masel, *Principles of Adsorption and Reaction on Solid Surfaces*, Wiley, 1996.

75. G. A. Somorjai, *Chemistry in Two Dimensions*, Cornell University Press, Ithaca, 1981.

76. A. W. Adamson, *Physical Chemistry of Surfaces*, John Wiley & Sons, New York, 5th edn., 1990.

Chapter 4 References.

1. C. Contado, Nanomaterials in Consumer Products: A Challenging Analytical Problem, *Front. Chem.*, 2015, **3**, 20.

2. T. A. Qiu, M. D. Torelli, A. M. Vartanian, N. B. Rackstraw, J. T. Buchman, L. M. Jacob, C. J. Murphy, R. J. Hamers and C. L. Haynes, Quantification of Free Polyelectrolytes Present in Colloidal Suspension, Revealing a Source of Toxic Responses for Polyelectrolyte-Wrapped Gold Nanoparticles, *Anal. Chem.*, 2017, **89**, 1823-1830.

3. X. L. Wang, S. S. Kelkar, A. G. Hudson, R. B. Moore, T. M. Reineke and L. A. Madsen, Quantitation of Complexed versus Free Polymers in Interpolyelectrolyte Polyplex Formulations, *ACS Macro Letters*, 2013, **2**, 1038-1041.

4. Z. V. Feng, I. L. Gunsolus, T. A. Qiu, K. R. Hurley, L. H. Nyberg, H. Frew, K. P. Johnson, A. M. Vartanian, L. M. Jacob, S. E. Lohse, M. D. Torelli, R. J. Hamers, C. J. Murphy and C. L. Haynes, Impacts of Gold Nanoparticle Charge and Ligand Type on Surface Binding and Toxicity to Gram-negative and Gram-positive Bacteria, *Chem. Sci.*, 2015, **6**, 5186-5196.

5. D. D. Iarikov, M. Kargar, A. Sahari, L. Russel, K. T. Gause, B. Behkam and W. A. Ducker, Antimicrobial Surfaces Using Covalently Bound Polyallylamine, *Biomacromolecules*, 2014, **15**, 169-176.

6. T. Ikeda, H. Yamaguchi and S. Tazuke, New Polymeric Biocides - Synthesis And Antibacterial Activities Of Polycations With Pendant Biguanide Groups, *Antimicrob. Agents Chemother.*, 1984, **26**, 139-144.

7. T. Ikeda, H. Hirayama, H. Yamaguchi, S. Tazuke and M. Watanabe, Polycationic Biocides with Pendant Active Groups - Molecular-Weight Dependence of Antibacterial Activity, *Antimicrob. Agents Chemother.*, 1986, **30**, 132-136.

8. E. Kiss, E. T. Heine, K. Hill, Y. C. He, N. Keusgen, C. B. Penzes, D. Schnoller, G. Gyulai, A. Mendrek, H. Keul and M. Moeller, Membrane Affinity and Antibacterial Properties of Cationic Polyelectrolytes With Different Hydrophobicity, *Macromol. Biosci.*, 2012, **12**, 1181-1189.

9. R. Kugler, O. Bouloussa and F. Rondelez, Evidence of A Charge-density Threshold for Optimum Efficiency of Biocidal Cationic Surfaces, *Microbiology*, 2005, **151**, 1341-1348.
10. S. Vaidyanathan, B. G. Orr and M. M. B. Holl, Role of Cell Membrane Vector Interactions in Successful Gene Delivery, *Acc. Chem. Res.*, 2016, **49**, 1486-1493.

11. C. Zhang, Z. M. Ying, Q. J. Luo, H. Du, Y. Wang, K. Zhang, S. G. Yan, X. D. Li, Z. Q. Shen and W. P. Zhu, Poly(hexamethylene guanidine)-based Hydrogels with Long Lasting Antimicrobial Activity and Low Toxicity, *J. Poly. Sci. A*, 2017, **55**, 2027-2035.

12. X. Gao and L. Huang, Potentiation of Cationic Liposome-mediated Gene Delivery by Polycations, *Biochemistry*, 1996, **35**, 1027-1036.

13. A. Alliband, F. A. Meece, C. Jayasinghe and D. H. Burns, Synthesis and Characterization of Picket Porphyrin Receptors That Bind Phosphatidylglycerol, an Anionic Phospholipid Found in Bacterial Membranes, *J. Org. Chem.*, 2013, **78**, 356-362.

14. O. Mertins and R. Dimova, Insights on the Interactions of Chitosan with Phospholipid Vesicles. Part II: Membrane Stiffening and Pore Formation, *Langmuir*, 2013, **29**, 14552-14559.

15. A. D. Robison, S. Sun, M. F. Poyton, G. A. Johnson, J. P. Pellois, P. Jungwirth, M. Vazdar and P. S. Cremer, Polyarginine Interacts More Strongly and Cooperatively than Polylysine with Phospholipid Bilayers, *J. Chem. Phys. B*, 2016, **120**, 9287-9296.

16. Y. Takechi, H. Tanaka, H. Kitayama, H. Yoshii, M. Tanaka and H. Saito, Comparative Study on the Interaction of Cell-penetrating Polycationic Polymers with Lipid Membranes, *Chem. Phys. Lipids*, 2012, **165**, 51-58.

17. A. A. Yaroslavov, E. G. Yaroslavova, A. A. Rakhnyanskaya, F. M. Menger and V. A. Kabanov, Modulation of Interaction of Polycations with Negative Unilamellar Lipid Vesicles, *Colloids Surf. B*, 1999, **16**, 29-43.

18. A. A. Yaroslavov, O. Y. Kuchenkova, I. B. Okuneva, N. S. Melik-Nubarov, N. O. Kozlova, V. I. Lobyshev, F. M. Menger and V. A. Kabanov, Effect of Polylysine on Transformations and Permeability of Negative Vesicular Membranes, *Biochim. Biophys. Acta*, 2003, **1611**, 44-54.

19. A. A. Yaroslavov, T. A. Sitnikova, A. A. Rakhnyanskaya, E. G. Yaroslavova, D. A. Davydov, T. V. Burova, V. Y. Grinberg, L. Shi and F. M. Menger, Biomembrane Sensitivity to Structural Changes in Bound Polymers, *J. Am. Chem. Soc.*, 2009, **131**, 1666-1667.

20. M. Kreuzer, M. Trapp, R. Dahint and R. Steitz, Polymer-Induced Swelling of Solid-Supported Lipid Membranes, *Membranes*, 2016, **6**, 15.

21. A. F. Xie and S. Granick, Phospholipid Membranes as Substrates for Polymer Adsorption, *Nat. Mater.*, 2002, **1**, 129-133.

22. A. A. Yaroslavov, N. S. Melik-Nubarov and F. M. Menger, Polymer-induced Flip-flop in Biomembranes, *Acc. Chem. Res.*, 2006, **39**, 702-710.

23. K. de Meijere, G. Brezesinski, T. Pfohl and H. Mohwald, Influence of the Polymer Charge Density on Lipid-polyelectrolyte Complexes at the Air/water Interface, *J. Chem. Phys. B*, 1999, **103**, 8888-8893.

24. S. Zhou, C. Burger, F. Yeh and B. Chu, Charge Density Effect of Polyelectrolyte Chains on the Nanostructures of Polyelectrolyte–Surfactant Complexes, *Macromolecules*, 1998, **31**, 8157-8163.

25. A. B. Chinen, J. R. Ferrer, T. J. Merkel and C. A. Mirkin, Relationships between Poly(ethylene glycol) Modifications on RNA-Spherical Nucleic Acid Conjugates and Cellular Uptake and Circulation Time, *Bioconjugate Chem.*, 2016, **27**, 2715-2721.

26. J. I. Cutler, E. Auyeung and C. A. Mirkin, Spherical Nucleic Acids, *J. Am. Chem. Soc.*, 2012, **134**, 1376-1391.

27. R. J. Banga, N. Chernyak, S. P. Narayan, S. T. Nguyen and C. A. Mirkin, Liposomal Spherical Nucleic Acids, *J. Am. Chem. Soc.*, 2014, **136**, 9866-9869.

28. J. Choi and M. F. Rubner, Influence of the Degree of Ionization on Weak Polyelectrolyte Multilayer Assembly, *Macromolecules*, 2005, **38**, 116-124.

29. P. Atkins and J. de Paula, *Atkins' Physical Chemistry*, OUP Oxford, 2010.

30. A. Y. Kostritskii, D. A. Kondinskaia, A. M. Nesterenko and A. A. Gurtovenko, Adsorption of Synthetic Cationic Polymers on Model Phospholipid Membranes: Insight from Atomic-Scale Molecular Dynamics Simulations, *Langmuir*, 2016, **32**, 10402-10414.

31. N. I. Kovtyukhova, P. J. Ollivier, B. R. Martin, T. E. Mallouk, S. A. Chizhik, E. V. Buzaneva and A. D. Gorchinskiy, Layer-by-layer Assembly of Ultrathin Composite Films from Micron-sized Graphite Oxide Sheets and Polycations, *Chem. Mater.*, 1999, **11**, 771-778.

32. N. Parveen and M. Schonhoff, Quantifying and Controlling the Cation Uptake upon Hydrated Ionic liquid-induced Swelling of Polyelectrolyte Multilayers, *Soft Matter*, 2017, **13**, 1988-1997.

33. A. I. Petrov, A. A. Antipov and G. B. Sukhorukov, Base-acid Equilibria in Polyelectrolyte Systems: From Weak Polyelectrolytes to Interpolyelectrolyte Complexes and Multilayered Polyelectrolyte Shells, *Macromolecules*, 2003, **36**, 10079-10086.

34. A. J. Chung and M. F. Rubner, Methods of Loading and Releasing Low Molecular Weight Cationic Molecules in Weak Polyelectrolyte Multilayer Films, *Langmuir*, 2002, **18**, 1176-1183.

35. B. Wang, Y. Y. Zhang, Z. W. Mao and C. Y. Gao, Cellular Uptake of Covalent Poly(allylamine hydrochloride) Microcapsules and Its Influences on Cell Functions, *Macromol. Biosci.*, 2012, **12**, 1534-1545.

36. S. W. Cranford, C. Ortiz and M. J. Buehler, Mechanomutable Properties of a PAA/PAH Polyelectrolyte Complex: Rate Dependence and Ionization Effects on Tunable Adhesion Strength, *Soft Matter*, 2010, **6**, 4175-4188.

37. Q. Ferreira, P. J. Gomes, P. A. Ribeiro, N. C. Jones, S. V. Hoffmann, N. J. Mason, O. N. Oliveira and M. Raposo, Determination of Degree of Ionization of Poly(allylamine hydrochloride) (PAH) and Poly 1- 4-(3-carboxy-4 hydroxyphenylazo)benzene sulfonamido -1,2-ethanediyl, sodium salt (PAZO) in Layer-by-Layer Films using Vacuum Photoabsorption Spectroscopy, *Langmuir*, 2013, **29**, 448-455.

38. J. M. Troiano, A. C. McGeachy, L. L. Olenick, D. Fang, D. Liang, J. Hong, T. R. Kuech, E. R. Caudill, J. A. Pedersen, Q. Cui and F. M. Geiger, Quantifying the Electrostatics of Polycation–Lipid Bilayer Interactions, *J. Am. Chem. Soc.*, 2017, **139**, 5808-5816.

39. D. A. Kondinskaia, A. Y. Kostritskii, A. M. Nesterenko, A. Y. Antipina and A. A. Gurtovenko, Atomic-Scale Molecular Dynamics Simulations of DNA-Polycation Complexes: Two Distinct Binding Patterns, *J. Chem. Phys. B*, 2016, **120**, 6546-6554.

40. E. F. Palermo and K. Kuroda, Chemical Structure of Cationic Groups in Amphiphilic Polymethacrylates Modulates the Antimicrobial and Hemolytic Activities, *Biomacromolecules*, 2009, **10**, 1416-1428.

41. A. Mecke, I. J. Majoros, A. K. Patri, J. R. Baker, M. M. B. Holl and B. G. Orr, Lipid Bilayer Disruption by Polycationic Polymers: The Roles of Size and Chemical Functional Group, *Langmuir*, 2005, **21**, 10348-10354.

42. E. Diamanti, P. Andreozzi, R. Anguiano, L. Yate, D. Gregurec, N. Politakos, R. F. Ziolo, E. Donath and S. E. Moya, The Effect of Top-layer Chemistry on the Formation of Supported Lipid Bilayers on Polyelectrolyte Multilayers: Primary versus Quaternary Amines, *Phys. Chem. Chem. Phys.*, 2016, **18**, 32396-32405.

43. L. L. Olenick, H. M. Chase, L. Fu, Y. Zhang, A. C. McGeachy, M. Dogangun, S. R. Walter, H.-f. Wang and F. M. Geiger, Single-component Supported Lipid Bilayers Probed using Broadband Nonlinear Optics, *Phys. Chem. Chem. Phys.*, 2018, **20**, 3063-3072.

44. J. M. Troiano, L. L. Olenick, T. R. Kuech, E. S. Melby, D. Hu, S. E. Lohse, A. C. Mensch, M. Dogangun, A. M. Vartanian, M. D. Torelli, E. Ehimiaghe, S. R. Walter, L. Fu, C. R. Anderton, Z. Zhu, H. Wang, G. Orr, C. J. Murphy, R. J. Hamers, J. A. Pedersen and F. M. Geiger, Direct Probes of 4 nm Diameter Gold Nanoparticles Interacting with Supported Lipid Bilayers, *J. Phys. Chem. C*, 2015, ***119*** 534-546.

45. T. H. Anderson, Y. Min, K. L. Weirich, H. Zeng, D. Fygenson and J. N. Israelachvili, Formation of Supported Bilayers on Silica Substrates, *Langmuir*, 2009, **25**, 6997-7005.

46. D. Blumenthal, L. Goldstien, M. Edidin and L. A. Gheber, Universal Approach to FRAP Analysis of Arbitrary Bleaching Patterns, *Sci. Rep.*, 2015, **5**.

47. M. Mosior and S. McLaughlin, Binding of Basic Peptides to Acidic Lipids in Membranes, *FASEB J.*, 1992, **6**, A88-A88.

48. J. Y. Kim, M. Mosior, L. A. Chung, H. Wu and S. McLaughlin, Binding of Peptides with Basic Residues to Membranes Containing Acidic Phospholipids, *Biophys. J.*, 1991, **60**, 135-148.

49. R. Pelton, Polyvinylamine: A Tool for Engineering Interfaces, *Langmuir*, 2014, **30**, 15373-15382.

50. M. Sander, J. E. Tomaszewski, M. Madliger and R. P. Schwarzenbach, Adsorption of Insecticidal Cry1Ab Protein to Humic Substances. 1. Experimental Approach and Mechanistic Aspects, *Environ. Sci. Technol.*, 2012, **46**, 9923-9931.

51. A. Katchalsky, J. Mazur and P. Spitnik, Polybase Properties of Polyvinylamine, *J. Poly. Sci.*, 1957, **23**, 513-532.

52. E. H. Westman, M. Ek, L. E. Enarsson and L. Wagberg, Assessment of Antibacterial Properties of Polyvinylamine (PVAm) with Different Charge Densities and Hydrophobic Modifications, *Biomacromolecules*, 2009, **10**, 1478-1483.

53. C. Delajon, T. Gutberlet, R. Steitz, H. Mohwald and R. Krastev, Formation of Polyelectrolyte Multilayer Architectures with Embedded DMPC Studied in Situ by Neutron Reflectometry, *Langmuir*, 2005, **21**, 8509-8514.

54. J. X. Shao, C. X. Wen, M. J. Xuan, H. Y. Zhang, J. Frueh, M. W. Wan, L. H. Gao and Q. He, Polyelectrolyte Multilayer-cushioned Fluid Lipid Bilayers: A Parachute Model, *Phys. Chem. Chem. Phys.*, 2017, **19**, 2008-2016.

55. P. Theato and R. Zentel, Formation of Lipid Bilayers on A New Amphiphilic Polymer Support, *Langmuir*, 2000, **16**, 1801-1805.

56. S. Volden, J. Genzer, K. Z. Zhu, M. H. G. Ese, B. Nystrom and W. R. Glomm, Charge- and Temperature-dependent Interactions between Anionic Poly (N-isopropylacrylamide) Polymers in Solution and A Cationic Surfactant at the Water/air Interface, *Soft Matter*, 2011, **7**, 8498-8507.

57. L. Q. Zhang, M. L. Longo and P. Stroeve, Mobile Phospholipid Bilayers on a Polyion/alkylthiol Layer Pair, *Langmuir*, 2000, **16**, 5093-5099.

Chapter 5 References.

1. D. J. Mitchell, D. T. Kim, L. Steinman, C. G. Fathman and J. B. Rothbard, Polyarginine Enters Cells More Efficiently than other Polycationic Homopolymers, *J. Pept. Res.*, 2000, **56**, 318-325.

2. D. D. Yi, G. M. Li, G. Li and W. Liang, Interaction of Arginine Oligomer with Model Membrane, *Biochem. Biophys. Res. Commun.*, 2007, **359**, 1024-1029.

3. Q. Cui, R. Hernandez, S. E. Mason, T. Fraunheim, J. A. Pedersen and F. M. Geiger, Sustainable Nanotechnology: Opportunities and Challenges for Theoretical/Computational Studies, *J. Phys. Chem. B*, 2016, **120**, 7297-7306.

4. C. J. Murphy, A. M. Vartania, F. M. Geiger, R. J. Hamers, J. A. Pedersen, Q. Cui, C. L. Haynes, E. E. Carlson, R. Hernandez, R. D. Klaper, G. Orr and Z. Rosenzweig, Biological Responses to Engineered Nanomaterials: Needs for the Next Decade, *ACS Cent. Sci.*, 2015, **1**, 117-123.

5. A. Colomer, A. Pinazo, M. T. Garcia, M. Mitjans, M. P. Vinardell, M. R. Infante, V. Martinez and L. Perez, pH-Sensitive Surfactants from Lysine: Assessment of Their Cytotoxicity and Environmental Behavior, *Langmuir*, 2012, **28**, 5900-5912.

6. A. D. Robison, S. Sun, M. F. Poyton, G. A. Johnson, J. P. Pellois, P. Jungwirth, M. Vazdar and P. S. Cremer, Polyarginine Interacts More Strongly and Cooperatively than Polylysine with Phospholipid Bilayers, *J. Phys. Chem. B*, 2016, **120**, 9287-9296.

7. L. E. Prevette, N. C. Benish, A. R. Schoenecker and K. J. Braden, Cell-penetrating Compounds Preferentially Bind Glycosaminoglycans over Plasma Membrane Lipids in a Charge Density- and Stereochemistry-dependent Manner, *Biophys. Chem.*, 2015, **207**, 40-50.

8. P. Novotna and M. Urbanova, Vibrational Circular Dichroism Study of Polypeptide Model-membrane Systems, *Anal. Biochem.*, 2012, **427**, 211-218.

9. M. Reuter, C. Schwieger, A. Meister, G. Karlsson and A. Blume, Poly-L-lysines and Poly-L-arginines Induce Leakage of Negatively Charged Phospholipid Vesicles and Translocate Through the Lipid Bilayer Upon Electrostatic Binding to the Membrane, *Biophys. Chem.*, 2009, **144**, 27-37.

10. F. Wei, S. J. Ye, H. C. Li and Y. Luo, Phosphate Ions Promoting Association between Peptide and Modeling Cell Membrane Revealed by Sum Frequency Generation Vibrational Spectroscopy, *J. Phys. Chem. C*, 2013, **117**, 11095-11103.

11. M. J. Wilhelm, M. S. Gh and H. L. Dai, Chemically Induced Changes to Membrane Permeability in Living Cells Probed with Nonlinear Light Scattering, *Biochemistry*, 2015, **54**, 4427-4430.

12. Y. Rao, S. J. J. Kwok, J. Lombardi, N. J. Turro and K. B. Eisenthal, Label-Free Probe of HIV-1 TAT Peptide Binding to Mimetic Membranes, *Proc. Natl. Acad. Sci. U.S.A.*, 2014, **111**, 12684-12688.

13. E. E. Kooijman, D. P. Tieleman, C. Testerink, T. Munnik, D. T. S. Rijkers, K. N. J. Burger and B. de Kruijff, An Electrostatic/hydrogen Bond Switch As the Basis for the Specific Interaction of Phosphatidic Acid with Proteins, *J. Biol. Chem.*, 2007, **282**, 11356-11364.

14. A. R. Ferhan, J. A. Jackman and N. J. Cho, Integration of Quartz Crystal Microbalance-Dissipation and Reflection-Mode Localized Surface Plasmon Resonance Sensors for Biomacromolecular Interaction Analysis, *Anal. Chem.*, 2016, **88**, 12524-12531.

15. J. A. Jackman, A. R. Ferhan and N. J. Cho, Nanoplasmonic Sensors for Biointerfacial Science, *Chem. Soc. Rev.*, 2017, **46**, 3615-3660.

16. S. Fukusho, H. Furusawa and Y. Okahata, In Vitro Selection and Evaluation of RNA Aptamers that Recognize Arginine-rich-motif Model Peptide on a Quartz-crystal Microbalance, *Chem. Commun.*, 2002, 88-89.

17. J. N. Anker, W. P. Hall, M. P. Lambert, P. T. Velasco, M. Mrksich, W. L. Klein and R. P. Van Duyne, Detection and Identification of Bioanalytes with High Resolution LSPR Spectroscopy and MALDI Mass Spectrometry, *J. Phys. Chem. C*, 2009, **113**, 5891-5894.

18. R. M. Onorato, A. P. Yoon, J. T. Lin and G. A. Somorjai, Adsorption of Amino Acids and Dipeptides to the Hydrophobic Polystyrene Interface Studied by SFG and QCM: The Special Case of Phenylalanine, *J. Phys. Chem. C*, 2012, **116**, 9947-9954.

19. R. L. York, G. J. Holinga and G. A. Somorjai, Investigation of the Influence of Chain Length on the Interfacial Ordering of L-Lysine and L-Proline and Their Homopeptides at Hydrophobic and Hydrophilic Interfaces Studied by Sum Frequency Generation and Quartz Crystal Microbalance, *Langmuir*, 2009, **25**, 9369-9374.

20. H. A. Rydberg, A. Kunze, N. Carlsson, N. Altgarde, S. Svedhem and B. Norden, Peptide-membrane Interactions of Arginine-tryptophan Peptides Probed Using Quartz Crystal Microbalance with Dissipation Monitoring, *Eur. Biophys. J. Biophys. Lett.*, 2014, **43**, 241-253.

21. H. M. Hiep, T. Endo, M. Saito, M. Chikae, D. K. Kim, S. Yamamura, Y. Takamura and E. Tamiya, Label-free Detection of Melittin Binding to A Membrane Using Electrochemical-localized Surface Plasmon Resonance, *Anal. Chem.*, 2008, **80**, 1859-1864.

22. C. Steinem, A. Janshoff and H. J. Galla, Evidence for Multilayer Formation of Melittin on Solid-supported Phospholipid Membranes by Shear-wave Resonator Measurements, *Chem. Phys. Lipids*, 1998, **95**, 95-104.

23. S. Svedhem, D. Dahlborg, J. Ekeroth, J. Kelly, F. Hook and J. Gold, In situ Peptide-modified Supported Lipid Bilayers for Controlled Cell Attachment, *Langmuir*, 2003, **19**, 6730-6736.

24. E. H. Chen, S. A. Saslow, S. T. Nguyen and F. M. Geiger, Zinc Ion-Hydroxyl Interactions at Undecanol-Funcationalized Fused Silica/Water Interfaces Quantified Using the Eisenthal chi(3) Technique, *J. Phys. Chem. C*, 2012, **116**, 19886-19892.

25. P. E. Ohno, S. A. Saslow, H.-f. Wang, F. M. Geiger and K. B. Eisenthal, Phase-referenced Nonlinear Spectroscopy of the alpha-Quartz/Water Interface, *Nat. Commun.*, 2016, **7**, 13587.

26. J.-L. Barrat and J.-P. Hansen, *Basic Concepts for Simple and Complex Liquids*, Cambridge University Press, Cambridge, UK, 2003.

27. N. Gal, A. Lassenberger, L. Herrero-Nogareda, A. Scheberl, V. Charwat, C. Kasper and E. Reimhult, Interaction of Size-Tailored PEGylated Iron Oxide Nanoparticles with Lipid Membranes and Cells, *ACS Biomater. Sci. Eng.*, 2017, **3**, 249-259.

28. S. Liu, J. X. Yang, H. Q. Ren, J. O'Keeffe-Ahern, D. Z. Zhou, H. Zhou, J. T. Chen and T. Y. Guo, Multifunctional Oligomer Incorporation: A Potent Strategy to Enhance the Transfection Activity of Poly(L-lysine), *Biomater. Sci.*, 2016, **4**, 522-532.

29. W. H. Chi, S. Liu, J. X. Yang, R. Y. Wang, H. Q. Ren, H. Zhou, J. T. Chen and T. Y. Guo, Evaluation of the Effects of Amphiphilic Oligomers in PEI based Ternary Complexes on the Improvement of pDNA Delivery, *J. Mater. Chem. B*, 2014, **2**, 5387-5396.

30. F. Zen, V. D. Karanikolas, J. A. Behan, J. Andersson, G. Ciapetti, A. L. Bradley and P. E. Colavita, Nanoplasmonic Sensing at the Carbon-Bio Interface: Study of Protein Adsorption at Graphitic and Hydrogenated Carbon Surfaces, *Langmuir*, 2017, **33**, 4198-4206.

31. A. J. Haes, S. Zou, J. Zhao, G. C. Schatz and R. P. Van Duyne, Localized Surface Plasmon Resonance Spectroscopy near Molecular Resonances, *J. Am. Chem. Soc.*, 2006, **128**, 10905-10914.

32. A. C. McGeachy, E. R. Caudill, D. Liang, Q. Cui, J. A. Pedersen and F. Geiger, Counting Charges on Membrane-bound Peptides, *Chem. Sci.*, 2018.

33. R. Michael, H. Fredrik, K. Anatol, B. Peter and K. Bengt, Quartz Crystal Microbalance Setup for Frequency and Q-factor Measurements in Gaseous and Liquid Environments, *Rev. Sci. Instrum.*, 1995, **66**, 3924-3930.

34. I. Reviakine, D. Johannsmann and R. P. Richter, Hearing What You Cannot See and Visualizing What You Hear: Interpreting Quartz Crystal Microbalance Data from Solvated Interfaces, *Anal. Chem.*, 2011, **83**, 8838-8848.

35. G. Sauerbrey, Verwendung von Schwingquarzen zur Wägung dünner Schichten und zur Mikrowägung, *Z. Phy.*, 1959, **155**, 206-222.

36. M. V. Voinova, M. Rodahl, M. Jonson and B. Kasemo, Viscoelastic Acoustic Response of Layered Polymer Films at Fluid-Solid Interfaces: Continuum Mechanics Approach, *Phys. Scr.*, 1999, **59**, 391.

37. A. B. Dahlin, P. Jonsson, M. P. Jonsson, E. Schmid, Y. Zhou and F. Hook, Synchronized Quartz Crystal Microbalance and Nanoplasmonic Sensing of Biomolecular Recognition Reactions, *ACS Nano*, 2008, **2**, 2174-2182.

38. E. Guzman, F. Ortega, M. G. Prolongo, V. M. Starov and R. G. Rubio, Influence of the Molecular Architecture on the Adsorption onto Solid Surfaces: Comb-like Polymers, *Phys. Chem. Chem. Phys.*, 2011, **13**, 16416-16423.

39. T. Inagaki, S. Aono, H. Nakano and T. Yamamoto, Like-Charge Attraction of Molecular Cations in Water: Subtle Balance between Interionic Interactions and Ionic Solvation Effect, *J. Phys. Chem. B*, 2014, **118**, 5499-5508.

40. A. Y. Kostritskii, D. A. Kondinskaia, A. M. Nesterenko and A. A. Gurtovenko, Adsorption of Synthetic Cationic Polymers on Model Phospholipid Membranes: Insight from Atomic-Scale Molecular Dynamics Simulations, *Langmuir*, 2016, **32**, 10402-10414.

41. N. BenTal, B. Honig, R. M. Peitzsch, G. Denisov and S. McLaughlin, Binding of Small Basic Peptides to Membranes Containing Acidic Lipids: Theoretical Models and Experimental Results, *Biophys. J.*, 1996, **71**, 561-575.

42. S. V. Solomatin, M. Greenfeld and D. Herschlag, Implications of Molecular Heterogeneity for the Cooperativity of Biological Macromolecules, *Nat. Struct. Mol. Biol.*, 2011, **18**, 732-734.

43. J. Y. Kim, M. Mosior, L. A. Chung, H. Wu and S. McLaughlin, Binding of Peptides with Basic Residues to Membranes Containing Acidic Phospholipids, *Biophys. J.*, 1991, **60**, 135-148.

44. F. Torrens, G. Castellano, A. Campos and C. Abad, Negatively Cooperative Binding of Melittin to Neutral Phospholipid Vesicles, *J. Mol. Struct.*, 2007, **834**, 216-228.

45. J. M. Troiano, A. C. McGeachy, L. L. Olenick, D. Fang, D. Liang, J. Hong, T. R. Kuech, E. R. Caudill, J. A. Pedersen, Q. Cui and F. M. Geiger, Quantifying the Electrostatics of Polycation–Lipid Bilayer Interactions, *J. Am. Chem. Soc.*, 2017.

46. J. M. Troiano, L. L. Olenick, T. R. Kuech, E. S. Melby, D. Hu, S. E. Lohse, A. C. Mensch, M. Dogangun, A. M. Vartanian, M. D. Torelli, E. Ehimiaghe, S. R. Walter, L. Fu, C. R. Anderton, Z. Zhu, H. Wang, G. Orr, C. J. Murphy, R. J. Hamers, J. A. Pedersen and F. M. Geiger, Direct Probes of 4 nm Diameter Gold Nanoparticles Interacting with Supported Lipid Bilayers, *J. Phys. Chem. C*, 2015, ***119*** 534-546.

47. A. Katchalsky, J. Mazur and P. Spitnik, Polybase Properties of Polyvinylamine, *J. Poly. Sci.*, 1957, **23**, 513-532.

48. J. Vondrasek, P. E. Mason, J. Heyda, K. D. Collins and P. Jungwirth, The Molecular Origin of Like-Charge Arginine-Arginine Pairing in Water *J. Phys. Chem. B*, 2009, **113**, 9041-9045.

49. G. Tesei, M. Vazdar, M. R. Jensen, C. Cragnell, P. E. Mason, J. Heyda, M. Skepo, P. Jungwirth and M. Lund, Self-association of A Highly Charged Arginine-rich Cell-penetrating Peptide, *Proc. Natl. Acad. Sci. USA*, 2017, **114**, 11428-11433.

50. M. Vazdar, E. Wernersson, M. Khabiri, L. Cwiklik, P. Jurkiewicz, M. Hof, E. Mann, S. Kolusheva, R. Jelinek and P. Jungwirth, Aggregation of Oligoarginines at Phospholipid Membranes: Molecular Dynamics Simulations, Time-Dependent Fluorescence Shift, and Biomimetic Colorimetric Assays *J. Phys. Chem. B*, 2013, **117**, 11530-11540.

51. J. Klug, D. Masone and M. G. Del Popolo, Molecular-level Insight into the Binding of Arginine to a Zwitterionic Langmuir Monolayer, *RSC Adv.*, 2017, **7**, 30862-30869.

52. G. Gonella, C. Lutgebaucks, A. G. F. de Beer and S. Roke, Second Harmonic and Sum-Frequency Generation from Aqueous Interfaces is Modulated by Interference, *J. Phys. Chem. C*, 2016, **120**, 9165-9173.

53. K. B. Eisenthal, Liquid Interfaces Probed by Second-harmonic and Sum-frequency Spectroscopy, *Chemical Reviews*, 1996, **96**, 1343-1360.

54. M. D. Boamah, P. E. Ohno, F. M. Geiger and K. B. Eisenthal, Relative Permittivity in the Electrical Double Layer from Nonlinear Optics, *arXiv 1702.02496 and in press at J. Chem. Phys. (2018)*, 2017, 222808.

55. I. Vorobyov and T. W. Allen, The Electrostatics of Solvent and Membrane Interfaces and the Role of Electronic Polarizability, *J. Chem. Phys.*, 2010, **132**, 185101.

56. D. J. Bonthuis and R. R. Netz, Beyond the Continuum: How Molecular Solvent Structure Affects Electrostatics and Hydrodynamics at Solid-Electrolyte Interfaces, *J. Phys. Chem B*, 2013, **117**, 11397-11413.

57. T. Ishiyama, D. Terada and A. Morita, Hydrogen-Bonding Structure at Zwitterionic Lipid/Water Interface, *J. Phys. Chem. Lett.*, 2016, **7**, 216-220.

58. P. Jedlovszky and M. Mezei, Orientational Order of the Water Molecules Across a Fully Hydrated DMPC Bilayer: A Monte Carlo Simulation Study, *J. Phys. Chem. B*, 2001, **105**, 3614-3623.

59. B. Ding and Z. Chen, Molecular Interactions between Cell Penetrating Peptide Pep-1 and Model Cell Membranes, *J. Phys. Chem. B*, 2012, **116**, 2545-2552.

60. L. Soblosky, A. Ramamoorthy and Z. Chen, Membrane Interaction of Antimicrobial Peptides using E-coli Lipid Extract as Model Bacterial Cell Membranes and SFG Spectroscopy, *Chem. Phys. Lipids*, 2015, **187**, 20-33.

61. P. E. Ohno, H.-f. Wang and F. M. Geiger, Second-order Spectral Lineshapes from Charged Interfaces, *Nat. Commun.*, 2017, **8**, 1032.

Chapter 6 References.

1. W. Dowhan, Molecular Basis for Membrane Phospholipid Diversity: Why are There So Many Lipids?, *Annu. Rev. Biochem.*, 1997, **66**, 199-232.

2. E. M. Mejia and G. M. Hatch, Mitochondrial Phospholipids: Role in Mitochondrial Function, *J. Bioenerg. Biomembr.*, 2016, **48**, 99-112.

3. J. M. Troiano, L. L. Olenick, T. R. Kuech, E. S. Melby, D. Hu, S. E. Lohse, A. C. Mensch, M. Dogangun, A. M. Vartanian, M. D. Torelli, E. Ehimiaghe, S. R. Walter, L. Fu, C. R. Anderton, Z. Zhu, H. Wang, G. Orr, C. J. Murphy, R. J. Hamers, J. A. Pedersen and F. M. Geiger, Direct Probes of 4 nm Diameter Gold Nanoparticles Interacting with Supported Lipid Bilayers, *J. Phys. Chem. C*, 2015, ***119*** 534-546.

4. E. H. Chen, S. A. Saslow, S. T. Nguyen and F. M. Geiger, Zinc Ion-Hydroxyl Interactions at Undecanol-Functionalized Fused Silica/Water Interfaces Using the Eisenthal chi((3)) Technique, *J. Phys. Chem. C*, 2012, **116**, 7016-7020.

5. M. Dogangun, M. N. Hang, J. M. Troiano, A. C. McGeachy, E. S. Melby, J. A. Pedersen, R. J. Hamers and F. M. Geiger, Alteration of Membrane Compositional Asymmetry by LiCoO2 Nanosheets, *ACS Nano*, 2015, **9**, 8755-8765.

6. J. M. Troiano, A. C. McGeachy, L. L. Olenick, D. Fang, D. Liang, J. Hong, T. R. Kuech, E. R. Caudill, J. A. Pedersen, Q. Cui and F. M. Geiger, Quantifying the Electrostatics of Polycation–Lipid Bilayer Interactions, *J. Am. Chem. Soc.*, 2017, **139**, 5808-5816.

7. M. A. Marchenkova, Y. A. Dyakova, E. Y. Tereschenko, M. V. Kovalchuk and Y. A. Vladimirov, Cytochrome c Complexes with Cardiolipin Monolayer Formed under Different Surface Pressure, *Langmuir*, 2015, **31**, 12426-12436.

8. S. Reymond-Laruinaz, L. Saviot, V. Potin and M. D. M. de Lucas, Protein-nanoparticle Interaction in Bioconjugated Silver Nanoparticles: A Transmission Electron Microscopy and Surface Enhanced Raman Spectroscopy Study, *Appl. Surf. Sci.*, 2016, **389**, 17-24.

9. A. A. Kapralov, I. V. Kurnikov, Vlasova, II, N. A. Belikova, V. A. Tyurin, L. V. Basova, Q. Zhao, Y. Y. Tyurina, J. F. Jiang, H. Bayir, Y. A. Vladimirov and V. E. Kagan, The Hierarchy of Structural Transitions Induced in Cytochrome c by Anionic Phospholipids Determines Its Peroxidase Activation and Selective Peroxidation During Apoptosis nn Cells, *Biochemistry*, 2007, **46**, 14232-14244.

10. C. E. B. Caesar, E. K. Esbjorner, P. Lincoln and B. Norden, Assigning Membrane Binding Geometry of Cytochrome c by Polarized Light Spectroscopy, *Biophys. J.*, 2009, **96**, 3399-3411.

11. K. T. Nguyen, An Electronically Enhanced Chiral Sum Frequency Generation Vibrational Spectroscopy Study of Lipid-Bound Cytochrome c, *Chem. Commun.*, 2015, **51**, 195-197.

12. R. Swanson, B. L. Trus, N. Mandel, G. Mandel, O. B. Kallai and R. E. Dickerson, Tuna Cytochrome-C at 2.0 A Resolution .1. Ferricytochrome Structure-Analysis, *J. Biol. Chem.*, 1977, **252**, 759-775.

13. I. Bertini, G. Cavallaro and A. Rosato, Cytochrome c: Occurrence and Functions, *Chem. Rev.*, 2006, **106**, 90-115.

14. A. Chakraborty and N. R. Jana, Design and Synthesis of Triphenylphosphonium Functionalized Nanoparticle Probe for Mitochondria Targeting and Imaging, *J. Phys. Chem. C*, 2015, **119**, 2888-2895.

15. S. Marrache and S. Dhar, Engineering of Blended Nanoparticle Platform for Delivery of Mitochondria-Acting Therapeutics, *Proc. Natl. Acad. Sci. U.S.A.*, 2012, **109**, 16288-16293.

16. N. Joshi, A. Mukhopadhyay, S. Basak, G. De and K. Chattopadhyay, Surface Coating Rescues Proteins from Magnetite Nanoparticle Induced Damage, *Part. Part. Sys. Charact.*, 2013, **30**, 683-694.

17. N. Luo, D. Ni, H. Yue, W. Wei and G. H. Ma, Surface-Engineered Graphene Navigate Divergent Biological Outcomes toward Macrophages, *ACS Appl. Mater. Interfaces*, 2015, **7**, 5239-5247.

18. U. Sakulkhu, M. Mahmoudi, L. Maurizi, J. Salaklang and H. Hofmann, Protein Corona Composition of Superparamagnetic Iron Oxide Nanoparticles with Various Physico-Chemical Properties and Coatings, *Sci. Rep.*, 2014, **4**.

19. H. Bayraktar, C. C. You, V. M. Rotello and M. J. Knapp, Facial Control of Nanoparticle Binding to Cytochrome c, *J. Am. Chem. Soc.*, 2007, **129**, 2732-2733.

20. Vlasova, II, A. A. Kapralov, Z. P. Michael, S. C. Burkert, M. R. Shurin, A. Star, A. A. Shvedova and V. E. Kagan, Enzymatic Oxidative Biodegradation of Nanoparticles: Mechanisms, Significance and Applications, *Toxicol. Appl. Pharmacol.*, 2016, **299**, 58-69.

21. A. Mansouri, M. Mousavi, F. Attar, A. A. Saboury and M. Falahati, Interaction of Manganese Nanoparticle with Cytochrome c: A Multi-spectroscopic Study, *Int. J. Biol. Macromol.*, 2018, **106**, 78-86.

22. M. Sathappa and N. N. Alder, The Ionization Properties of Cardiolipin and Its Variants in Model Bilayers, *Biochim. Biophys. Acta*, 2016, **1858**, 1362-1372.

23. T. P. Petralli-Mallow, A. L. Plant, M. L. Lewis and J. M. Hicks, Cytochrome c At Model Membrane Surfaces: Exploration via Second Harmonic Generation-Circular Dichroism and Surface-Enhanced Resonance Raman Spectroscopy, *Langmuir*, 2000, **16**, 5960-5966.

24. J. S. Salafsky and K. B. Eisenthal, Protein Adsorption at Interfaces Detected by Second Harmonic Generation, *J. Phys. Chem. B*, 2000, **104**, 7752-7755.

25. M. De, C. C. You, S. Srivastava and V. M. Rotello, Biomimetic Interactions of Proteins with Functionalized Nanoparticles: A Thermodynamic Study, *J. Am. Chem. Soc.*, 2007, **129**, 10747-10753.

26. C. C. You, M. De, G. Han and V. M. Rotello, Tunable Inhibition and Denaturation of Alpha-Chymotrypsin with Amino Acid-Functionalized Gold Nanoparticles, *J. Am. Chem. Soc.*, 2005, **127**, 12873-12881.

27. S. Morandat and K. El Kirat, Cytochrome c Provokes the Weakening of Zwitterionic Membranes as Measured by Force Spectroscopy, *Colloids Surf. B*, 2011, **82**, 111-117.

28. G. P. Gorbenko, V. Trusova and J. G. Molotkovsky, Forster Resonance Energy Transfer Study of Cytochrome c-Lipid Interactions, *J. Fluoresc.*, 2018, **28**, 79-88.

29. A. Magarkar, V. Dhawan, P. Kallinteri, T. Viitala, M. Elmowafy, T. Rog and A. Bunker, Cholesterol Level Affects Surface Charge of Lipid Membranes in Saline Solution, *Sci. Rep.*, 2014, **4**.

30. F. de Meyer and B. Smit, Effect of Cholesterol on the Structure of a Phospholipid Bilayer, *Proc. Natl. Acad. Sci. U.S.A.*, 2009, **106**, 3654-3658.

31. J. Seemork, T. Sansureerungsikul, K. Sathomsantikun, T. Sinthusake, K. Shigyou, T. Tree-Udom, B. Jiangchareon, K. Chiablaem, K. Lirdprapamongkol, J. Svasti, T. Hamada, T. Palaga and S. Wanichwecharungruang, Penetration of Oxidized Carbon Nanospheres through Lipid Bilayer Membrane: Comparison to Graphene Oxide and Oxidized Carbon Nanotubes, and Effects of pH and Membrane Composition, *ACS Appl. Mater. Interfaces*, 2016, **8**, 23549-23557.

32. L. Y. Zhang, B. Q. Xu and X. Q. Wang, Cholesterol Extraction from Cell Membrane by Graphene Nanosheets: A Computational Study, *J. Phys. Chem. B*, 2016, **120**, 957-964.

33. D. D. Sun, X. B. Lin and N. Gu, Cholesterol affects C-60 Translocation Across Lipid Bilayers, *Soft Matter*, 2014, **10**, 2160-2168.

34. T. R. Kuech, Doctor of Philosophy, University of Wisconsin-Madison, 2015.

35. S. H. De Paoli, L. L. Diduch, T. Z. Tegegn, M. Orecna, M. B. Strader, E. Karnaukhova, J. E. Bonevich, K. Holada and J. Simak, The Effect of Protein Corona Composition on the Interaction of Carbon Nanotubes with Human Blood Platelets, *Biomaterials*, 2014, **35**, 6182-6194.

36. A. K. Murthy, R. J. Stover, W. G. Hardin, R. Schramm, G. D. Nie, S. Gourisankar, T. M. Truskett, K. V. Sokolov and K. P. Johnston, Charged Gold Nanoparticles with Essentially Zero Serum Protein Adsorption in Undiluted Fetal Bovine Serum, *J. Am. Chem. Soc.*, 2013, **135**, 7799-7802.

37. E. E. Ross, T. Spratt, S. C. Liu, L. J. Rozanski, D. F. O'Brien and S. S. Saavedra, Planar Supported Lipid Bilayer Polymers Formed by Vesicle Fusion. 2. Adsorption of Bovine Serum Albumin, *Langmuir*, 2003, **19**, 1766-1774.

38. A. E. Nel, L. Madler, D. Velegol, T. Xia, E. M. V. Hoek, P. Somasundaran, F. Klaessig, V. Castranova and M. Thompson, Understanding Biophysicochemical Interactions at the Nano-Bio Interface, *Nat. Mater.*, 2009, **8**, 543-557.

39. B. Sengupta, W. E. Gregory, J. Y. Zhu, S. Dasetty, M. Karakaya, J. M. Brown, A. M. Rao, J. K. Barrows, S. Sarupria and R. Podila, Influence of Carbon Nanomaterial Defects on the Formation of Protein Corona, *RSC Advances*, 2015, **5**, 82395-82402.

40. E. K. Moen, B. L. Ibey and H. T. Beier, Detecting Subtle Plasma Membrane Perturbation in Living Cells Using Second Harmonic Generation Imaging, *Biophys. J.*, 2014, **106**, L37-L40.

41. C. Macias-Romero, M. E. P. Didier, V. Zubkovs, L. Delannoy, F. Dutto, A. Radenovic and S. Roke, Probing Rotational and Translational Diffusion of Nanodoublers in Living Cells on Microsecond Time Scales, *Nano Lett.*, 2014, **14**, 2552-2557.

42. J. Culic-Viskota, W. P. Dempsey, S. E. Fraser and P. Pantazis, Surface Functionalization of Barium Titanate SHG Nanoprobes for in Vivo Imaging in Zebrafish, *Nat. Protoc.*, 2012, **7**, 1618-1633.

Alicia C. McGeachy
2145 Sheridan Road Evanston, IL 60208
Phone: 718-715-6977 • School E-Mail: aliciamcgeachy2013@u.northwestern.edu

EDUCATION

PhD CHEMISTRY- NORTHWESTERN UNIVERSITY 08/13-05/18
B.S. CHEMISTRY- SPELMAN COLLEGE 08/09-12/12

SELECT AWARDS AND ACTIVITIES

- Edward Alexander Bouchet Graduate Honor Society (2018)
- Andrew W. Mellon Foundation Conservation Fellowship (2018)
- Robert L. Burwell Summer Scholar: Recognizing Excellence in Physical Chemistry (2017)
- Chicagoland Science Penpals (2017)
- Student Diversity Award, The Graduate School, Northwestern University (NU) (2017)
- Museum of Science and Industry, Intern (2017)
- Advancing Science Conference Grant (2016/2017)
- The Graduate School, Northwestern University Diversity Peer Mentor (2016)
- NUBonD (NU Building on Diversity), Founding Member (2016-Present)
- Center for Sustainable Nanotechnology, Student Board/ Executive Committee Liaison (2016)
- Center for Sustainable Nanotechnology, Peer Editor (2015)
- Center for Sustainable Nanotechnology, Student Board Representative (2015-2017)
- National Science Foundation Graduate Research Fellowship (2014-2017)

RESEARCH EXPERIENCE

Northwestern University, Dept. of Chemistry 09/13-05/18
Advisor: Dr. Franz M. Geiger, CCI Center for Sustainable Nanotechnology
Probing the Nano-Bio Interface with Nonlinear Optics

- Applied nonlinear, surface-selective electronic and vibrational laser spectroscopies to characterize interactions occurring between nanoparticles and biological interfaces
- Explored the fundamental factors governing the interactions between nanoparticles and biochemically relevant interfaces
- Published three first author articles in peer-reviewed journals
- Co-founded a student-led diversity and inclusion group, NUBonD
- Mentored five junior graduate students and two undergraduate students
- Formally mentored one graduate student through The Graduate School Diversity Peer Mentor Program
- Awarded a National Science Foundation Graduate Research Fellowship
- Communicated science research at six national conferences in both oral and poster formats
- Contributed five blog posts to SustatinableNano and edited fourteen other blog posts in my role of Peer Editor for SustainableNano

- Recruited students on behalf of the Graduate School at four national conferences and biannual events at Spelman College
- Participated in the Graduate Engagement Opportunity Community Practicum

Spelman College, Dept. of Chemistry 09/12-12/12
Advisor: Dr. Jean Marie Dimandja, ASPIRING Researchers Program
In-Situ Derivatization of Biological Compounds in Polar Organic Media

- Worked on derivatization process in the preparation of samples for the analysis of organic compounds in biological matrices by gas chromatography
- Explored the effects of using various solvents on retention time of several amino acids to understand how retention time is affected by different conditions including temperature ramps.

Jet Propulsion Laboratory, California Institute of Technology 06/12-08/12
Advisor: Dr. Mark Anderson
Sample Acquisition Using Meta-Stable Helium

- Prepared 60 samples for analysis by infrared spectroscopy in an effort to minimize contamination.
- Used meta-stable helium with direct analysis in real time time-of-flight mass spectrometry to analyze porous rock samples impregnated with polycyclic aromatic hydrocarbons and amino acids.
- Developed and refined an analytical method for samples collected in future in situ planetary missions.
- Prepared 6 technical reports for publication in major journals.

Goddard Institute for Space Studies (NASA NYC Research Initiative) 06/11-08/11
Advisors: Dr. Dorothy Peteet, Dr. Jonathan Nichols, Argie Miller
Carbon Sequestration with Climate Change in Alaskan Peatlands

- Performed loss on ignition testing for 200 samples from two sites in Alaska in order to examine carbon accumulation in relation to climate change.
- Screened 60 macrofossil samples from Bear Bog and Gold Mine, Alaska that were used to create a climate relative timeline at the two locations over the last 11,000 years based on peat and pollen accumulation.
- Cored a sample from Four Sparrows Marsh in Brooklyn, NY.

Marshall Space Flight Center 06/10-08/10
Advisors: Dr. James Perkins, Dr. James Morgan, Dr. Jessica Albrecht
Identification and Analysis of Polyurethane Foam Components A and B

- Organized and maintained documentation and performed routine laboratory maintenance necessary for compliance with National Environmental Laboratory Accreditation Program requirements.
- Developed standards and created chemical composition profile using the NIST (National Institute of Science and Technology) database. Standards were used to analyze the composition of polyurethane foam used in ARES project.

PUBLICATIONS (REVERSE ORDER)

Doğangün, M.;† Ohno, P. E.;† Liang, D.; **McGeachy, A. C.**; Bé, A. G.; Dalchand, N.; Li, T.; Cui, Q.; Geiger, F. M., Hydrogen Bond Networks Near Supported Lipid Bilayers from Vibrational Sum Frequency Generation Experiments and Atomistic Simulations. *J. Phys. Chem. B* **2018**, *122*, 4870-4879.

McGeachy, A. C.;† Caudill, E. R.;† Liang, D.;† Cui, Q.; Pedersen, J. A.; Geiger, F., Counting Charges on Membrane-bound Peptides. *Chem. Sci.* **2018**, *9*, 4285-4298.

McGeachy, A. C.; Dalchand, N.; Caudill, E. R.; Li, T.; Doğangün, M.; Olenick, L. L.; Chang, H.; Pedersen, J. A.; Geiger, F. M., Interfacial Electrostatics of Poly(vinylamine hydrochloride), Poly(diallyldimethylammonium chloride), Poly-L-lysine, and Poly-L-Arginine Interacting with Lipid Bilayers. *Phys. Chem. Chem. Phys.* **2018**, *20*, 10846-10856.

Olenick, L. L.; Chase, H. M.; Fu, L.; Zhang, Y.; **McGeachy, A. C.**; Doğangün, M.; Walter, S. R.; Wang, H.-f.; Geiger, F. M., Single-Component Supported Lipid Bilayers Probed Using Broadband Nonlinear Optics. *Phys. Chem. Chem. Phys.* **2018**, *20*, 3063-3072.

Doğangün, M.; Hang, M. N.; Machesky, J.; **McGeachy, A. C.**; Dalchand, N.; Hamers, R. J.; Geiger, F. M., Evidence for Considerable Metal Cation Concentrations from Lithium Intercalation Compounds in the Nano-Bio Interface Gap. *J. Phys. Chem. C* **2017**, *121*, 27473-27482.

Troiano, J. M.; **McGeachy, A. C.**; Olenick, L. L.; Fang, D.; Liang, D.; Hong, J.; Kuech, T.; Caudill, E.; Pedersen, J. A.; Cui, Q.; Geiger, F.M., Quantifying the Electrostatics of Polycation-Lipid Bilayer Interactions. *J. Am. Chem. Soc.* **2017**, *139*, 5808-5816.

McGeachy, A. C.; Troiano, J. M.; Olenick, L. L.; Lankone, R.; Melby, E.; Kuech, T.; Ehimiaghe, E.; Fairbrother, D. H.; Pedersen, J. A.; Geiger , F. M., Resonantly Enhanced Nonlinear Optical Probes of Oxidized Multiwalled Carbon Nanotubes at Supported Lipid Bilayers. *J. Phys. Chem. B* **2017**, *121*, 1321-1329.

Peteet, D.; Nichols, J.; Moy, C.; Castaneda, I.; **McGeachy, A. C.**; Perez, M., Recent and Holocene Climate Change Controls on Vegetation and Carbon Accumulation in Alaskan Coastal Muskegs. *Quat. Sci. Rev.* **2016**, *131*,168-178.

Doğangün, M.; Hang, M. N.; Troiano, J. M.; **McGeachy, A. C.**; Melby, E. S.; Pedersen, J. A.; Hamers, R. J.; Geiger, F. M., Alteration of Membrane Compositional Asymmetry by $LiCoO_2$ Nanosheets. *ACS Nano* **2015,** *9*, 8755-8765.

Nichols, J.; Peteet, D.; Moy, C.; Castaneda, I.; **McGeachy, A**. **C.**; Perez, M., Impacts of Climate and Vegetation Change on Carbon Accumulation in a South-central Alaskan Muskeg Assessed with Novel Organic Geochemical Techniques. *Holocene* **2014**, *24*, 1146-1155.

†Indicates co-first authorship.

SELECT PRESENTATIONS

Oral Presentations

Black Creativity Jr. Science Café, Museum of Science and Industry, *Chicago, IL* 02/18

National Organization for the Professional Advancement of Black Chemists and Chemical Engineers Conference, *Raleigh, NC* 11/16
252nd American Chemical Society Fall National Meeting. *Philadelphia, PA* 08/16
Northwestern University, Seven Minutes of Science Symposium, *Evanston, IL* 09/15

Poster Presentations
National Organization for the Professional Advancement of Black Chemists and Chemical Engineers Conference, *Minneapolis, MN* 10/17
National Organization for the Professional Advancement of Black Chemists and Chemical Engineers Conference, *Orlando, FL* 09/15
Gordon Research Conference: Environmental Nanotechnology, *West Dover, VT* 06/15